UNIVERSITY OF CALIFORNIA, SAN DIEGO

Studies of Membrane Protein Folding by Bimolecular Fluorescence Quenching

A Thesis submitted in partial satisfaction of the requirements for the degree

Master of Science

in

Chemistry

by

Ivan Andrew Kozachenko

Committee in charge:

Professor Judy E. Kim, Chair

Professor Elizabeth A. Komives

Professor Michael J. Tauber

2016

The Thesis of Ivan Andrew Kozachenko is approved, and it is acceptable in quality and form for publication on microfilm and electronically:

Chair

University of California, San Diego

2016

DEDICATION

I would like to dedicate my thesis to my father, Ken, mother, Maria, grandmother, Jane and sister, Eva as well as Dr. Kim, Dr. Brian Leigh, Dr. Guipeun Kang and Ignacio Lopez-Peña, without whom this work would not have been possible.

I give a special thanks to Dr. Tauber, Dr. Magde, Dr. Komives, all other members of the Kim and Tauber groups (Deeann Asamoto, Joel Rivera, Justine Liang, Sam Doyle, Maria Angellela, Andrew Tai, Jen Daluz, Steven Ortiz, John Wenger, Fabian Heinzel) and professors who made contributions to my education, this work and a positive influence on my time at UCSD.

I give a special thanks to my professors from Mesa College, Dr Gergens, Dr. Zand, Dr. Hjorth-Gustin, Mr. Fremland and Dr. Alexander who were great influences to my academic progress.

I would also like to add a note in loving memory of my late best friend, Alex Daniel Rodriguez.

IAK

EPIGRAPH

In a world of casual inquiries make me a seeker

Jeanne Mayo 1995

TABLE OF CONTENTS

LIST OF ABBREVIATIONS

MP ..... membrane protein

OmpA ..... Outer Membrane Protein A

E. coli ..... Escherichia Coli

trp or W ..... tryptophan

acr ..... acrylamide

SV ..... Stern-Volmer

phe or F. ..... phenylalanine

NATA ..... N-acetyl-L-tryptophanamide

SUV ..... small unilamellar vesicle

DMPC ..... dimyristoylphosphatidylcholine

DPPC ..... dipalmitoylphosphatidylcholine

KPi ..... pH 7.3 potassium phosphate buffer

PVDF ..... polyvinylidene fluoride

T_c ..... Phase transition temperature (melting/freezing)

ANTS 8-aminonaphthalene-1,3,6-trisulfonate

DPX ..... *p*-xylene-bis(N-pyridinium bromide)

SFCA ..... Surfactant free cellulose acetate

tx100 ..... triton X-100

DLS ..... dynamic light scattering

tyr or Y ..... tyrosine

K_{SV} ..... Stern Volmer quenching constant

K_D ..... Stern Volmer quenching constant for dymanic qucnehing

w/ ..... with

w/o ..... without

exp ..... exponential

dexp ..... double exponential

DOPC ..... dioleylphosphatidylcholine

TDFQ..... Distance determination by time-dependent fluorescence quenching

SA..... solvent acessibility

IPTG ..... isopropyl β-D-1-thiogalactopyranoside

LIST OF FIGURES

LIST OF TABLES

ACKNOWLEDGEMENTS

I would like to acknowledge Dr. Judy Kim for inviting me to lab as an undergraduate, and being a mentor and basis of support for me at UCSD. If it were not for her, I would probably not have had the opportunity to gain the experience and knowledge that I have in my undergraduate and graduate time at UCSD.

I would like to acknowledge Ignacio Lopez-Peña for doing most of the writing of the macros that made the data workup for these experiments feasible. I did help.

I would like to acknowledge Dr. Douglas Magde for the Dynamic Light Scattering experiments, autocorrelation of the data and for all the discussions and explanations that were so helpful.

I would like to acknowledge Dr. Brian Leigh for constructing a spreadsheet that assisted in preparation of the samples. Aside from that Brian was a great mentor, and friend.

I would like to acknowledge Dr. Guipeun Kang for her mentorship and encouragement. She taught me the process of protein expression and many other techniques, and encouraged me to stay in lab at a point where I was considering leaving. I thank her for that.

I would like to acknowledge my professors and committee members Dr. Elizabeth A. Komives and Dr. Michael J. Tauber for their professorship and encouragement.

I would like to acknowledge my professors from Mesa College Dr Gergens, Dr. Zand, Dr. Hjorth-Gustin, Mr. Fremland and Dr. Alexander who were great influences to my academic progress.

I would like to acknowledge John Wenger and Steven Ortiz who both assisted in some of the quenching experiments that are included in this thesis.

It should be acknowledged that this thesis is in the process of being formatted for publication.

ABSTRACT OF THE THESIS

Studies of Membrane Protein Folding by Bimolecular Fluorescence Quenching

By

Ivan Andrew Kozachenko

Master of Science in Chemistry

University of California, San Diego, 2016

Professor Judy Kim, Chair

This project investigates changes in protein solvation during the folding reaction of Outer membrane protein A (OmpA) of *Escherichia Coli*, and correlates this dehydration process with shifts in local polarity. Changes in solvent accessibility were probed by fluorescence quenching experiments and Stern-Volmer analysis while polarity was monitored via emission maxima; site-specific insights were gained by probing single tryptophan OmpA mutants (W7, W15, W57, W102, W129, and W143). Fluorescence experiments were performed on OmpA denatured in 8.0 M urea, folded in small unilamellar vesicles (SUVs), adsorbed on SUVs, and aggregated in 0.5 M

urea. Time resolved experiments were performed during the folding reaction. The Stern-Volmer quenching constant (K_{SV}) and fluorescence maxima (λ_{max}) showed a correlation where high values of K_{SV} corresponded to red-shifted λ_{max}. K_{SV} and λ_{max} values decayed from unfolded values of 8.6-10 M^{-1} and 351-354 nm to folded values of 0.6-2.0 M^{-1} and 325-338 nm. Double exponential fits to the K_{SV} and λ_{max} data showed fast (τ ~ 3–11 minutes) and slow components (τ ~ 26–49 minutes). The majority of λ_{max} shift occurs in the fast step, while the majority of dehydration occurs in the slower step. The fast component was attributed to a transition of the trp residues of unfolded OmpA to a partially adsorbed state in the bilayer headgroup. A slower, dehydration event took place in which the protein fully inserted into the bilayer. These results complement previously proposed mechanisms of concerted folding, and provided insights into changes in solvation that accompanies formation of native structure.

Introduction

General background. Membrane proteins (MP) are essential for cellular processes because they function as receptors, transporters and enzymes,[1] and they represent at least 26%[2,3] of the human genome. In contrast to soluble proteins, relatively little is known about MPs. Only about 0.7% of protein data bank (PDB) structures are of MPs;[4] there are 585 MPs of known structure[5] in contrast to about 84,000 total proteins in the protein data bank. In a SciFinder literature search, 7.3% of results for "proteins" refer to "membrane proteins".[6]

Membrane proteins are divided into two classes; integral MPs span the lipid bilayer and peripheral MPs are only embedded on the surface or weakly associated with the bilayer.[7] Integral MPs are of great importance because they are the means by which cells interact with their external environment. Misfolding of MPs is implicated in many common diseases like cancer, cardiovascular disease and cystic fibrosis.[3] The five most common cancers, breast, prostate, lung, colorectal and cervical are all associated with transmembrane (TM) receptor proteins that initiate intracellular signaling pathways.[8] Ion channels in smooth muscle are responsible for maintaining vascular tone, which modulates the resistance of the circulatory system, having implications to hypertension.[9,10] Oxidized forms of low density lipoprotein, a lipid-associated protein that transports lipids through the bloodstream, have been associated with atherosclerosis, a common cause of cardiovascular disease.[11] Cystic fibrosis is caused by mutations in the cystic fibrosis transmembrane regulator (CFTR) protein, an ion channel found in epithelial cells of the respiratory system, sweat glands and pancreas.[12] In cystic fibrosis, the faulty ion channel prohibits transport of saline, causing mucus buildup and infection. As a consequence of the important role that they play in biochemical systems, MPs constitute at least 60%[13,3] of human drug targets and are a large area of research. Recently, a new drug, Ivacaftor, was approved for the treatment of cystic fibrosis in patients with certain mutations of the CFTR.[14] Despite progress, information on the structure and dynamics of MPs is lacking. Further study of the folding and insertion of MPs into their native environments is an important pursuit for the advancement of research and healthcare.

Outer membrane protein A (OmpA) of *Escherichia coli* (*E. coli*) is a suitable system for the study of the folding and insertion of integral MPs into lipid bilayers. The intrinsic hydrophobicity of most MPs is an obstacle to the conventional techniques applied to the expression, purification and crystallization of proteins.[3] Most MPs require detergents for their solvation, and most α-helical proteins are too hydrophobic for refolding studies without detergents.[15] β-barrel MPs, like OmpA, feature alternations of hydrophobic and hydrophilic residues in the TM β-strands, making them moderately hydrophobic,[16] and reducing 'frustration' in their folding-energy landscape.[17] β-barrel MPs are native to Gram negative bacteria, and organelles (especially mitochondria) of eukaryotic cells[18] (including those of humans), where they have been shown to be essential for the biogenesis of the outer membrane.[19] They are thought to be the means by which our microbiome intake dietary polysaccharides for fermentation,[20] a process which is responsible for 10-15% of our daily calorie intake.[21] Research on the dynamics of β-barrels like OmpA is important because it may have influence on current research on the human microbiome,[22] the development of antimicrobial drugs and vaccines[23,24] and the study of human β-barrel MPs.

OmpA, also known as Outer membrane protein II* (in the older literature),[25] is a 325 residue[26] (35,177 Da)[27] integral MP that resides in the outer membrane of *E. coli*. OmpA forms an N-terminal (residues 1 to ~170), 8-stranded, transmembrane β-barrel and has a C-terminal (residues ~170-325), soluble, periplasmic domain[28] (Figure1). In its native environment, OmpA influences cell shape,[29] is necessary for the action of colicin,[30] and with lipopolysaccharide serves as a receptor for F-mediated conjugation and bacteriophage TuII.[31,32] In contrast to many MPs, OmpA is fully soluble in 8 M urea solution,[33] and has been shown to spontaneously fold and insert into curved[34] lipid bilayers, in an oriented fashion, upon dilution of denaturant, and in the absence of detergents.[35] The absence of necessity for detergents is a key benefit of OmpA in terms of protein folding studies.[36] Another attribute of OmpA is the existence of high resolution structural data. X-ray diffraction[37] (PDB ID 1QJP) and NMR[38] (PDB ID 1G90) spectroscopy studies have provided atomic resolution structures of the OmpA transmembrane domain (Figure

1). These properties make OmpA an ideal system for the study of integral membrane protein folding.

Fluorescence spectra of OmpA. OmpA has five native, fluorescent tryptophan residues at positions 7, 15, 57, 102 and 143 (Figure 1) of its primary structure. In this thesis, I will use the conventional abbreviations for tryptophan of 'trp' or 'W'. Like most integral membrane proteins, the trp residues are located near the membrane-aqueous interface.[39,40] The trp residue at position 7 (W7) is located on the periplasmic region of the outer membrane while tryptophan residues 15, 57, 102 and 143 are located on the extracellular side of the outer membrane. We have generated a sixth mutant Y129W that allows us to investigate a second tryptophan residue on the periplasmic region.

The fluorescence of these residues has been used in many studies to gain information on the structure and dynamics of OmpA. The increase of fluorescence quantum yield and blue-shift of the emission maximum of the indole moiety upon transition from aqueous to apolar environment has widely been exploited.[41] Fluorescence spectra for W7, W15, W57, W102, W129, and W143 in folded and unfolded conformations are shown in Figures 2 and 3 (experimental conditions described in the Materials and Methods section). The unfolded and folded states of OmpA in micelles[42] and SUVs[35] were studied by this fluorescence assay. Similar assays were used to study the kinetics of the folding and insertion process via investigations of the emission of the individual trp residues, providing support for a concerted folding mechanism.[43] The association of OmpA with the chaperone protein Skp was monitored by the same type of fluorescence assay applied to protein-protein interactions.[44] More recently, Förster resonance energy transfer (FRET) studies have determined distances between the native tryptophan residues and cysteine linked dye molecules at different unfolding states of OmpA. These studies determined the distance across the pore to be roughly 19 Å, and the transmembrane distance to be roughly 29 Å.[45] More information is yet to be revealed through fluorescence spectroscopy techniques.

Fluorescence quenching. Another fluorescence spectroscopy technique that has been used to gain valuable information about OmpA is fluorescence quenching. The following description of fluorescence quenching is adapted mainly from Lakowicz.[46] Fluorescence quenching is any process that decreases the fluorescence quantum yield of a fluorophore. Various processes, including isomerization, energy transfer, excited state chemical reactions, ground-state complex formation, and collisional quenching, can be responsible for quenching. Many molecules including molecular oxygen, halogenated compounds, and aromatic and aliphatic amines are quenchers.

In this study, tryptophan fluorescence was collisionally quenched by acrylamide. Although the quenching mechanism is not perfectly clear, the singlet excited state of trp is thought to form a transient charge transfer complex with acrylamide, which returns the fluorophore to the ground state.[47,48,49] In collisional quenching, the quencher diffuses to the fluorophore within the lifetime of the excited state, makes van der Waals contact (< 5 Å),[49] and returns the fluorophore to the ground state. Collisional or dynamic quenching is modeled by the Stern-Volmer (SV) equation (Eq 1).

$$\frac{F_0}{F} = K_{SV}[Q] + 1 = k_q \tau_0 [Q] + 1 \qquad \text{Equation 1}$$

In Eq. 1, F_0 represents the fluorescence intensity of the fluorophore in the absence of quencher, while F indicates the fluorescence intensity in the presence of quencher. When quencher is absent ([Q] = 0), F_0 is equal to F so the ratio F_0/F equals 1. The concentration of quencher is denoted [Q] (or [Acr] for acrylamide). The SV quenching constant, K_{SV}, referred to as K_D in the case of a dynamic quenching processes, is an indirect measure of solvent accessibility (SA) when using soluble quenchers. K_D is equal to the product of the lifetime of the excited state of the fluorophore τ_o, and the bimolecular quenching rate constant k_q. Another interesting interpretation of K_{SV}, which has units of concentration (M), is that the reciprocal, K_{SV}^{-1} is the concentration of quencher that decreases fluorescence intensity by 50%. Dynamic quenching usually results in linear SV plots. Previous studies have shown that the quenching of tryptophan fluorescence by

acrylamide is primarily a dynamic process,[50] although slight deviation of the SV curve has been noted in fluorescence quenching studies of proteins.[51]

Fluorescence quenching may also occur through a static process. Upward-curving SV plots are indicative of a combination of dynamic and static quenching; the latter occurs when the fluorophore and quencher form a non-fluorescent, ground-state complex. The presence of static quenching has been observed in single trp containing proteins, in the presence of acrylamide.[51] It is considered that indole and acrylamide have a relatively weak association, and do not form a true, non-fluorescent, ground state complex. In this mechanism, the indole and acrylamide are closely approximated in a "sphere of action" volume such that fluorescence is immediately quenched when the quencher is within a certain distance from the fluorophore. The upward curvature of these plots may reflect two populations of trp residues, one larger population that is being purely dynamically quenched and one smaller population that is pseudo-statically quenched in 'dark complexes'. This type of combined static+dynamic quenching is described by the following equation.

$$\frac{F_0}{F} = (K_D[Q] + 1)e^{V[Q]} \qquad \text{Equation 2}$$

In Eq. 2, K_D represents an analogous SV quenching constant for dynamic quenching, and V represents a volume element around the fluorophore in which interaction with the quencher creates a dark pseudo complex; the parameter V should be a constant for a given fluorophore-quencher pair. One value of V determined for the trp analog, N-acetyl-L-tryptophanamide (NATA), and acrylamide quencher is 1.44 L/mol. This value of V equates to a sphere of diameter 17 Å nm around each fluorophore. Previously reported diameter values for the indole fluorophore and acrylamide are 4.4 Å and 3.4 Å.[49] Representative SV data for NATA, are shown in Figure 4. Also shown in figure 4 are the structures of tryptophan and acrylamide. The upward curvature of the NATA SV plot is evident, and the data are fit to both dynamic (Eq. 1) and dynamic+static (Eq. 2) models shown as the black and green fits, respectively. In this situation, NATA is solvent-exposed, and acrylamide can readily quench the fluorescence; hence the slope of the SV graph,

and the corresponding K_{SV} or K_D values, are large (NATA exposed). If NATA were completely buried, and acrylamide could not access NATA to quench the fluorescence, the SV plot would be a horizontal line with slope of zero; this hypothetical SV graph is shown as a dashed line (NATA protected). If NATA were partially-exposed to solvent, the slope would fall in between these two extremes.

Fluorescence quenching is readily applicable to the study of protein-lipid interactions. The requirement of van der Waals contact for both static and dynamic quenching, and the exclusion of water[52] (and soluble quenchers) from lipid bilayers allows these experiments to provide information on accessibility of quencher to fluorophore. Membrane-bound and soluble quenchers can be used to determine relative locations of fluorophores in proteins as well as determine the accessibility of the quencher, and therefore solvent, to the fluorophore. Fluorescence quenching studies have previously been conducted on OmpA and have revealed valuable information. Acrylamide has been used to establish K_{SV} values for the adsorbed, folded and inserted forms of OmpA in dioleylphosphatidylcholine (DOPC, T_c -17 °C)[53] and DMCP[36] vesicles. Fluorescence quenching studies (using acrylamide) that probed the association of wild type OmpA (wt-OmpA) with the chaperone Skp determined a K_{SV} value of 2.7 M^{-1}.[54] This indicated that in complex with Skp, the solvent accessibility of the trp residues is comparable to a membrane bound 'adsorbed' folding intermediate. Time resolved distance determination by fluorescence quenching (TDFQ) experiments (using brominated lipids) were performed on OmpA to track the distance between individual trp residues and the center of the lipid bilayer during the folding process.[43,53,36] Steady-state quenching studies with OmpA and soluble quenchers have established K_{SV} values for folded and unfolded states, but, have not tracked the evolution of K_{SV} during the folding process.

In this work, the folding and insertion of OmpA into lipid bilayers has been studied by measuring the change in K_{SV} over the time of the folding reaction. Again, K_{SV} is an indirect measure of solvent accessibility. This is an important topic because water plays an important role in protein folding and function.[55,56] Water is important in catalysis[57] and hydrogen bonding networks, its dielectric coefficient mediates electrostatic interactions[58], and it is an intrinsic part of

the hydrophobic interactions that are important to most protein folding processes.[59,60] The temporal evolution of K_{SV} throughout protein folding provides new insight into the kinetics of desolvation that compliments previous time-resolved studies of OmpA. This thesis introduces a valuable method of monitoring the dynamics of MPs, and that shows promise for new applications to other families of MPs, protein-protein interactions, and perhaps the dynamics of other biological macromolecules.

Materials and Methods

Protein preparation. Mutants that contain single trp residues (referred to as "single trp mutants") of OmpA were expressed and purified following an established procedure.[61,35] OmpA mutants were prepared with single trp residues at native (7, 15, 57, 102, 143) or non-native (129) positions. In these mutants, the remaining four or five (in the case of 129) native trp residues were mutated to phenylalanine (phe or F). Briefly, an OmpA-free cell stock JF733[25] was transformed with a plasmid containing the OmpA gene under the control of the lac operon. The protein was overexpressed using isopropyl β-D-1-thiogalactopyranoside (IPTG), and the cells were lysed by sonication after treatment with lysozyme. The membranes were collected by centrifugation, and OmpA was extracted with 8 M urea and isopropanol. The crude protein was purified on a Q sepharose Fast Flow (GE Healthcare Life Sciences) anion exchange column and eluted by a NaCl gradient. The enriched fractions were combined, rinsed of NaCl, and concentrated by ultrafiltration (Millipore ultracel NMWL 3 or 10 KDa). OmpA single trp mutants were stored in the denatured state (8.0 M urea, 20 mM potassium phosphate buffer, pH 7.3), with stock concentrations of 150-400 μM.

Preparation of samples for fluorescence experiments. Small unilamellar vesicles (SUVs) of dimyristoylphosphatidylcholine (DMPC, phase transition temperature T_c = 24°C) and dipalmitoylphosphatidylcholine (DPPC, T_c = 41°C) were prepared according to a previously published procedure.[61] The lipids were purchased from Avanti Polar Lipids. Briefly, 1 mL of 25 mg/ml lipid in chloroform was dried under nitrogen gas. The dry lipid film was resuspended in 5 mL of pH 7.3 potassium phosphate buffer (KPi), sonicated with a probe sonicator tip, and the SUVs were filtered through a 0.22 μm pore polyvinylidene fluoride (PVDF) filter, making a 5 mg/mL lipid stock solution. The SUVs were allowed to equilibrate overnight above their phase transition temperature. The diameter of the vesicles was determined to be roughly 50 nm (with a smaller population of larger, ~180 nm vesicles) by dynamic light scattering experiments (see description below). DMPC SUVs were used for the study of the folding and insertion of OmpA at

37°C; DPPC SUVs were used to study the adsorbed state of OmpA at room temperature (~21°C).

For each quenching experiment, five 200 µL samples were prepared with concentrations of acrylamide ranging from 0.0 M to 0.4 M; acrylamide was dispensed from a 1.0 M stock solution. Protein was added to pre-made solutions that contained SUVs and acrylamide (if appropriate) in KPi. Protein and urea were supplied from a secondary stock protein solution that contained 80-140 µM OmpA and 5 M Urea. OmpA has been determined to be unfolded in 5 M urea.[62] The secondary protein stock was vortexed before aliquots were distributed to each sample. The final protein concentration of all samples was 8-14 µM, as determined by the absorption spectrum of protein in 0.0 M acrylamide. For each experiment, we aimed for a final OmpA concentration of 10 µM, but inaccuracies in stock protein concentration resulted in final concentrations of 8-14 µM, as determined by the absorption spectrum of protein in 0.0 M acrylamide. The final urea concentration was 0.5 M for all samples. The final lipid to protein ratio was 300:1 which resulted in a roughly 2 mg/mL lipid concentration. All solutions were prepared in pH 7.3 KPi. All samples were mixed by stirring and pipetting the solution up and down with the pipette tip after injecting 20 µL of the secondary protein stock. This mixing was done immediately (≤10 s) before the first fluorescence spectrum was acquired. Each cuvette was capped with a parafilm-sealed teflon cap. Special care in sample preparation, especially the delivery of acrylamide and protein stock was crucial to ensure that the fluorescence intensity showed the proper trend to increasing concentrations of acrylamide.

Spectroscopic measurements of fluorescence quenching. Fluorescence spectra were acquired on a Jobin Yvon Fluorolog Spectrofluorometer from 300 nm to 500 nm at 4 nm step size with 0.5-second integration time and 3 nm entrance and exit bandpass; the excitation wavelength was 290 nm. Temperature was maintained at 37°C for the OmpA folding study and at room temperature (~21°C) for the adsorbed (DPPC), unfolded (8.0 M urea) and aggregated (0.5 M urea) OmpA experiments. For the folding experiment, acquisition of fluorescence spectra commenced upon addition of 20 µL of the secondary OmpA stock (80-140 µM OmpA and 5 M

urea) into five 2×10 mm quartz cuvettes, each of which contained 180 µL of a pre-made solution of phosphate buffer, DMPC SUVs and varying amounts of acrylamide. The samples with final volume 200 µL were excited along the 2 mm path and fluorescence was acquired along the 10 mm path. Spectra were acquired for each sample at 5-minute intervals for two hours, and then at 20-minute intervals until six hours had passed. A total of five samples with acrylamide concentrations 0.0 M, 0.1 M, 0.2 M, 0.3 M and 0.4 M were analyzed for each experiment. This method required that a fluorescence spectrum be acquired every minute during the first two hours so SV plots could be generated. This time constraint influenced the choice of protein concentration and relatively large step size such that sufficient signal could be detected over the entire span of the emission spectrum (300-500 nm) of the indole moiety. In the beginning of the experiment, an iterative, systematic and well-coordinated procedure needed be followed; this procedure included vortexing the secondary protein stock, injecting protein into a solution of 0.0 M acrylamide, starting the clock, acquiring spectra, changing filenames, switching to the second cuvette, vortexing and injecting protein into the second cuvette that contained 0.1 M acrylamide, acquiring spectra, changing filenames, switching to the third cuvette, etc. This procedure resulted in initiation of five folding reactions with five different acrylamide concentrations over a 5-minute period. This was an intense procedure, and required practice to obtain reliable success. An assistant helped in the first 5 minutes and then afterwards, the focus was to switch cuvettes and change filenames for the next six hours. Absorbance spectra of each sample were acquired on an Agilent 8453 UV-visible spectrophotometer along the 10 mm path length of the cuvette after the experiments were completed (6 hours).

Analogous experiments were conducted for one hour at ambient temperature (~21°C) with DPPC SUVs instead of DMPC SUVs to investigate the kinetics of adsorption of OmpA. Spectra were collected every five minutes for the first half hour and then every 10 minutes for the last half hour. Aside from the decreased duration of the experiment, lower temperature, and gel (solid) phase vesicles, all aspects of the adsorbed experiment and data workup were the same as the 6-hour folding experiment with DMPC SUVs described in the previous paragraph.

Control experiments were conducted at ambient temperature for unfolded (8 M urea) and aggregated (0.5 M urea) OmpA in the absence of SUVs; these experiments revealed the level of quenching for the fully denatured and aggregated states of OmpA. For these experiments, samples were incubated for ~5 minutes, then fluorescence spectra were collected with 1-nm step size and 1- second integration time. All other fluorescence spectra acquisition parameters as well as protein and acrylamide concentrations were the same as the previously described quenching experiments. Data workup for these experiments only required the calculation of a single K_{SV} value.

Vesicle leakage assays. Vesicle leakage assays were conducted to investigate the stability and permeability of the SUVs. Prior to sonication, the aqueous DMPC solution contained 50 mM 8-aminonaphthalene-1,3,6-trisulfonate (ANTS), a fluorophore, 50 mM *p*-xylene-bis(N-pyridinium bromide) (DPX), a quencher, and 2.5 mg/ml resuspended DMPC. The decrease in lipid stock concentration to 2.5 mg/ml relative to folding experiments (5 mg/ml) was necessary to avoid undesired flocculation of lipid+dye solutions. After sonication, 3.0 mL of the 2.5 mg/ml DMPC SUV stock solution with quencher and fluorophore was passed down a warm (~45 °C) Econo-Pac® 10DG desalting column to separate vesicles encapsulating ANTS+DPX from free ANTS and DPX by size exclusion. After discarding the initial dead volume of 3.0 mL, 0.5 mL fractions were collected. The first 3.5 mL of elution were tested for encapsulation of ANTS and DPX by acquisition of fluorescence spectra before and after lysing the SUVs in the presence of 0.1% (v/v)[63] Triton X-100; this concentration of Triton X-100 was obtained by 10x dilution of an initial 1% Triton X-100 solution. ANTS fluorescence spectra were collected from 400 nm to 670 nm with 1 nm step size, 1-second integration time, and 3 nm entrance and exit bandpass; the excitation wavelength was 380 nm.[64] Increase in fluorescence intensity after lysis indicated that the first 1.0 mL of elution was the most enriched in SUVs encapsulating ANTS and DPX.

The effects of acrylamide and OmpA on the integrity of the SUVs were probed. In one experiment, two 180 µL samples of dye-encapsulated DPMC SUVs from the first 1.0 mL of elution were prepared with and without 0.4 M acrylamide and incubated at 37°C.

The fluorescence spectrum of ANTS and UV-vis absorbance were monitored over a period of 6 hours. In a separate experiment, a sample of the ANTS/DPX encapsulating SUVs was prepared with ~10 uM OmpA in a manner analogous to the folding experiment. The fluorescence of tryptophan (excitation at 290 nm and emission scan from 300-500 nm) and ANTS (excitation at 380 nm and emission scan from 300-500 nm) were monitored over time. For both experiments involving ANTS/DPX encapsulating SUVs, fluorescence spectra were acquired over 6 hours, at 20 minute intervals for the first 3 hours and then at 30 minute intervals for the last 3 hours. One preliminary experiment was conducted with fluorescence measurements at 1.5 hour intervals. The samples were then lysed by adding 20 µL of 1% Triton X-100 to create a 0.1% Triton X-100 solution, and then fluorescence and absorbance spectra were measured again.

Dynamic light scattering experiments. Dynamic light scattering (DLS) experiments were conducted in collaboration with Dr. Douglas Magde to evaluate the diameter of the SUVs and to investigate potential effects of acrylamide on their size and stability. Samples of 2 mg/ml DMPC were prepared in the presence of 0.0, 0.2 and 0.4 M acrylamide, and maintained at 37 degrees Celsius. DLS measurements were taken at 3 hour intervals. A Coherent Verdi Diode Pumped Laser with a Nd:YVO_4 crystal as the lasing medium provided monochromatic, coherent light of 532 nm wavelength after second harmonic generation of the fundamental 1064 nm emission. The green, 532 nm output of 1.01 Watts was attenuated with neutral density filters to ~ 50 mW, focused with a 100 mm focal length lens and directed through the sample in a 1x1 cm quartz cuvette. Rayleigh scattered light that was polarized in the horizontal plane was passed through a small aperture (< 1 mm diameter) and collected at 90 degrees by a SPEX double monochromator (250 mm focal length). Photons were detected by an Amprex Model 56 photomultiplier tube, and output was amplified by a factor of ten, discriminated to produce standard pulses suitable for counting and then accumulated in a multichannel scaler. For each acquisition, there were 524,288 bins accumulated, each for 20 µs, for a total of 10.5 s; for each sample, 20 acquisitions were acquired. For each acquisition, the fluctuation in the intensity of the

scattered signal, which is related to the number of scattered photons, (first 4000 bins) was analyzed via the autocorrelation function (equation 3) by custom computer programs.

$$\boldsymbol{G(\tau_i) = \langle I(0) I(\tau_i) \rangle = \lim_{T\to\infty} \frac{1}{T} \int_0^T I(t) I(t+\tau_i) dt} \qquad \text{Equation 3}$$

In equation 3, $G(\tau_i)$ is the autocorrelation function,[65] I is the intensity of scattered signal at a particular time, T is the number of bins acquired, and τ_i is an integral multiple of the time increment or bin size, Δt.

Fluorescence quenching data analysis. The raw fluorescence spectrum exhibits fluorescence signal from OmpA as well as scattering from SUVs. The fluorescence originates from the single tryptophan and 17 native tyrosine residues in OmpA; subtraction of the contribution from tyrosine did not affect observed K_{SV} values (see below). Therefore, all spectra were treated in the following manner, without removal of tyrosine signal. OmpA fluorescence spectra were isolated by subtracting a scalar multiple of the vesicle background from each raw spectrum to generate a corrected spectrum; OmpA corrected spectrum = raw OmpA spectrum − *c**vesicle spectrum, where *c* is a scalar between the values of 0.5 and 1.5. The selection of *c* was based on the shape of the resulting curves, which depended on the blue shift of the fluorescence maxima and the increase in fluorescence quantum yield at a particular time during the folding reaction. For each time point, a graph of the quenching trend was constructed (see Figure 5 for representative quenching trends of folded and unfolded OmpA). The value of *c* was chosen such that the region near 300 nm, where the scattering signal is greatest, exhibited reasonable shape without obvious over- or under-subtraction. At the earliest times, the region near 300 nm was nearly horizontal, and during the folding process, slopes approached 60 degrees. Although this process is somewhat subjective, values of c were chosen without regard to whether the expected trends were achieved; this blind method hopefully reduced bias in the interpretation. Indeed, some quenching trends did not display the expected outcomes, and showed overlap of fluorescence spectra of the different samples.

The isolated and corrected OmpA fluorescence spectra, called F_{obs}, were further corrected for attenuation of the excitation beam and emission signal by quencher and fluorophore (known as the inner filter effect) yielding F_{corr} [46]. The inner filter effect equation is displayed below.

$$F_{corr} = F_{obs} 10^{\left(\frac{A_{ex}+A_{em}}{2}\right)} \qquad \text{Equation 4}$$

In Eq. 4, A_{ex} and A_{em} denote the absorbance at the excitation and emission wavelengths, respectively (A_{ex} is measured at 290 nm). Despite the blue-shift of the fluorescence maximum from ~350 nm to ~330 nm, the wavelength used for A_{em} was kept constant at 350 nm. The difference in absorption from 350 nm to 330 nm is negligible in terms of the inner filter effect correction. In some studies on OmpA, A_{em} has been disregarded because the samples absorbed very little at the emission wavelengths, so self-absorption was considered to affect only the excitation beam[53]. To determine A_{ex} and A_{em}, absorption values which were acquired along the 10 mm path length of the cuvette were multiplied by 0.2 to take into account that excitation for fluorescence measurements was along the 0.2 mm pathlength. The assumption of 0.2 mm pathlength for both excitation and emission paths is an estimate because the pathlength of the emitted light is probably around 0.5 mm (full pathlength of cuvette along emission direction is 1 cm). However, given the negligible effect of A_{em} (value of A_{em} at 350 nm was typically 0.003 over 1 cm pathlength), the use of 0.2 mm vs 0.5 mm pathlength for emission does not significantly affect the self-absorption correction. Fluorescence spectra were not normalized for protein concentration because the absorbance of acrylamide overlapped with protein absorption, so it was difficult to ascertain the protein concentration based on UV-Vis absorption. Because protein concentrations could not be easily measured for each sample, it was especially important that my technique be careful and reproducible. It was assumed that the concentration of protein in 0.1, 0.2, 0.3, and 0.4 M acrylamide was identical to that in 0.0 M acrylamide; the latter was determined by UV-vis absorption measurements. Gaussian fits were applied to the peaks of all corrected fluorescence spectra to determine maximum fluorescence intensities (F_{max}) and maximum fluorescence wavelengths (λ_{max}).

Stern Volmer plots were constructed from the F_{max} of all five samples at each time point during the folding reaction, regardless of slight differences in λ_{max}. Briefly, the corrected fluorescence intensity of each sample (0.1-0.4 M acrylamide) (F_{max} , abbreviated simply as F) was compared to the corrected fluorescence intensity in the absence of quencher (0.0 M acrylamide) (F_0) by the ratio F_0/F and plotted versus the concentration of acrylamide. For the 6- or 1- hour DMPC and DPPC experiments, respectively, Sterm-Volmer plots were constructed for each time point. The plots were fit to the dynamic quenching models, see Eq. 1, to yield K_{SV} values as a function of folding time. K_{SV} vs time data were averaged for multiple trials and fit to single (Equation 5) or double (Equation 6) exponential decay functions.

$$\boldsymbol{K_{SV}(t) = y_0 + Ae^{-k(t)}} \qquad \text{Equation 5}$$

$$\boldsymbol{K_{SV}(t) = y_0 + A_1e^{-k_1(t)} + A_2e^{-k_2(t)}} \qquad \text{Equation 6}$$

In these equations, y_o is the asymptotic K_{SV} value as $t\rightarrow\infty$, A, A_1, and A_2 are the amplitudes associated with each decay constant, and k, k_1, and k_2 are the decay constants (where $k = 1/\tau$, where τ is interpreted as a decay time). The decay time is the time that it takes for 1/e of the OmpA population to fold into the lipid bilayer. Equations of the same form were also used to fit the DLS data.

ANTS DPX data analysis. The raw ANTS DPX data were subtracted of their water Raman signal and were not normalized for concentration of fluorophore. The absorbance and fluorescence data were overlaid to emphasize leakage of ANTS and DPX and to make comparison of the different conditions. Plots of fluorescence maxima (514 nm) for each fraction, before and after lysis were constructed to visualize the efficacy of the separation process to select the best fraction for experiments. Similar plots were constructed to compare the leakage of ANTS DPX in the presence of acrylamide or OmpA.

DLS Data Analysis The averaged autocorrelation curves were fit to single and double exponential decay equations (Equations 5 and 6). The scattering vector q was calculated for the experimental setup[65] (Equation 7).

$$\boldsymbol{q = \frac{4\pi n}{\lambda} sin \frac{\theta}{2}} \qquad \text{Equation 7}$$

In Equation 7, n is the refractive index of the solvent (1.33 for water), λ is the wavelength of incident light (532 nm), and θ is the observation angle (90°). For each individual exponential term (from single and double exponential fits), a diffusion constant, D, was calculated from the scattering vector and the exponential decay constants (k, k_1, k_2)[65] (Equation 8).

$$\boldsymbol{D = \frac{k}{2q^2}} \qquad \text{Equation 8}$$

The diffusion constant was inputted into the Stokes-Einstein equation (Equation 9) to yield the hydrodynamic radius, which is the radius of a sphere with an equal diffusion coefficient [65].

$$\boldsymbol{R_h = \frac{k_b T}{6\pi\eta D}} \qquad \text{Equation 9}$$

In Equation 9, k_B is the Boltzmann constant, T is the temperature in Kelvin (303.15K), and η is the viscosity of the solvent (0.798 mPa·s) .[61]

Results

The folding and insertion of OmpA into SUVs of DMPC was studied by time resolved fluorescence quenching techniques. The sensitivity of the fluorescence of the individual trp residues to increasing concentrations of acrylamide was monitored over the time of their insertion into the lipid bilayer. Five samples of 8-14 μM OmpA were prepared with SUVs of DMPC and increasing concentrations of acrylamide (0.0, 0.1, 0.2, 0.3 and 0.4 M). For each experiment, 185 spectra were acquired (37 spectra for each acrylamide concentration corresponding to 37 time points). Full data sets for all experiments are included in the supplemental information (Figures S1-S39). Representative quenching data for the W102 OmpA mutant are shown in Figures 5-10. It should be noted that these images represent the highest quality data (W102) collected in all experiments. Corrected fluorescence spectra in which vesicle scattering has been subtracted are shown in Figure 5 for W102 OmpA immediately following initiation of the folding reaction (solid) and after 6-hours of folding (dashed); the blue-shift and increase in fluorescence quantum yield associated with folding are evident. In these and subsequent analysis steps, the fluorescence intensities were not normalized for protein concentration due to the fact that acrylamide overwhelmed the absorbance in the region of tryptophan so concentrations could not be spectroscopically measured. The strong absorption by acrylamide at 280 nm is evident in Figure 6, which shows absorption spectra of five W102 samples in different acrylamide concentrations.

The fluorescence wavelengths (λ_{max}) and maximum intensities (F_{max}) were plotted as a function of folding time. These properties were determined via Gaussian fits to the fluorescence spectra in the range 301 to 370 nm. IGOR macros were written, with the help of Ignacio Lopez-Peña, to apply the Gaussian fits to the data and are included in Figure A1. The characteristic blue-shift during folding is shown in Figure 7 for W102 OmpA for all five acrylamide concentrations (panel A). For all OmpA mutants, the spectra blue-shifted at least 15 nm, from unfolded values of 351-354 nm, to folded values of 326-338 nm for the 0.0 M acrylamide samples. The λ_{max} versus time plots for the 0.0 M acrylamide samples were averaged over all trials for each mutant (Figure 7, panel B) and exponential and double exponential fits were

applied (described below). The blue shift was more prominent in the presence of acrylamide. Enhanced blue shift in the presence of acrylamide is not observed in NATA fluorescence quenching data. This indicates that the enhanced blue shift with acrylamide is most likely an artifact of the protein environment rather than an indication of more thorough immersion of the indole moiety into the apolar environment of the lipid bilayer. Because of the large number of spectra for two variables (acrylamide concentration and folding time), quenching trends for all time points cannot be simultaneously presented. Instead, the essential data are collected into a graph that plots maximum fluorescence intensity (corrected for vesicle scattering and inner-filter effect) as a function of folding time for all acrylamide concentrations; we refer to this graph of intensity vs time as the 'rainbow' graph because of the visual appearance. A representative rainbow graph is shown in Figure 8.

Stern Volmer plots were generated for each time point during folding. A Custom IGOR macro (Figure A2) was written to convert the data in the rainbow plot into Stern-Volmer plots for each time point of the experiment (Figure 9). Some Stern-Volmer plots, such as those of W102 in Figure. 9, exhibited slight upward curvature, indicating the presence of static/sphere-of-action quenching mechanisms. For reasons that are not clear, sphere of action quenching was not observed in all experiments. In the experiments that exhibited upward curvature, this curvature disappeared as the folding proceeded because the trp residue was no longer accessible to bulk solvent and acrylamide. In the absence of ubiquitous sphere of action quenching and knowledge of how to deal with the transition from dynamic+static quenching to pure dynamic (or pure static) quenching during folding, Stern-Volmer plots were fitted to the linear, dynamic quenching model for determination of K_{SV} values. Linear fits were not forced to have a y-intercept value of 1, but the fits never significantly deviated from this ideal y-intercept. K_{SV} data were plotted as a function of folding time, and these plots exhibited exponential decay (Figure 10).

This data analysis procedure was performed for all six OmpA mutants: W7, W15, W57, W102, W143, and W129. The corresponding data for each mutant (analogous to Figures 5-10) are shown in the Appendix 1 (Figures S1-S39). As mentioned above, tyrosine emission was not

subtracted prior to calculation of K_{SV} values because the presence of tyrosine did not affect the results. The insensitivity of K_{SV} to tyrosine is shown in Figures S40, S41 and S42, where a slightly modified data analysis procedure in which tyrosine signal as measured from a tryptophan-free OmpA mutant, called W0, was removed from raw fluorescence spectra of OmpA. The W0 fluorescence data in Figure S40 were subtracted from the W102 data in Figure S23 by the same method described for subtraction of vesicle scatter in the OmpA folding experiment to yield the plots in Figure S41. The resulting trp only K_{SV} versus time data was very similar to the tyrosine inclusive data set (Figure S42, panel C), which indicated that tyrosine signal does not significantly affect the results of the experiment.

Three trials were conducted for each mutant of OmpA (except W15 OmpA which was studied 5 times). The plots of K_{SV} as a function of folding time were averaged for each mutant and are shown in Figure 11. Plots showing the average K_{SV} versus time data with their experimental error are shown in figure S43. These K_{SV} versus time plots were fitted to single and double exponential functions (Eqs 5 and 6), and are shown in Figure 12. Results from the fits are summarized in Table 1. In general, the decays are very similar. Residual plots that compare the experimental data to the fit (residual = observed – fit) were constructed (Figure S44). These plots show complete overlap of single and double exponential fits for the W7 and W102 mutants, indicating that the single and double exponential fits are equivalent. The residuals for W57 were nearly as overlaid as those for W7 and W102. The residuals for the W15, W129 and W143 mutants indicated that the double exponential fit was more appropriate.

The fluorescence emission wavelengths (Figure 7) were also fit to single and double exponential functions so we could compare timescales for the emission blue-shift with evolution of K_{SV}. The fits are in Figure S45 and their residual plots are in Figure S46, and fit parameters are shown in Table 2. For all mutants, the double exponential functions exhibited superior fits.

Data for the adsorbed (on DPPC SUVs), fully unfolded (in 8.0 M urea) and aggregated (0.5 M urea) OmpA were analyzed by similar methods. In these experiments, the fluorescence

spectra did not evolve over time, so single K_{SV} values were obtained for each mutant. The DPPC samples were monitored over the period of an hour. The K_{SV} vs time plots were fitted to flat lines for determination of K_{SV} for the adsorbed state. Representative quenching data for unfolded and adsorbed OmpA are shown in Figures 13 and 14, respectively, and K_{SV} values for all three conditions are tabulated in Table 3 (also see Figures S47-S60). Graphs for aggregated OmpA are very similar to those of unfolded OmpA, except for generally lower K_{SV} values; those data are included in Appendix 1 (Figures S61 and S62).

Vesicle integrity and permeability in the presence of acrylamide and OmpA were analyzed by leakage assays and DLS measurements. Figure 15 shows the separation of SUVs encapsulating ANTS and DPX from free quencher and fluorophore by size exclusion chromatography. Figure 16 shows fluorescence maxima (514 nm) of fractions #1-6 before and after lysis with 0.1% Triton X-100 (final concentration). Also shown in Figure 16 is a fluorescence spectrum of fraction 2 before and after lysis. Figure 17 shows the evolution of ANTS+DPX leakage over time for the highest acrylamide concentration studied here, 0.4 M. Corresponding control experiments of SUV stability in the absence of acrylamide were also performed. Comparison of these fluorescence data indicate that acrylamide causes the vesicles to leak their encapsulated ANTS and DPX. The integrity of the vesicle, however, is not compromised by acrylamide. DLS data in Table 4 indicate that the size of the SUVs is unaffected by the presence of acrylamide. The maintenance of an intact vesicle is also evidenced in the fluorescence data in Figure 17 (panels A and C) which shows that the scattering component near ~300 nm remains unchanged and only disappears upon lysis with Triton X-100, despite the leaky nature of the vesicles. Data for a preliminary ANTS DPX experiment is shown in Figures S63 and S64. In this data set, A sudden decrease in vesicle scatter in the absorbance spectra can be noticed after lysis with Triton X-100 (Figure S64 panels B and D). Analogous experiments with ~10 μM OmpA in place of acrylamide showed similar results, although OmpA did not make the vesicles as leaky (Figures S65 and S66).

DLS experiments were conducted to assess the effects of time and acrylamide on the size of the vesicles. Samples were prepared with 0.0, 0.2 and 0.4 M acrylamide and monitored by DLS at 3 hour intervals for 6 hours. Figure 18 shows representative DLS data for one 10-second acquisition, and a resulting autocorrelation curve. Figure S67 shows autocorrelation curves for all 9 acquisitions. Exponential and double exponential fit data has been tabulated in Table 4. The hydrodynamic Radii (R_h) calculated from the decay constants are tabulated there as well. A residual plot shows that the double exponential fit to the 0 hour, 0 M acrylamide autocorrelation data is more appropriate than the single exponential fit (Figure S68).

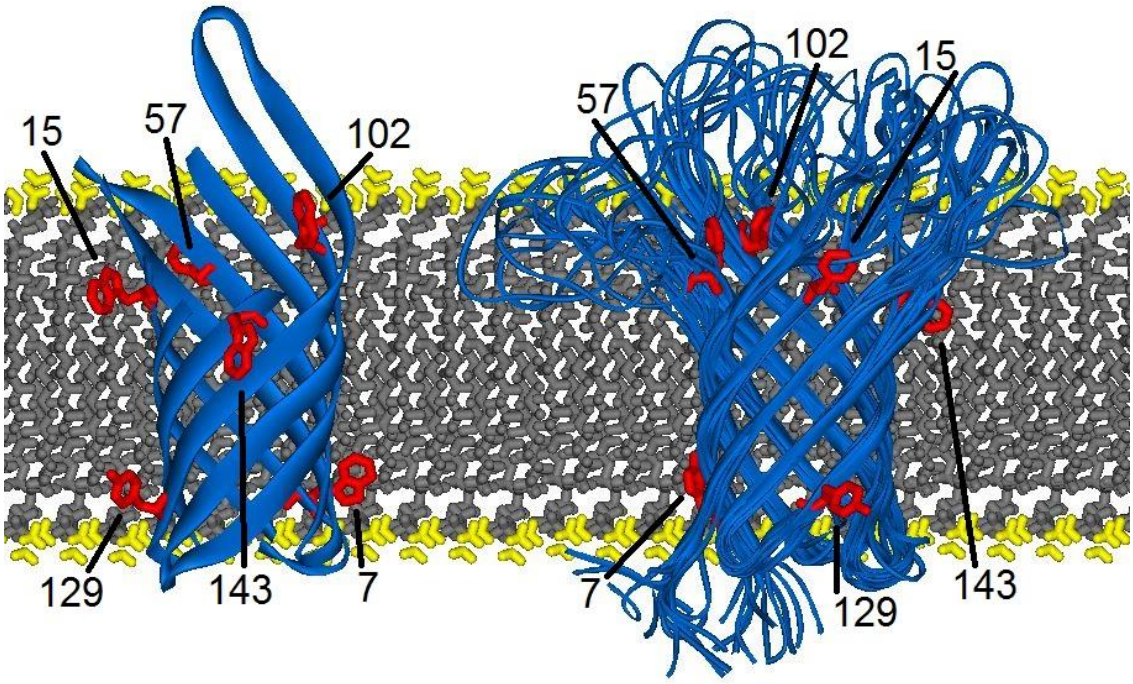

Figure 1. OmpA structure. Depicted here are the X-ray (left) (PDB ID 1QJP) and NMR (right) (PDB ID 1G90) structures of the transmembrane portions of OmpA superimposed on a DPPC lipid [66] bilayer. Both structures show the native residues at positions 7, 15, 57, 102, 129 and 143 in red. The X-ray structure is wild-type OmpA, whereas the NMR structure is the W7 OmpA mutant (10 conformers). For both structures, the protein was a truncated variant in which the soluble tail was not expressed.

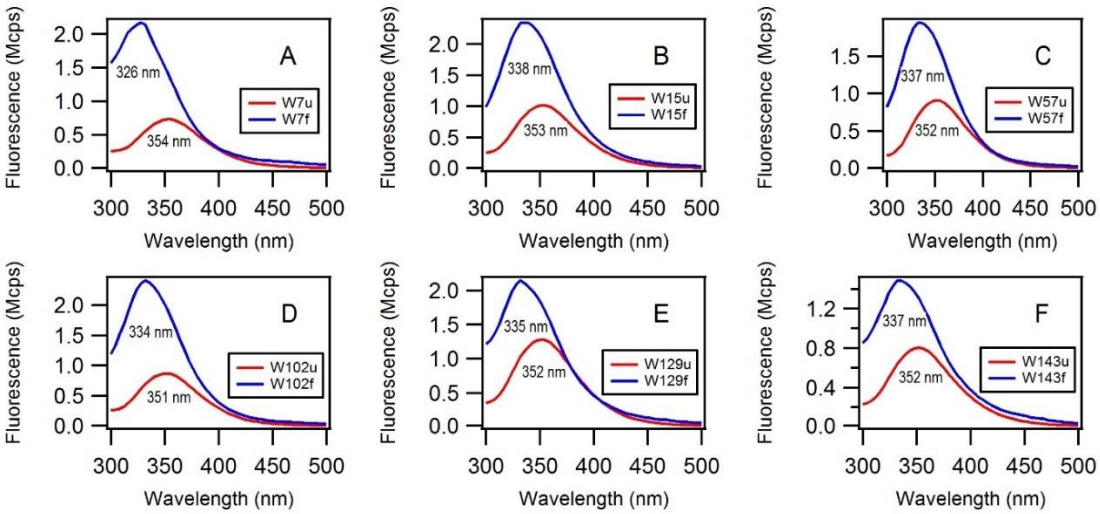

Figure 2. Fluoresence spectra of folded and unfolded OmpA. Depicted here are the fluorescence spectra for the single trp OmpA mutants W7 (A), W15 (B), W57 (C), W102 (D), W129 (E) and W143 (F) in the unfolded state (denoted 'u') and in the folded state (denoted 'f'). The individual graphs have been labeled with the average λ_{max} values from the various trials on each single trp mutant.

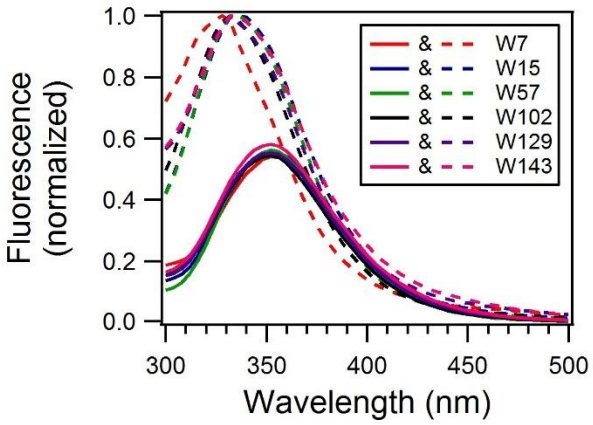

Figure 3. Overlay of fluorescence spectra of folded and unfolded conformations of all OmpA mutants. Shown here is an overlay of the fluorescence spectra in Figure 2 to allow straightforward comparison of emission peaks and quantum yields. The spectra for the unfolded OmpA are in solid lines and the spectra for the folded OmpA are in dashed lines; the spectra for the various single trp mutants are color coded. The fluorescence spectra of folded OmpA have been normalized to a value of 1.0, and the unfolded spectra are scaled based on the difference in quantum yields between folded and unfolded states.

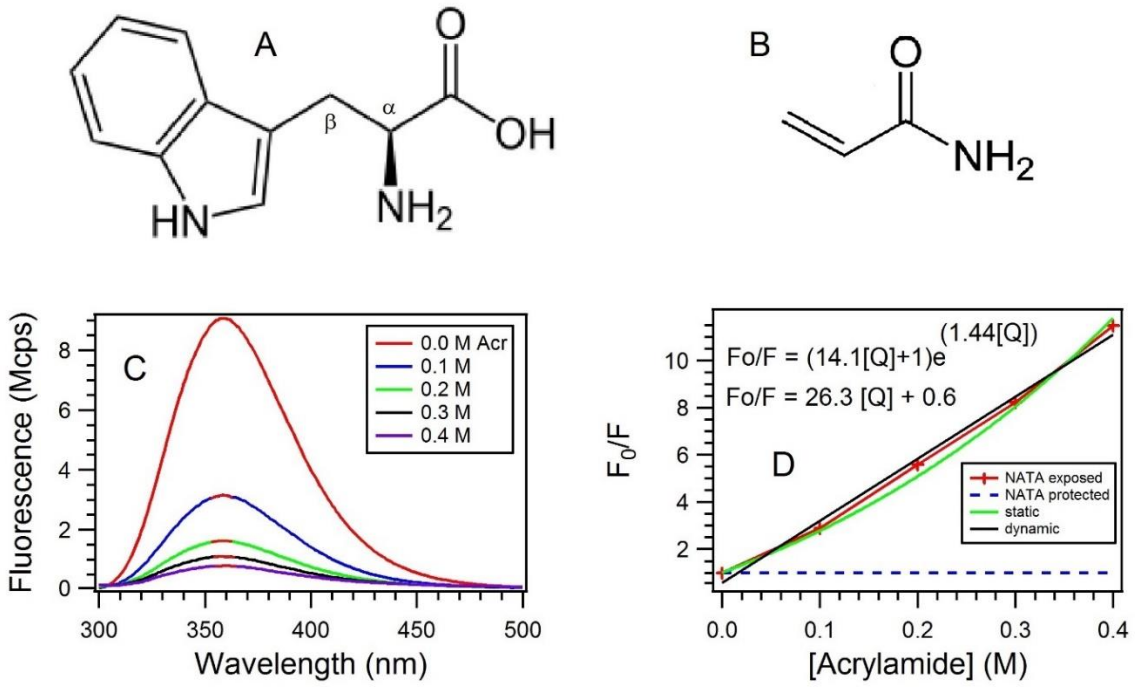

Figure 4. Quenching of NATA fluorescence by Acrylamide. Panel A shows the structure of L-tryptophan. NATA is an analog of tryptophan with an acetylated N-terminus and an amide group replacing the carboxylic acid group on the C-terminus. NATA is less photoreactive than tryptophan and has a better approximation of the polypeptide backbone than tryptophan or indole, making it a good model compound for the study of tryptophan fluorescence in proteins.[47] Indole is the aromatic bicyclic ring structure with hydrogen replacing the β carbon. Panel B shows the structure of acrylamide. Panel C shows fluorescence spectra of NATA at different concentrations of acrylamide in a plot that is referred to as a quenching trend. Panel D shows a SV plot constructed from the fluorescence maxima data from panel A. Black and green fits are from equations 1 (dynamic model) and 2 (dynamic+static model), respectively, where [Q] is concentration of acrylamide quencher. Also displayed is a hypothetical SV plot for an indole fluorophore that is completely protected from solvent and quencher in an inaccessible buried pocket (NATA protected).

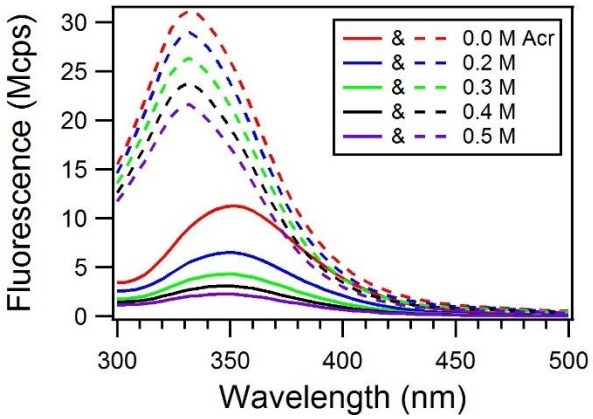

Figure 5. Quenching Trends. Fluorescence spectra of W102 OmpA in the presence of DMPC SUVs with 0.0 M (red), 0.1 M (blue), 0.2 M (green), 0.3 M (black) and 0.4 M (purple) acrylamide immediately upon initiation of the folding reaction, which we approximate as 0 hours (solid lines), and 6 hours (dashed lines) after initiation of the folding reaction.

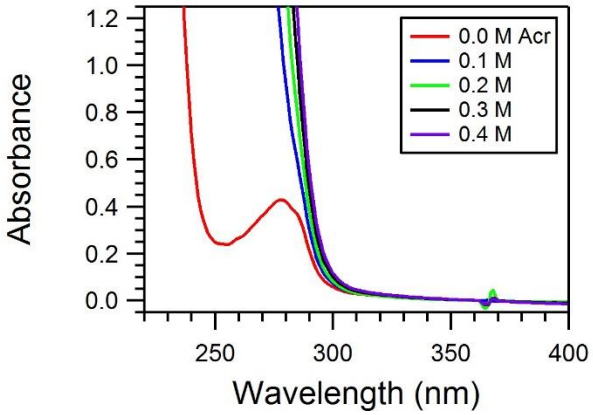

Figure 6. Absorbance Data. Displayed here are absorption spectra for the W102 OmpA mutant at different concentrations of acrylamide. The trp absorbance is completely overwhelmed by the acrylamide absorbance, thus preventing determination of protein concentrations for the individual samples by spectrophotometry.

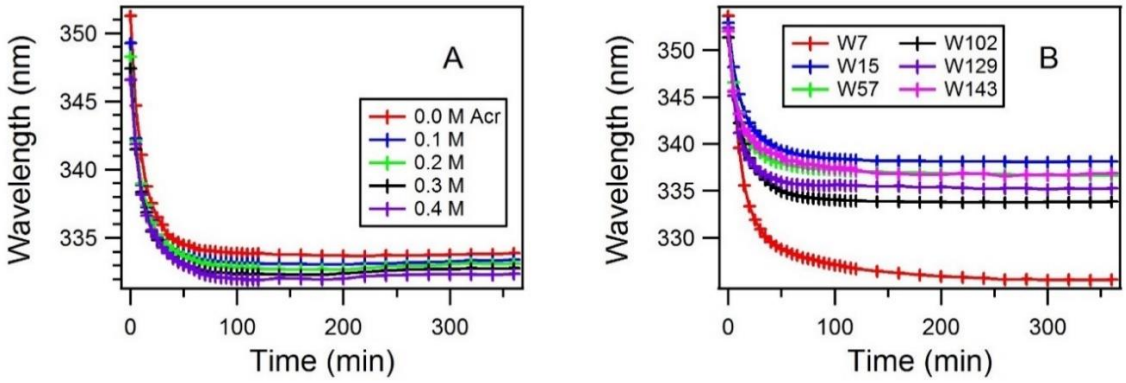

Figure 7. Fluorescence maxima. The plot in panel A shows the shift in fluorescence λ_{max}, determined from Gaussian fits of the fluorescence spectra at different times throughout the folding experiment (for the W102 mutant). Displayed in panel B are the average fluorescence λ_{max} versus time for each mutant in 0.0 M acrylamide. Exponential and double exponential fits to the data in panel B are shown in Figure S45, and fit parameters have been tabulated in Table 2. Residuals plots are shown in Figure S46).

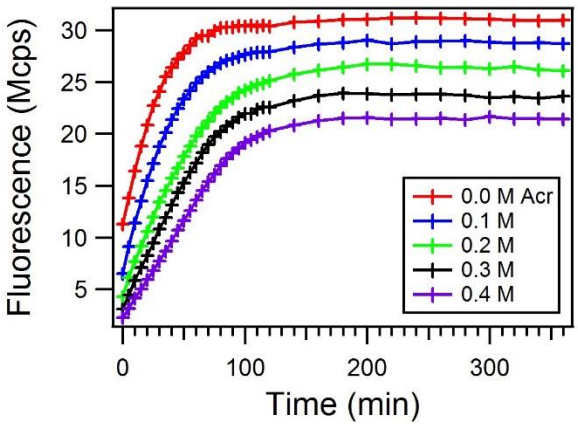

Figure 8. The Rainbow Graph. Fluorescence intensity maxima of W102 OmpA in the presence of DMPC SUVs with 0.0 M (red), 0.1 M (blue), 0.2 M (green), 0.3 M (black) and 0.4 M (purple) acrylamide at indicated time points during the folding reaction. The maxima do not correspond to a single emission wavelength.

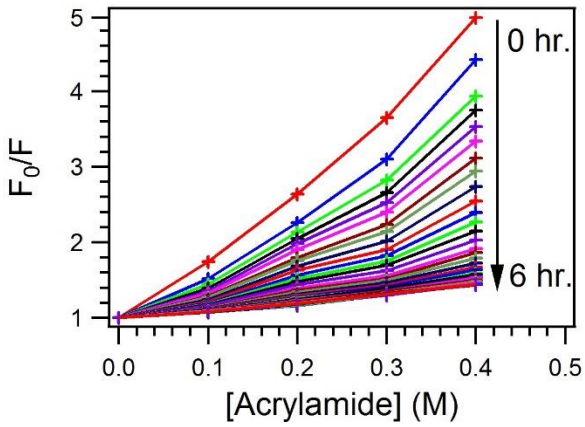

Figure 9. Stern-Volmer Plots. Stern-Volmer plots for W102 OmpA derived from the data in Figure 8; solid lines that connect the data points are drawn to guide the eye. The linear slope of the plots (K_{SV}) decreases over the time of the folding process. The upward curvature is indicative of the presence of static quenching mechanisms.

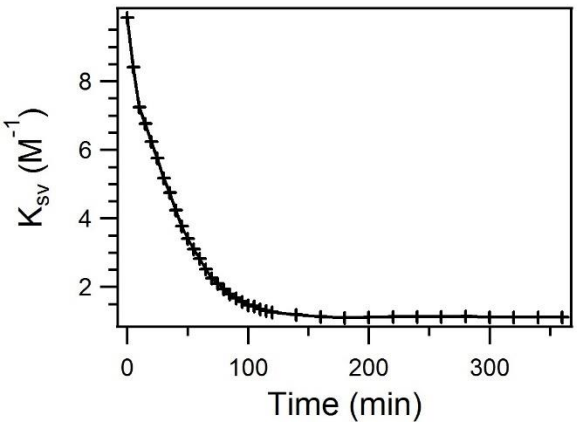

Figure 10. K_{SV} vs. Time. Graph of K_{SV} as a function of folding time for W102 OmpA derived from the data in Figure 9. Curve connecting points is to guide the eye.

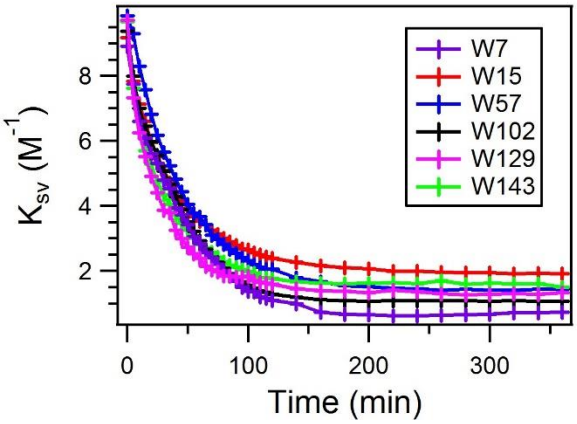

Figure 11. K_{SV} Averages. Average K_{SV} as a function of folding time for mutants studied in this project. Averages were determined based on multiple trials (see text). Curves connecting points are to guide the eye. K_{SV} decayed from 8.9 to 0.7 M^{-1} for OmpA W7, from 9.2 to 1.9 M^{-1} for OmpA W15, from 9.9 to 1.4 M^{-1} for OmpA W57 from, from 9.4 to 1.1 M^{-1} for OmpA W102, from 9.7 to 1.3 M^{-1} for OmpA W129 and from 9.7 to 1.5 M^{-1} for OmpA W143.

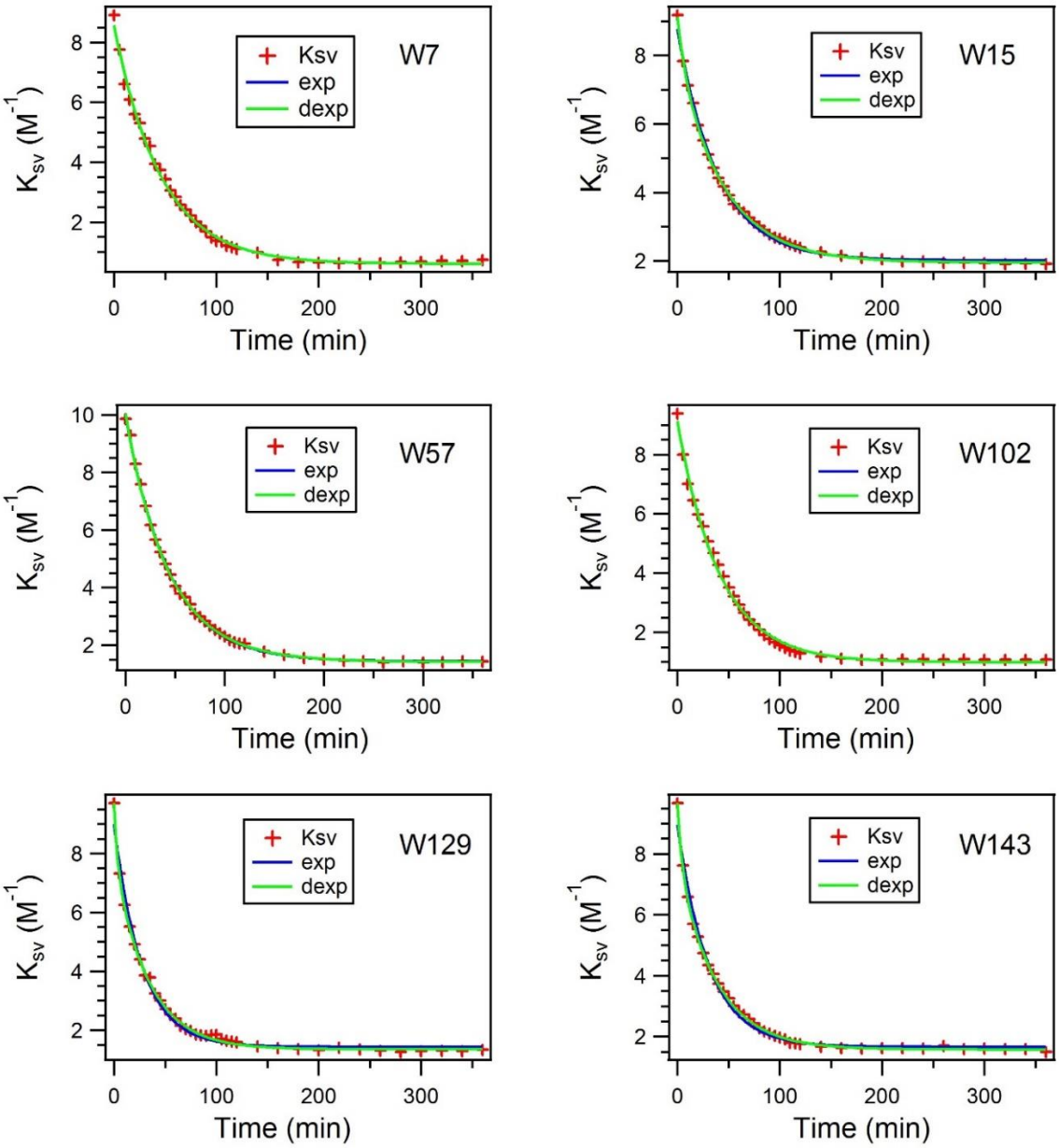

Figure 12. Single- and double-exponential fits to average K_{sv} plots. Displayed here are ovelays of the single (blue curves) and double (green curves) exponential fits to the average K_{SV} data (red crosses) of each mutant presented in Figure 11. In some graphs the single and double exponential fits are indistinguishable, and the blue and green curves overlap perfectly.

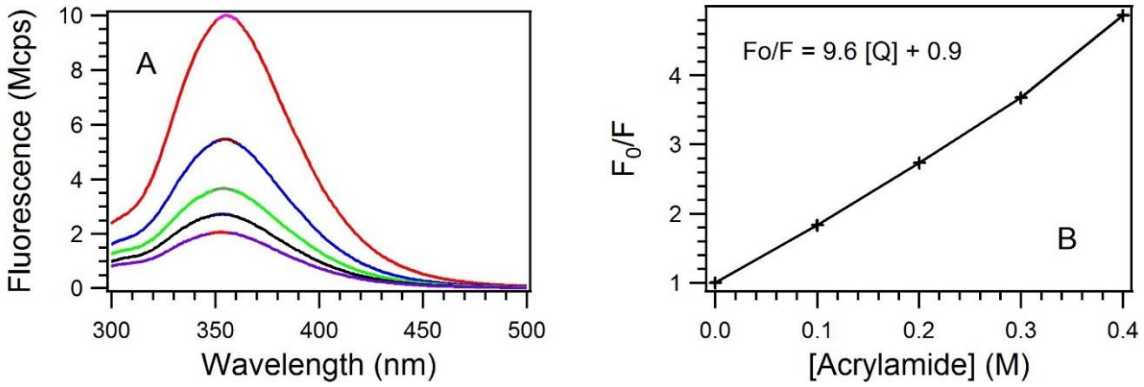

Figure 13. OmpA in 8.0 M urea. Panel (A) shows the quenching trend and (B) shows the resulting SV plot for the W7 OmpA mutant in 8 M urea and the resulting equation where [Q] is acrylamide concentration.

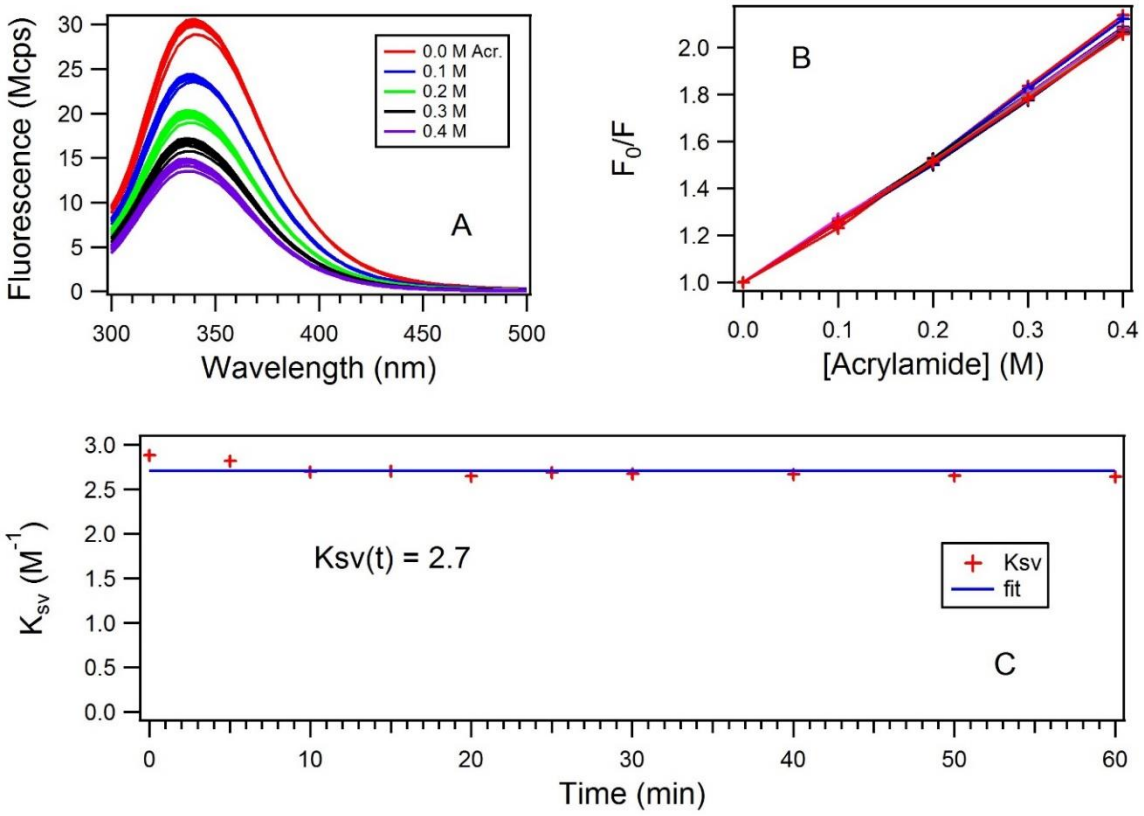

Figure 14. OmpA adsorbed onto DPPC SUVs. Data are for W57 OmpA mutant in the presence of DPPC vesicles (A) Quenching trend; (B) SV plots for all 10 time points; and (C) plot of K_{SV} versus time (C). In Panel A,the overlapping spectra for a given acrylamide concentration correspond to fluorescence spectra collected at 10 timepoints over the period of an hour.

Figure 15. Size exclusion chromatography of dye-encapsulated SUVs. Displayed from left to right are the fractions that eluted from the size-exclusion column after the dead volume was discarded. The first, and sometimes second, fractions (labeled 1 and 2) were usually determined to have the highest enrichment of SUV encapsulated ANTS and DPX. Columns that appear yellow had high concentration of free (unencapsulated) dye.

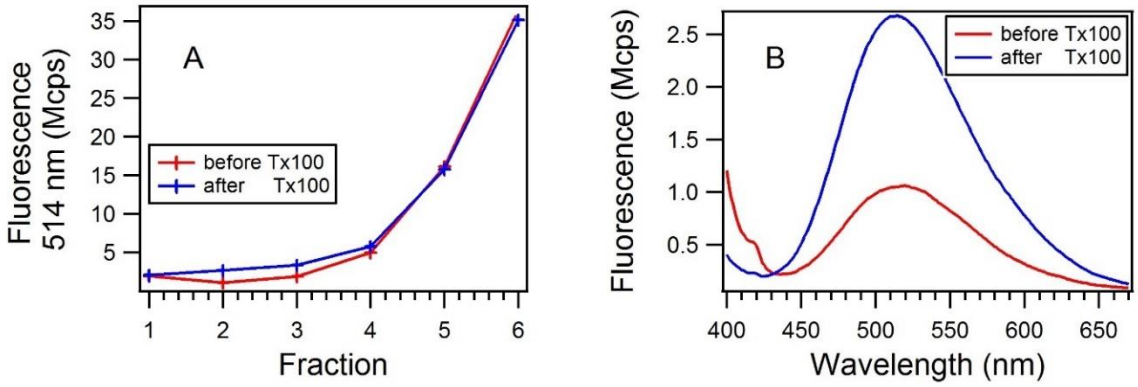

Figure 16. Disruption of DMPC SUVs that contained ANTS and DPX. Panel (A) Fluorescence chromatogram of fractions #1-6 of DMPC vesicles encapsulating ANTS and DPX before and after lysis with 0.1% Triton X-100 (Tx100). Fraction number on x-axis is same as Figure 15. For this particular experiment, fraction 1 was accidentally left out in room temperature, whereas the other fractions were incubated at 37 °C. This difference in handling may be responsible for the lack of significant increase in fluorescence after lysis for fraction 1. Fraction 2 however showed a sizeable increase in fluorescence after lysis (panel B), and was a suitable sample for the vesicle leakage assay.

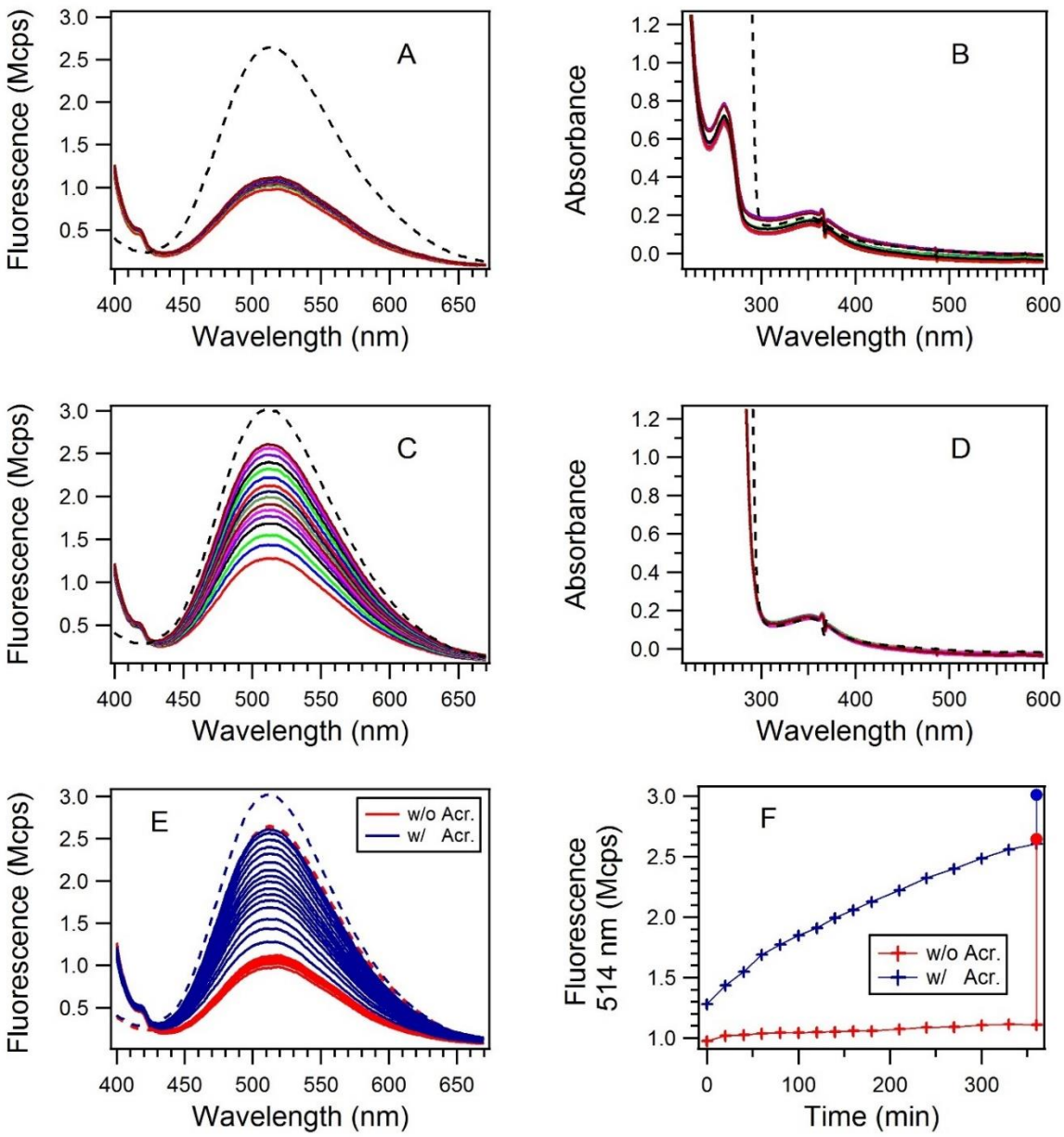

Figure 17. Leakage assay spectra. An aliquot of fraction 2 was diluted to, and monitored by fluorescence and UV-Vis absorbtion spectroscopy (panels A and B, respectively) over the period of 6 hours. Spectra were recorded every 20 minutes for the first 3 hours and then every 30 minutes for the last 3 hours. Another aliquot of fraction 2 was diluted, and 0.4 M acrylamide was added. This sample was monitored by the same method (panels C and D). In panels (A) thru (E), the spectra upon lysis with 0.1% Triton X-100 are shown as dashed curves. Panel E shows an overlay of the fluorescence spectra of the two samples in panels A (red) and B (blue) for ease of comparison, with dashed curves representing post-lysis with Triton X-100. Panel F shows the maximum fluorescence intensities over time; the maximum intensities after lysis are shown as filled circles.

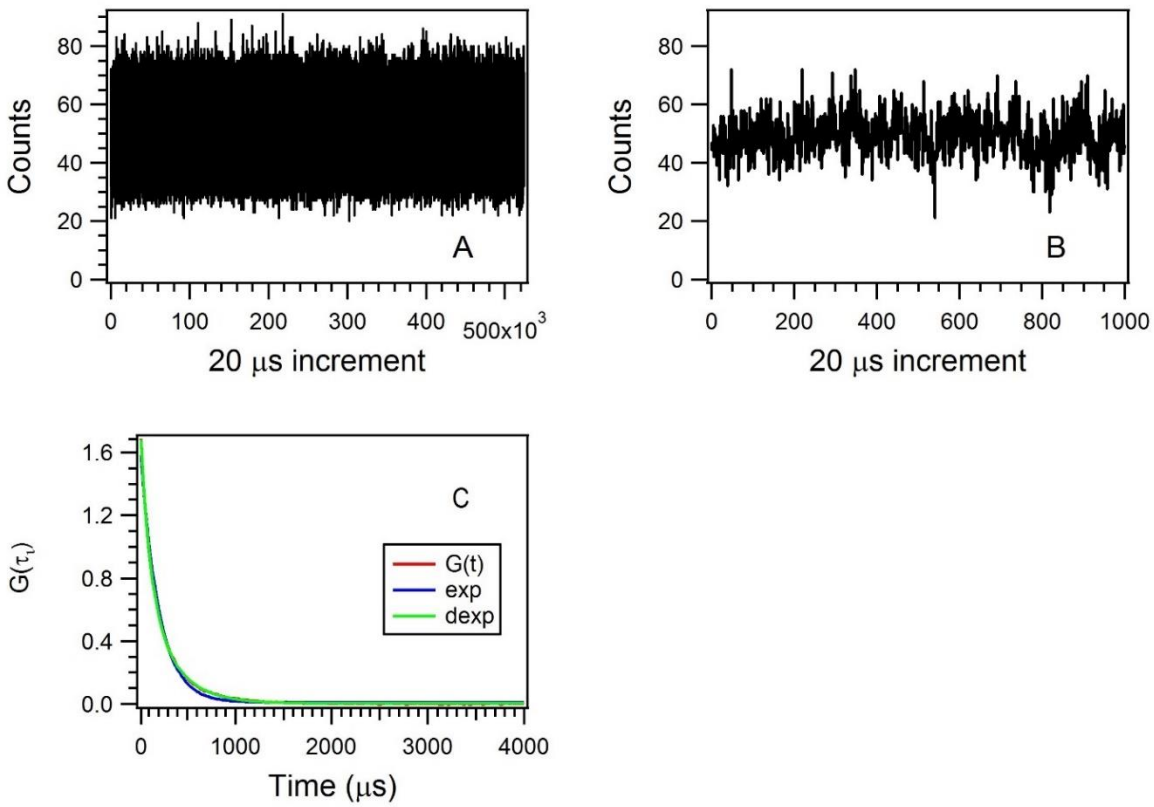

Figure 18. DLS data. Panel A shows a representative plot of counts per bin for a single acquisition of DLS data. Panel B shows a zoomed in view of the first 1000 bins to illustrate the fluctuations. Panel C shows the auto correlation (G(t)) of the fluctuations in Rayleigh scattering of the 0.0 M acrylamide sample at the 0 hour timepoint. Overlayed on the plot of G(t) are exponential (blue) and double exponential (green) fits. The double exponential fit (green curve) has almost complete overlap with G(t) shown in red, while the single exponential shows deviation.

Table 1. K_{SV} fits. Kinetic constants based on single (exp) and double exponential (dexp) fits (Figure 12) of the K_{SV} vs time averages depicted in Figure 11.

	W7	**W15**	**W57**	**W102**	**W129**	**W143**
exp						
A	8.0	6.8	8.6	8.1	7.6	7.3
k	0.022	0.025	0.023	0.024	0.037	0.033
τ (min)	45	40	43	41	27	31
y_0	0.6	2.0	1.4	1.0	1.4	1.7
χ^2	0.622	0.379	0.137	0.670	1.35	1.18
dexp						
A_1	4.1	6.0	1.8	4.0	6.5	6.3
k_1	0.022	0.022	0.016	0.024	0.030	0.027
τ_1 (min) / %	46 / 51%	45 / 84%	62 / 21%	42 / 50%	33 / 78%	37 / 77%
A_2	3.9	1.1	6.9	4.1	1.8	1.8
k_2	0.022	0.12	0.025	0.025	0.31	0.23
τ_2 (min) / %	46 / 49%	8 / 16%	40 / 79%	41 / 50%	3 / 22%	4 / 23%
y_0	0.6	2.0	1.4	1.0	1.3	1.6
χ^2	0.622	0.073	0.129	0.670	0.173	0.082

Table 2. λ_{max} fits. Kinetic constants based on single (exp) and double exponential (dexp) fits of the λ_{max} vs time averages depicted in Figure 7, panel B.

	W7	W15	W57	W102	W129	W143
exp						
A	26	14	15	17	16	13
k	0.062	0.062	0.076	0.064	0.096	0.066
τ (min)	16	16	13	16	10	15
y_0	327	338	337	334	336	337
χ^2	24.8	2.83	4.85	2.56	3.30	13.4
dexp						
A_1	6	6	3	9	4	5.7271
k_1	0.012	0.032	0.021	0.039	0.036	0.022
τ_1 (min) / %	84 / 20%	31 / 41%	48 / 22%	25 / 50%	27 / 26%	45 / 38%
A_2	23	9	12	9	13	10
k_2	0.092	0.12	0.12	0.13	0.15	0.17
τ_2 (min) / %	11 / 80%	9 / 59%	9 / 78%	8 / 50%	7 / 74%	6 / 62%
y_0	325	338	337	334	335	337
χ^2	0.419	0.0408	0.166	0.0551	0.393	0.489

Table 3. Adsorbed, denatured and aggregated OmpA. K_{SV} values (M^{-1}) for the adsorbed and fully denatured and aggregated states of OmpA mutants.

	W7	W15	W57	W102	W129	W143
adsorbed (DPPC)						
	2.4	2.7	2.7	3.4	1.6	3.0
denatured (8 M urea)						
	9.6	8.3	9.4	10.5	11.9	8.7
aggregated (0.5 M urea)						
	8.7	6.0	8.7	9.2	9.8	9.2

Table 4. DLS data. The exponential (exp) and double-exponential (dexp) fit data of the autocorrelation curves in Figure S62, as well as the calculated hydrodynamic radii are tabulated here

Time (hours)	**0**	**3**	**6**	**0**	**3**	**6**
0.0 M Acr				**0.2 M Acr**		
exp				**exp**		
A	1.74	1.59	1.56	1.66	1.40	1.42
k (μs^{-1})	0.0053	0.0055	0.0056	0.0050	0.0053	0.0056
y_0	0.01	0.01	0.01	0.01	0.01	0.01
χ^2	0.059	0.051	0.051	0.066	0.040	0.040
R(H) (nm)	52	50	49	55	51	49
dexp				**dexp**		
A_1	0.84	0.68	0.69	0.70	0.63	0.69
k_1 (μs^{-1})	0.0034	0.0033	0.0034	0.0029	0.0032	0.0035
A_2	1.09	1.08	1.04	1.13	0.92	0.89
k_2 (μs^{-1})	0.010	0.010	0.011	0.0091	0.0099	0.011
y_0	0.00	0.00	0.00	0.00	0.00	0.00
χ^2	0.002	0.001	0.002	0.003	0.002	0.001
$R(H)_1$ (nm)	82	84	82	95	85	78
$R(H)_2$ (nm)	27	27	26	30	28	25
0.4 M Acrylamide						
exp						
A	1.60	1.44	1.53			
k (μs^{-1})	0.0049	0.0053	0.0057			
y_0	0.01	0.01	0.01			
χ^2	0.054	0.041	0.040			
R(H) (nm)	56	52	48			
dexp						
A_1	0.74	0.66	0.68			
k_1 (μs^{-1})	0.0031	0.0032	0.0035			
A_2	1.01	0.93	1.00			
k_2 (μs^{-1})	0.0093	0.0098	0.010			
y_0	0.00	0.00	0.00			
χ^2	0.001	0.001	0.001			
$R(H)_1$ (nm)	90	85	79			
$R(H)_2$ (nm)	29	28	27			

Discussion

An important goal of this project is to investigate changes in protein solvation during the folding reaction of a membrane protein, and to correlate this dehydration process with shifts in local polarity. Here, changes in solvent accessibility were probed by steady-state and time-resolved tryptophan fluorescence quenching experiments and Stern-Volmer analysis on single tryptophan OmpA mutants while shifts in polarity were monitored by fluorescence maxima. We aim to complement our interpretation with other published studies that focused on secondary structures (e.g. circular dichroism experiments), tertiary structures (e.g. FRET), and distance evolution during folding (e.g. heavy-atom quenching experiments).

Solvent-accessibility for steady-state structures. The OmpA mutants were studied in various steady-state conformations, including fully denatured in 8 M urea, fully folded in DMPC SUVs, adsorbed on DPPC SUVs, and aggregated in 0.5 M urea. A summary of K_{SV} values is shown in Table 5. For all six OmpA mutants in the denatured state of 8 M urea, K_{SV} values ranged between 8.3 and 11.9 M^{-1}. This range of values agrees well with K_{SV} values reported for wild-type OmpA in 4 M urea, ~10.4 M^{-1} (estimate from graph)[36] and in glycine buffer at 40 °C, 11.7 M^{-1}.[53] When the protein was fully folded after 6 hours, the K_{SV} values had dropped to their lowest fitted values of 2.0 - 0.6 M^{-1}. A previously recorded value for the fully folded state of wild-type OmpA in DMPC vesicles at 30 °C is 2.2 M^{-1};[36] in DOPC vesicles at 40 °C, K_{SV} was 1.8 M^{-1}.[53] The decrease in K_{SV} values reported here and in previous reports is consistent with tryptophan residues that become less solvent exposed upon insertion into the lipid bilayer.[53,36] However, it should be noted that these previous studies investigated native OmpA which contained all five tryptophan residues and therefore, the reported K_{SV} values reflect an average for all five fluorophores. Our study is an improvement on these previous studies because we probe site-specific changes in K_{SV} values during the folding reaction.

It is valuable to compare the level of solvent exposure in other conformations that may be relevant to the folding, reaction such as the aggregated and adsorbed states. In this thesis, the aggregated state is defined as OmpA that has inclubated in 0.5 M urea for about 5 minutes,

where the protein is shown to exhibit spectroscopic blue-shifts that support partial burial of the tryptophan residues.[35] The structure of aggregated OmpA has been reported to be a mixture of α-helix and β-strand in the periplasmic domain and unstructured in the TM β-barrel region based on circular dichroism.[35,67] The K_{SV} values ranged between 9.8 and 6.0 M^{-1}. These values are generally lower than or comparable to the K_{SV} values extrapolated to t = 0 during the folding reaction, which ranged 10.0 to 8.6 M^{-1}. A previously measured value for the aggregated state of wild-type OmpA in glycine buffer with 0.08 M urea at 2 °C is 5.3 M^{-1}.[53] Our values are higher than this previous report, and the discrepancy can be attributed to the different incubations times of 10 min in this previous report (compared to less than 5 minutes in our study), variation in urea concentration of 0.08 vs 0.5 M, and also because our measurements were made at room temperature, not 2 °C.

OmpA in the adsorbed state on DPPC vesicles exhibited K_{SV} values between 1.6 and 3.4 M^{-1}, and these values all fall between theose of the aggregated and fully folded states. A previously recorded value for the adsorbed state of wild-type OmpA in DMPC vesicles at their solid-like gel phase at 10 °C is 2.8 M^{-1}.[36] I performed a time study on the adsorption process, but K_{SV} values were not observed to decay significantly (see Figure 14), indicating that the temporal evolution of the adsorption process may not be resolved by this technique. The adsorption and folding experiments differed in that the adsorption studies were performed at ~21 °C whereas folding experiments in DMPC proceeded at 37 °C; at 21 °C, DPPC is in the gel phase, which means the bilayer has greater thicknes than fluid-phase DMPC bilayers.[68] Given these variations, it appears that the adsorbed state trapped on DPPC vesicles is different from any adsorbed state that might be associated with OmpA folding into DMPC vesicles.

The solvent accessibility can be compared for adsorbed and aggregated states. Both structures exhibit different degrees of secondary structure; the adsorbed state exhibits beta-barrel features similar to the native state based on circular dichroism studies, and there appears to be greater secondary structure for the adsorbed state than aggregated state.[35,67] In these previous studies as well as our current report, the tryptophan residues in the adsorbed species are less

solvent-exposed than in the aggregated state. The fact that tryptophan residues have moderate solvent accessibility in aggregated OmpA is consistent with the fact that OmpA, like many beta-barrel membrane proteins, is not highly hydrophobic and therefore, is not expected to aggregate as easily as alpha-helical MPs.[16,17] Upon forming greater secondary structure as an adsorbed species, the tryptophans become more buried.

Evolution of solvent accessibility during folding. We hypothesized that the observed K_{sv} values would progressively decrease, with the highest values in the denatured state, followed by an exponential decrease to moderate K_{sv} values of the aggregated and adsorbed states, and finally converge to the smallest values for the fully folded conformation. This trend was observed for the W7 and W102 OmpA mutants. Considering the possibility that there are site-specific similarities in solvent exposure between the unfolded and aggregated states, a more general expectation would be that K_{SV} values would progressively decrease from the beginning the folding experiment, to high K_{SV} values similar to those of the aggregated state, to K_{SV} values similar to the adsorbed state, and finally to low values of the fully folded state. This trend of K_{SV} values met this expectation for all mutants except W129 and W7, in which the aggregated K_{SV} value was similar to K_{SV} at the beginning of the folding reaction.

The temporal evolution of K_{SV} could be satisfactorily modeled with single and double exponential functions (Figure 12). For W7 and W102 mutants, the use of double exponential functions did not improve the fit substantially. As can be seen in Table 1 and summarized in Table 5, double exponential fits resulted in a dominant rate constant that persisted for all mutants; the minor component contributed less than 23% across all samples, and was generally a fast component (3-8 min) with the exception of W57 that exhibited a minor long component of 62 minutes. The dominant time constant was 40-45 minutes for all mutants except W129 and W143, which exhibited dominant time constants between 33 and 37 minutes. The consistency in time constants indicates that all tryptophan residues are being desolvated on a comparable timescale (~35-45 min), but that there are differences in dehydration kinetics at the various topological areas of the protein/membrane interface.

Evolution of local environment during folding. Analogous analyses based on emission maxima can be performed for the OmpA mutants, and are summarized in Table 6. The general trend is that the emission maxima blue-shifted as the protein folded into the bilayer. For the denatured state in 8 M urea, λ_{max} values ranged between 355 and 354 nm for all mutants; these values are higher than the K_{SV} values at the start of the folding reactions. For the aggregated state, λ_{max} values ranged between 353 and 351 nm for all mutants. In the DPPC adsorbed state, λ_{max} values ranged between 342 and 332 nm, which are intermediate values between the aggregated/unfolded and fully folded λ_{max} values for all but one mutant of OmpA. For W129, the adsorbed λ_{max} value was lower than the fully folded value. In the fully folded state, λ_{max} ranged between 338 and 326 nm.

The site-specific variations in emission maxima provide insight into the local environement near each tryptophan residue. The most blue-shifted λ_{max} was observed for the W7 OmpA mutant, which reached 326 nm. This value indicates that W7 resides in the most apolar environment of all the trp residues of OmpA. This environment is consistent with the large number of aromatic residues near the region of tryptophan 7.[26] Fluorescence λ_{max} values for the other mutants were: W102 (334 nm), W129 (335nm), W143 (337 nm), W57 (337nm), and W15 (338nm). Previously reported ordering of λ_{max} for single-trp mutants of OmpA (except W129) in DOPC vesicles shows the same increasing trend, although the values are not exactly the same.[43]

The differences in folded λ_{max} may reflect local differences among the tryptophan residues. For example, W15 exhibits a relatively red λ_{max} of 338 nm, which is consistent with the existence of a hydrogen-bond according to the crystal structure,[38,37] or other perturbation such as cation-π interactions according to UV resonance Raman.[62, 69] We were surprised that W102 exhibits a strongly blue-shifted emission maximum of 334 nm because it is the only tryptophan residue that faces the interior of the protein pore as opposed to the bilayer; despite it's nominal exposure to passively diffusing water and other small molecules, tryptophan 102 appears to remain in a hydrophobic environment. The mutant W129 exhibits a moderate blue-shifted emission maximum of 335 nm; this is a non-native tryptophan residue, and the native Y129 is in a hydrophobic,

aromatic pocket in the periplasmic region, like W7. Despite the similar environment of W7 and W129, the emission maxima differ by 9 nm. The variations in emission maxima reflect local environment. It does not seem that there are any topological correlation between these values, as W143 and W57 which have the same λ_{max} values are on opposite sides of the reported crystal structures, and W7 and W15, which are on the same β- strand have the greatest disparity in λ_{max} values.

The evolution of the emission maxima (Figure 7) were also modeled with single and double exponential decay functions. λ_{max} decayed from unfolded state values of 355 - 351 nm at the start of the experiment, to folded state values between 338 and 326 nm. This trend is similar to previously reported study of the same OmpA mutants in DOPC vesicles at 40 °C.[43] In contrast to K_{SV} data, the emission maxima were all more appropriately fit to double exponential decay. The time constants in Table 2 and summarized in Table 6 indicate that there are fast and slow time constants, with generally larger contributions to the overall decay from the fast component. For the W15 -W143 mutants, the fast components are ~6 to 9 min (50-78% of the decay) while the slow components are 26 to 49 min (22-50%). The W7 mutant is a special case, having a fast component of 11 minutes (80%), and a slow component of 83 (20%) minutes. A long decay has previously been observed for W7, and has been attributed to a third, transition between a partially folded membrane bound intermediate and the native state.[43] It seems intuitive that trp7 would have distinct kinetics in view of the unique behavior of its λ_{max} vs time data in comparison to the other mutants (Figure 7). It is not certain whether this unique, long decay represents resolution of a transition distinct from those observed in the other mutants or a more thorough immersion of W7 in the bilayer than the other trp residues.

Vesicle properties. The primary measurements in this thesis are fluorescence quenching trends on account of bimolecular collision. The fact that acrylamide and other small molecules have been shown by osmotic shrinking experiments to diffuse through lipid bilayers at a relatively fast rate is crucial for the interpretation of these experiments.[70] Additionally, it is important that we

perform control experiments to establish that the kinetics of K_{SV} and λ_{max} values are not artifacts because of the presence of acrylamide.

We probed the effect of acrylamide on the diffusion properties of the SUVs via leakage assays; these leakage assays revealed the rates at which encapsulated molecules diffused out of the interior of the SUVs in the presence of extravesicular acrylamide and protein (Table 7). Our data show that the presence of acrylamide causes DMPC vesicles to leak encapsulated ANTS and DPX, indicating that acrylamide does cause the vesicles to be more permeable. However, the time evolution of ANTS/DPX leakage in the presence of acrylamide is much slower than the folding reaction with a dominant τ value of 510 minutes (88%) and a faster τ value of 98 minutes (12%) from a double exponential fit. As comparison, the dominant τ value in the absence of acrylamide was 560 minutes (87%). In the presence of OmpA, the dominant τ value for leakage was 530 minutes (81%). Despite the leakage, the SUVs remained intact. DLS and fluorescence data indicate that the size of the SUVs was unchanged by the presence of acrylamide, and that the SUVs continued to scatter light in the presence of acrylamide. The size of the vesicles is important because OmpA has been shown to fold and insert into highly curved SUVs and not into less curved large unilamellar vesicles.[35,34] The DLS measurements determined that the majority of the vesicles were SUVs of ~ 50 nm diameter, which is the appropriate size for OmpA folding reactions.[35] A smaller population of larger, ~180 nm vesicles may have been produced by the filtration process (220 nm pore PVDF), and could have caused decreased folding yields, resulting in higher K_{SV} values from solvent exposed trp residues.

We also investigated the effect of acrylamide on the emission maximum. Acrylamide was observed to cause enhanced blue shifts of OmpA fluorescence in the denatured, aggregated, adsorbed and fully folded forms (Table 8). This blue shift was not noticed in the trp analog NATA, which suggests that the observed blue shifts with acrylamide are an effect of the protein environment. It is reasonable for acrylamide to cause OmpA to have different denatured, aggregated, and adsorbed structures because acrylamide is a moderately hydrophobic molecule in relatively high concentrations of up to 0.4 M. It is difficult to explain why folded OmpA exhibits

a greater blue shift in the presence of acrylamide than in the absence. One possibility is that the presence of acrylamide causes OmpA to fold deeper into the bilayer, or that it causes a higher fraction of protein to fold correctly. Alternatively, the presence of diffusing acrylamide in the bilayer may cause a slightly different folded structure in the bilayer. These and other possible effects of acrylamide are the focus of future investigations.

Figure 19 shows normalized kinetics for λ_{max}, K_{SV}, and vesicle leakage. All data are presented as decay curves on a scale of 0 to 1 to allow for facile comparison of these kinetics. For leakage assays, the data are presented as decrease in SUV integrity as assessed by decrease in encapsulation efficacy. The curves in Figure 19 show that the observed kinetics associated with λ_{max} and K_{SV} are much faster than those of vesicle leakage, indicating that the changes in λ_{max} and K_{SV} are largely independent of the effects of acrylamide on vesicle integrity.

Correlation between K_{SV} and emission maxima. A comparison of the steady state λ_{max} and K_{SV} values for the fully folded states of the OmpA single trp mutants shows a correlation between the λ_{max} and K_{SV} values, where the lowest K_{SV} value is reported for the most blue-shifted mutant. Stern-Volmer constants and λ_{max} values for the mutants are: W7 (K_{SV} 0.7, λ_{max} 326); W102 (K_{SV} 1.1, λ_{max} 334); W129 (K_{SV} 1.3, λ_{max} 335); W57 (K_{SV} 1.4, λ_{max} 337); W143 (K_{SV} 1.5, λ_{max} 337); and W15 (K_{SV} 1.9, λ_{max} 338). The correlation between the values is not perfectly linear but nonetheless, appears to be significant (Figure 20). Comparison of the exponential fits to K_{SV} and λ_{max} values shows that the dominant component (50-78%) of λ_{max} decay is the fast component ($\tau = 6 - 11$ minutes) whereas for K_{SV}, the dominant component is the slow decay (τ = 33-46 min). For K_{SV}, the fast component (τ = 3-8 min) of decay is of lesser magnitude (< 23%). This results in λ_{max} decaying quicker overall 33-45 min.

The observation that there is a fast and dominant blue-shift of the emission maximum that precedes changes in hydration (K_{SV}) suggests that there are at least two observable changes in protein environment during the folding reaction. We can interpret the data to state that the majority of blue shift occurs in the fast step, while the majority of desolvation occurs in a slower

step. Previous folding studies of OmpA single trp mutants in DOPC vesicles at 2 degrees C reported similar decay constants from double exponential fits to the fluorescence data.[43] In this previous study, the fast component ((τ_{fast} = 1.4 - 1.8 min)(relative amplitude 0.46 – 0.66)) of fluorescence quantum yield increase was attributed to adsorption of OmpA to the bilayer surface, and the slower component was attributed to transition from the adsorbed state to a partially folded and inserted intermeidate. Other time resolved studies of OmpA folding and insertion (performed by another member of our group, Dr. Guipeun Kang) have probed the formation of secondary[71] and tertiary[72] structure. Secondary structure formation was probed by a time resolved circular dichroism study, which determined a τ value of 37 minutes for the formation of the beta structure of the transmembrane domain of OmpA. This τ value is comparable to time constants determined in this experiment, which indicates that water may be involved in the formation of secondary structure during insertion and folding. The formation of tertiary structure was probed by Förster resonance energy transfer (FRET) experiments that determined changes in the distance between a tryptophan FRET donor and a cysteine-linked FRET acceptor dye molecule over the time of the folding reaction.[72] For a donor/acceptor pair at positions 7 and 129 (directly across the pore on the periplasmic side) these studies determined that a rapid collapse occurs within 2 minutes and then the majority of pore formation is complete after 50 minutes. A final set of relevant data come from fluorescence quenching experiments with brominated lipids in specific locations along the hydrocarbon chain of the bilayer.[53] These experiments were conducted at 2 °C in brominated DOPC vesicles that probed the movement of the trp residues along the bilayer normal, and revealed two time constants of 2 minutes for the first, fast transition that was attributed to adsorption, and 87 minutes for the second, slow transition attributed to insertion. The slow time constant from this experiment is reminiscent of the slow decay of λ_{max} for W7. All of these previous experiments (summarized in Table 9) indicate a fast transition immediately upon initiation of the folding reaction and a subsequent slow transition.

We propose that the fast step that is obvious in λ_{max} decay represents a transition from a fully sovent exposed, unfolded conformation to one where the trp residues are in a less polar

environment in the polar head group of the lipid bilayer, where acrylamide is likely to exist (figure 21). The existence of acrylamide in the headgroup region can be justified by comparison of relevant dielectric constants. Water has a dielectric constant of about 74 at 37 °C,[73] the dielectric constant of the phosphatidyl choline polar region has been calculated to be 23-29,[74,75] and the dielectric of the lipid core is about 2.[76] The dielectric constant of acrylamide has been estimated to be around 43; this value was calculated by a proportional estimate from dielectric constants of acetamide in solid (dielectric of 4)[77] and liquid forms (dielectric 59)[77] and a dielectric constant for solid acrylamide of 2.9.[78] The moderately polar region of the bilayer headgroup favorablly accommodates the trp residues and acrylamide when OmpA initially associates with the lipid bilayer, and this association would result in the observed blue-shift of emission maxima but relatively high accessbility of acrylamide to tryptophan. The fast component is therefore attributed to a transition of the trp residues of OmpA from a fully solvent exposed state with high K_{SV} and red λ_{max} values corresponding to those of the unfolded state, to a partially adsorbed state in the bilayer headgroup that has a decreased dielectric constant (blue-shifted λ_{max}) but relatively high acrylamide concentration. This conclusion is consistent with the results of brominated quenching experiments that determined the distance of the trp residues in the first membrane bound folding intermediate to be ~14-16 Å from the center of the DOPC lipid bilayer, a distance that is consistent with the polar region of the bilayer.[53,79]

The slow component is attributed to a transition of the trp residues from the polar region of the lipid bilayer into the fatty core of the bilayer, upon which K_{SV} and λ_{max} values decrease further to the fully folded values. This slow transition is illustrated in Figure 21. The fact that the final K_{SV} values of folded OmpA are not zero can be explained by the presence of acrylamide in the bilayer itself; in this scenario, the mechanism for quenching is likely to be static given that the diffusion of acrylamide in the bilayer is likely to be slow.

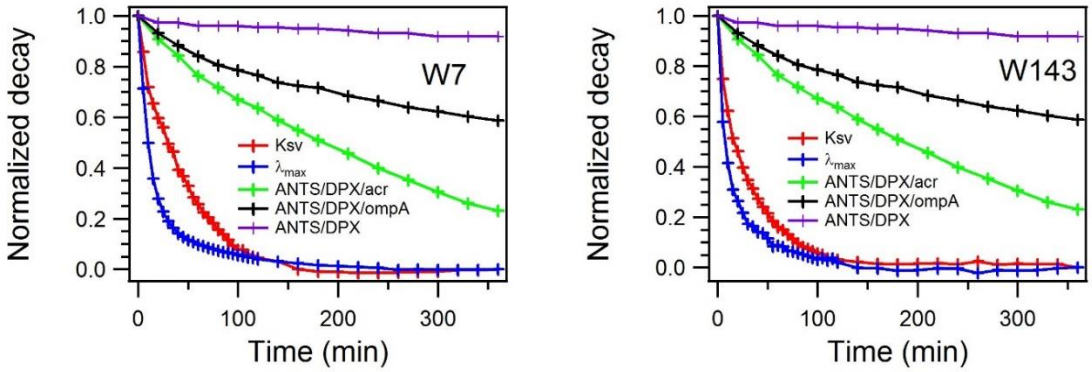

Figure 19. Comparison of K_{SV}, λ_{max}, and leakage assays. Shown in these graphs are normalized decay plots for K_{SV}, λ_{max}, and ANTS/DPX data over the time of the folding reaction for W7 (left) and W143 (right). The plots of K_{SV} (red) and λ_{max} (blue) show that λ_{max} decays faster than K_{SV}. The decay plots for the leakage assays were generated by subtracting the post lysis fluorescence intensity (figure 17 panel F) from each fluorescence maxima (514 nm) vs time data set, multiplying by -1 and then normalizing to the highest value of the resulting curve.

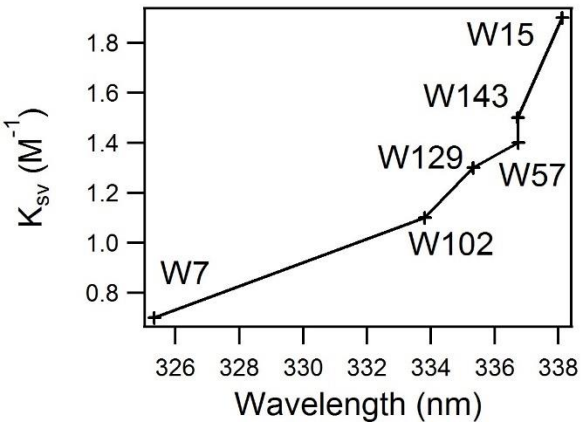

Figure 20. Correlation of K_{SV} and λ_{max}. Shown here is the correlation between K_{SV} and λ_{max} values that were determined from the average K_{SV} and λ_{max} versus time data at the fully folded state (t = 6 hours).

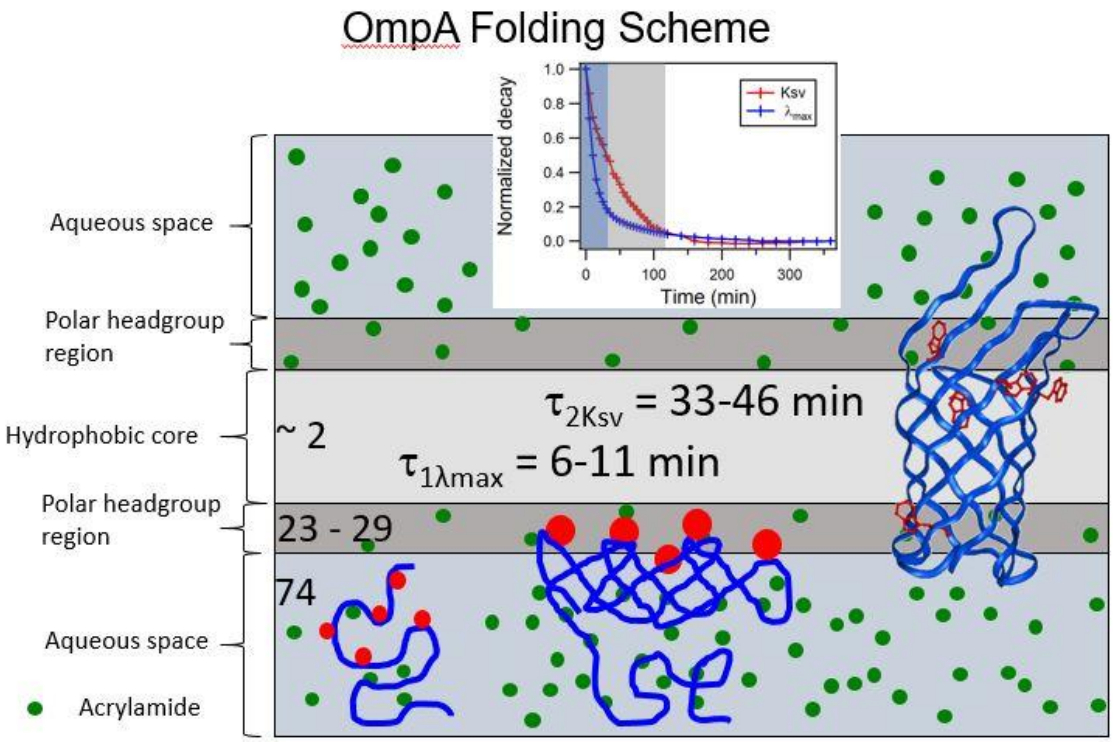

Figure 21. OmpA Folding Scheme. Shown here is a folding scheme for OmpA. The lipid bilayer is shown as the hydrophobic core with dielectric 2 (light gray) and the polar headgroup regions with dielectric 23-29 (dark gray). The values for dielectric constants are shown in the figure. Aqueous space (dielectric 74) is shown in light blue. OmpA is shown in blue, with the tryptophan residues as red balls. The unfolded protein (left) transforms to a lipid-associated structure (middle) in the fast step of folding; this process is described with a time constant associated with the fast blue-shift in λ_{max} ($\tau_{1\lambda max}$ = 6 – 11 min). The second, slow transition, is associated with OmpA fully inserting and folding the final structure (right). During this transition, the tryptophan residues are unable to interact extensively with the quencher and therefore, the time constant associated with this step is given by the time constant for change in the value for K_{SV} (τ_{2Ksv} = 33 – 46 min). Placed above the scheme is the plot of normalized decay for K_{SV} and λ_{max} for the W7 mutant. The fast and slow transitions are shaded in blue and grey respectively.

Table 5. Summary of K_{SV} values and corresponding decay times. *Values of K_{SV} at t = 0 and 6 hr were determined from double exponential fit parameters. **Values of τ were determined from double exponential fits to data, and reflect the fast and slow components and corresponding relative amplitudes. For two mutants (W7 and W102), fast and slow components were identical, and reported as a single value

K_{SV} (M^{-1})	**W7**	**W15**	**W57**	**W102**	**W129**	**W143**
denatured	9.6	8.3	9.4	10.5	11.9	8.7
t = 0 h*	8.6	9.1	10.0	9.1	9.7	9.7
aggregated	8.7	6.0	8.7	9.2	9.8	9.2
adsorbed	2.4	2.7	2.7	3.4	1.6	3.0
t = 6 h*	0.6	2.0	1.4	1.0	1.3	1.7
Decays**						
τ (min)	46	45 : 8	40 : 62	41	33 : 3	37 : 4
Relative amplitude	1.00	0.84 : 0.16	0.80 : 0.20	1.00	0.78 : 0.22	0.77 : 0.23

Table 6. Summary of λ_{max} and corresponding decay times. *Values of λ_{max} at t = 0 and 6 hr were determined from double exponential fit parameters. **Values of τ were determined from double exponential fits to data, and reflect the fast and slow components and corresponding relative amplitudes.

λ_{max} (nm)	**W7**	**W15**	**W57**
denatured	356	355	355
t = 0 h*	354	353	352
aggregated	353	352	352
adsorbed	339	339	341
t = 6 h*	325	338	337
Decays**			
τ (min)	11 : 83	9 : 31	9 : 49
Relative amplitude	0.80 : 0.20	0.60 : 0.40	0.78 : 0.22

λ_{max} (nm)	**W102**	**W129**	**W143**
denatured	354	356	355
t = 0 h*	351	352	352
aggregated	351	353	353
adsorbed	342	333	341
t = 6 h*	334	335	337
Decays**			
τ (min)	8 : 26	7 : 28	6 : 45
Relative amplitude	0.50 : 0.50	0.74 : 0.26	0.63 : 0.37

Table 7. Single and double exponential fits to ANTS/DPX decays. Tabulated here are exponential fit parameters for single and double exponential fits to the ANTS/DPX decays in Figure 17 and S64 and S65.

	ANTS/DPX/Acr	ANTS/DPX/OmpA	ANTS/DPX
Double exponential			
y_0	-0.35	0.34	0.86
A_1	0.17	0.53	0.11
k_1 (min^{-1})	0.010	0.0019	0.0018
τ_1 (min) / %	98 / 12%	530 / 81%	560 / 87%
A_2	1.17	0.13	0.017
k_2 (min^{-1})	0.0020	0.021	0.012
τ_2 (min) / %	510 / 88%	49/ 19%	57 / 13%
Single exponential			
y_0	-0.10	0.55	0.88
A_1	1.08	0.44	0.11
k (min^{-1})	0.0033	0.0058	0.0030
τ (min)	310	170	330

Table 8. λ_{max} values for indole with and without protein. The following table was prepared to show the difference in λ_{max} values at increasing concentrations of acrylamide in the presence and absence of protein structure. In all folding states of the protein, denatured (8 M urea), beginning of folding reaction (t = 0 hours), aggregated, adsorbed, and fully folded (t = 6 hours), λ_{max} shows a decreasing trend with increasing concentrations of acrylamide, but in the absence of protein environment (NATA), the effect is not observed.

[Acr] (M)	NATA	8 M urea	t = 0 hours	aggregated	adsorbed	t = 6
0.0	359	356	353	351	339	338
0.1	358	355	351	350	336	337
0.2	359	354	350	349	335	337
0.3	358	354	350	349	335	336
0.4	359	354	349	348	334	336

Table 9. Comparison of timescales from various studies of OmpA folding. Tabulated here are timescales derived from previous experiments on fluorescence intensity,[43] circular dichroism [71], tertiary structure,[72] and insertion.[53] Amplitudes from these previous studies are omitted. Data from this study are indicated as asterisks.

	Technique	A_1	τ_1 (min)	A_2	τ_2 (min)
Environment polarity	Fluorescence		1.4 - 1.8		30 – 40
Secondary structure	Circular Dichroism	1	37		
Tertiary structure	FRET		2		50
Insertion	TDFQ		2		87
λ_{max} *	Fluorescence	0.50-0.80	6-11	0.20-0.50	26-49
Solvent accessibility*	Quenching	0.16-0.23	3-8	0.84-0.77	33-46
*This work					

Conclusion

The aim of this study was to gain a more in-depth view of the folding and insertion of OmpA into lipid bilayers. The experiments involved measurement and analysis of the kinetics of site specific desolvation and changes in polarity that occur upon transition from aqueous environment to membrane-associated states. Steady state quenching experiments as well as a time resolved fluorescence quenching technique were applied to the folding of six single tryptophan mutants of OmpA into fluid bilayers of DMPC at 37 °C. The experiments revealed K_{SV} values for the denatured, aggregated and fully folded states of OmpA, and K_{SV} and λ_{max} data that were fit to single and double exponential decay functions. Double exponential fits to K_{SV} data showed a minor component of fast decay (τ ~ 3 – 8 minutes) and a dominant component of slow decay (τ ~ 33 – 46 minutes). Double exponential fits to λ_{max} data showed a dominant component of fast decay (τ ~ 6 – 11 minutes) and a minor component of slow decay (τ ~ 26 – 49 minutes). The different trends indicated that the majority of blue shift happens in the fast step, while the majority of desolvation occurs in the slow step. In consideration of differences in polarity of the lipid headgroup region and the bilayer core, the fast step was attributed to transition from the aqueous environment to the polar headgroup region and the slow step was attributed to transition from the polar headgroup region to the bilayer core. The results of the experiment are consistent with the results of previous studies of OmpA folding by time resolved fluorescence experiments. What this study offers in addition to those studies is the elucidation of the desolvation and changes in the polarity of the environment of the individual trp fluorophores.

Future studies should focus on the role of static quenching on the reported K_{SV} data to investigate whether the conversion from dynamic+static quenching to purely dynamic quenching during the folding process reveals new insights into the folding mechanisms. The effects of acrylamide on the folding reaction and kinetics should also be further investigated by, for example, comparison with other quenchers such as iodide. . Future time resolved quenching experiments could investigate other folding pathways by variation of lipid composition.

Temperature studies may also help provide new insights into the thermodynamics of the folding reaction. Finally, it would be valuable to perform similar experiments on other membrane proteins, such as alpha-helical systems and oligomeric membrane proteins such as the trimeric OmpF.

Appendix 1: Supplemental Information

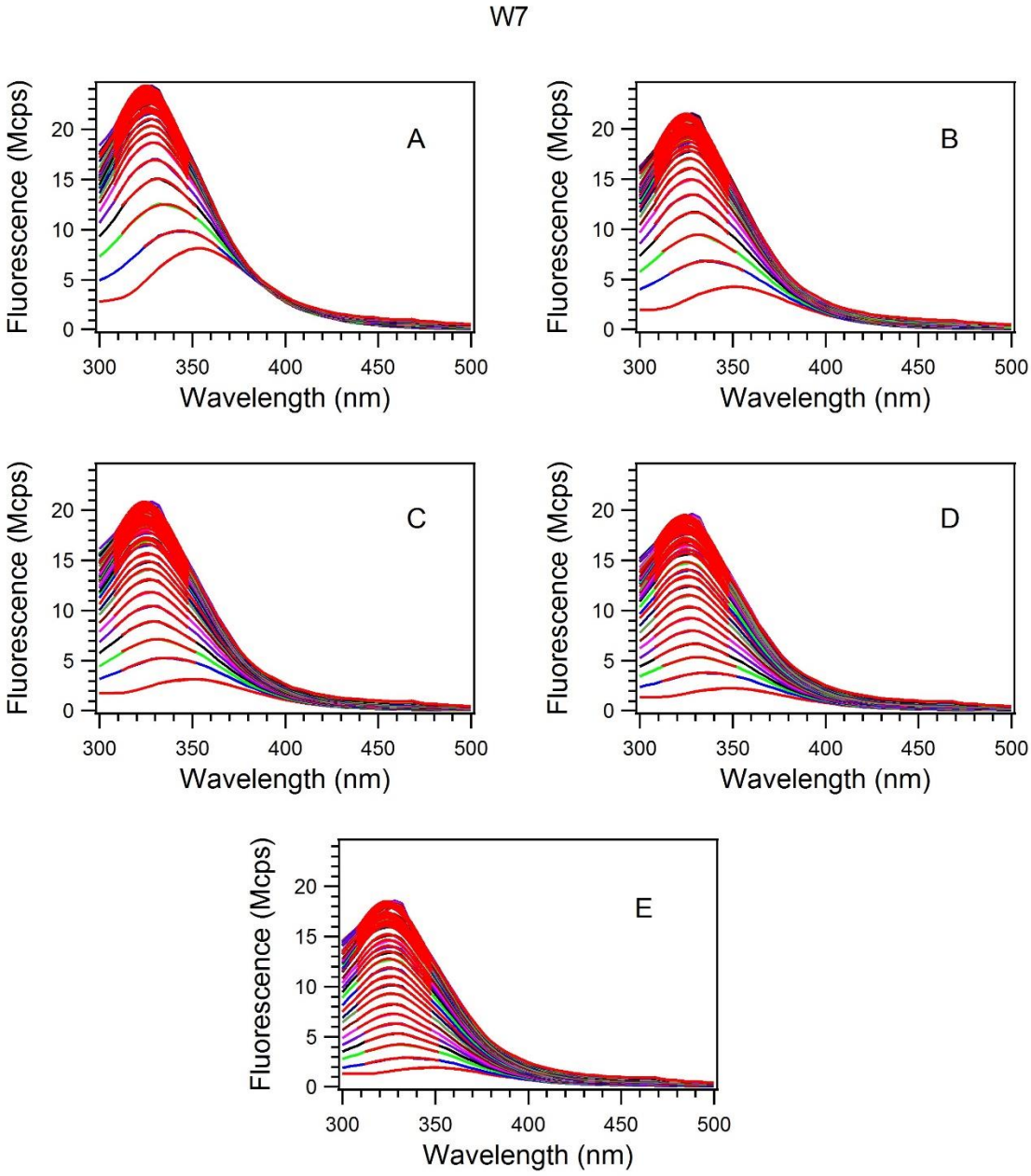

Figure S1: W7 Experiment 1 Data. Depicted are the fluorescence spectra for the 0.0M (A), 0.1M (B), 0.2M (C), 0.3M (D) and 0.4M (E) acrylamide samples for all 6 hours of the experiment. Gaussian fits are in red.

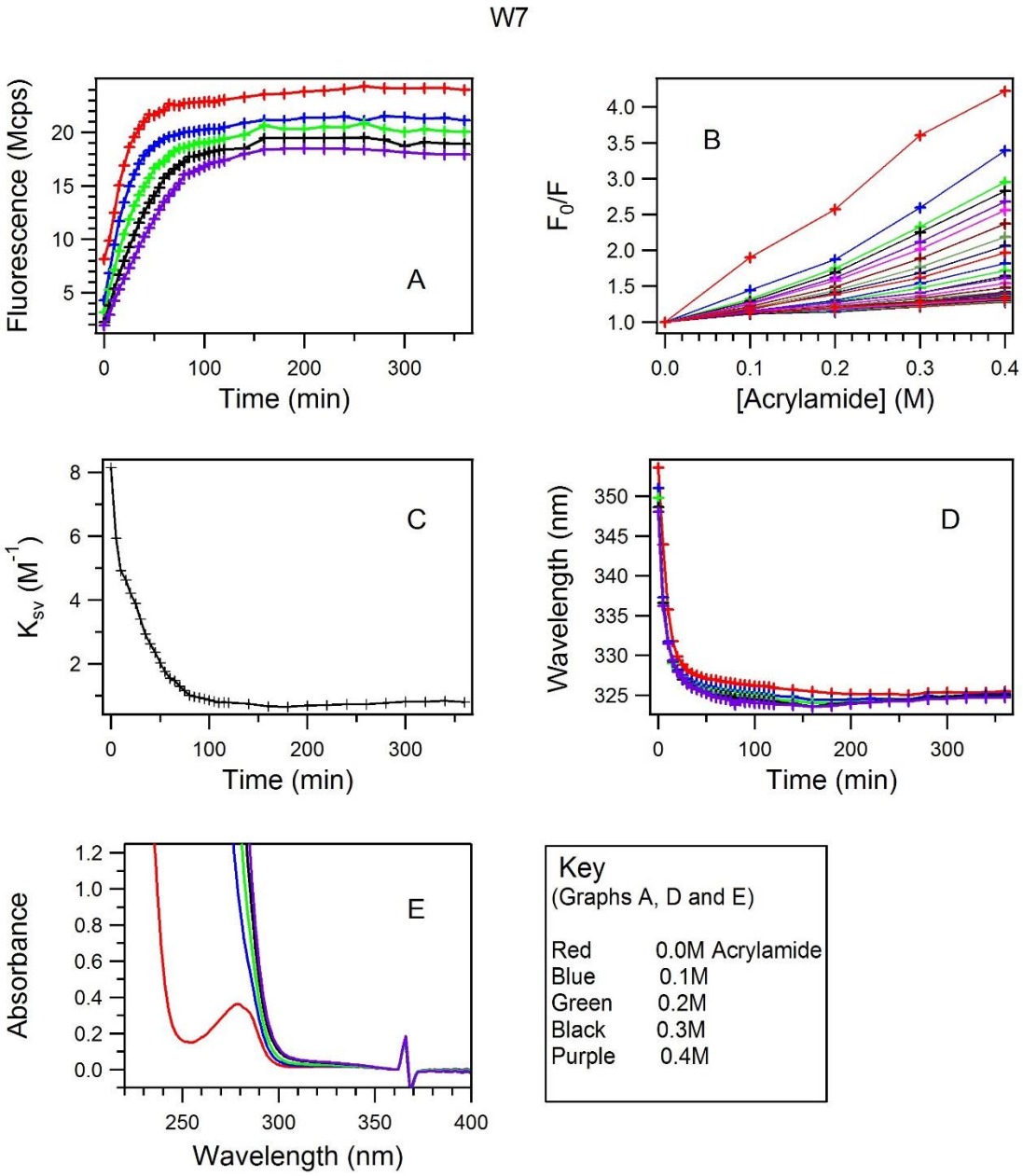

Figure S2: W7 Experiment 1 Data Workup. Panel A depicts fluorescence maxima from the gaussian fits for each sample and time point. For panels A, D and E, red corresponds to the 0.0M acrylamide sample, blue to the 0.1M sample, green to the 0.2M sample, black to the 0.3M sample and purple to the 0.4M sample. Panel B depicts Stern-Volmer plots for each time point in the experiment. Panel C depicts the linear slope (K_{SV}) of the Stern-Vomer plots in panel B over the time of the experiment. Panel D depicts the shift of maximum wavelength of emission for all samples over the time of the experiment. Panel E depicts absorbance spectra for all samples.

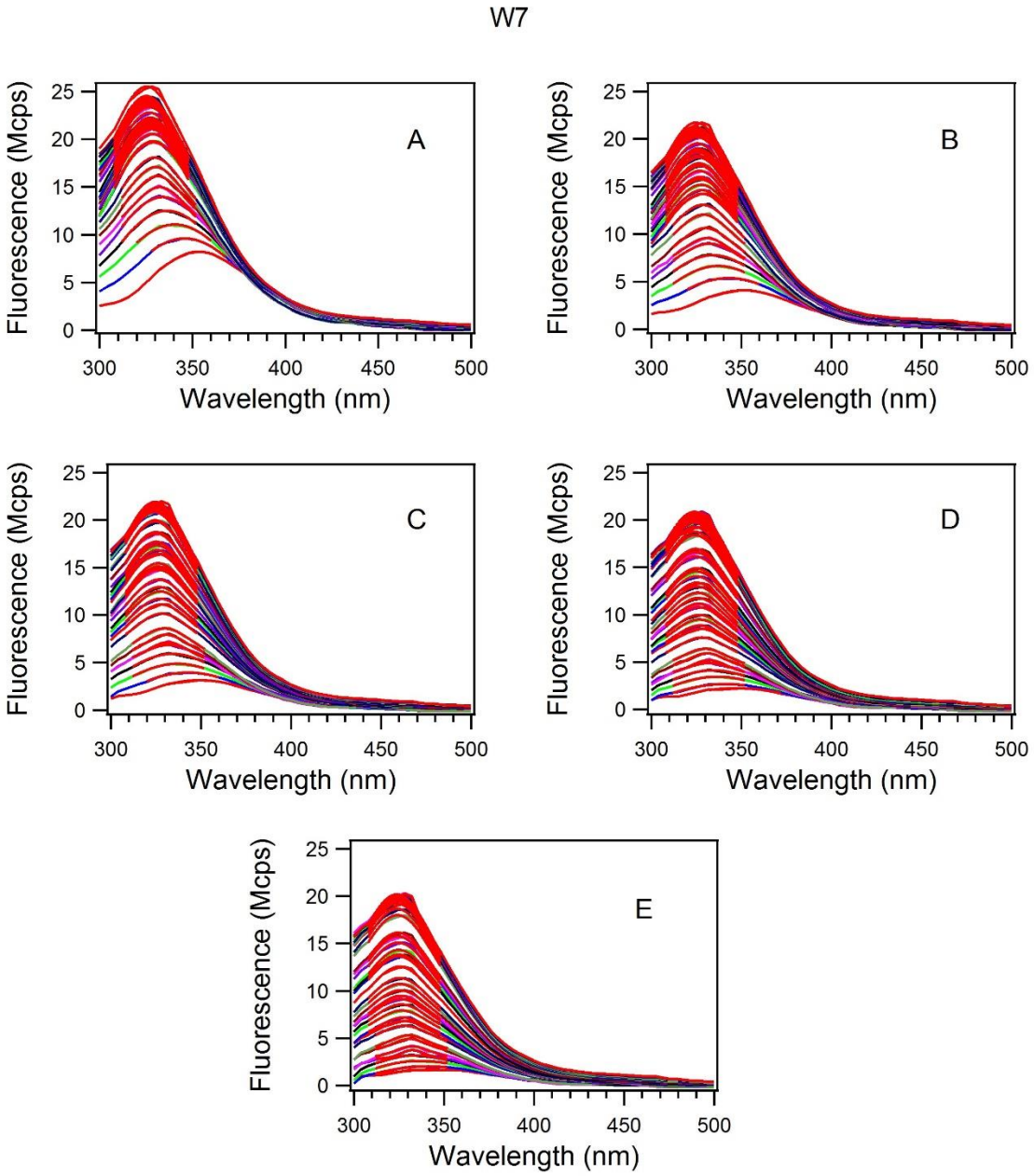

Figure S3: W7 Experiment 2 Data. Depicted are the fluorescence spectra for the 0.0M (A), 0.1M (B), 0.2M (C), 0.3M (D) and 0.4M (E) acrylamide samples for all 6 hours of the experiment. Gaussian fits are in red.

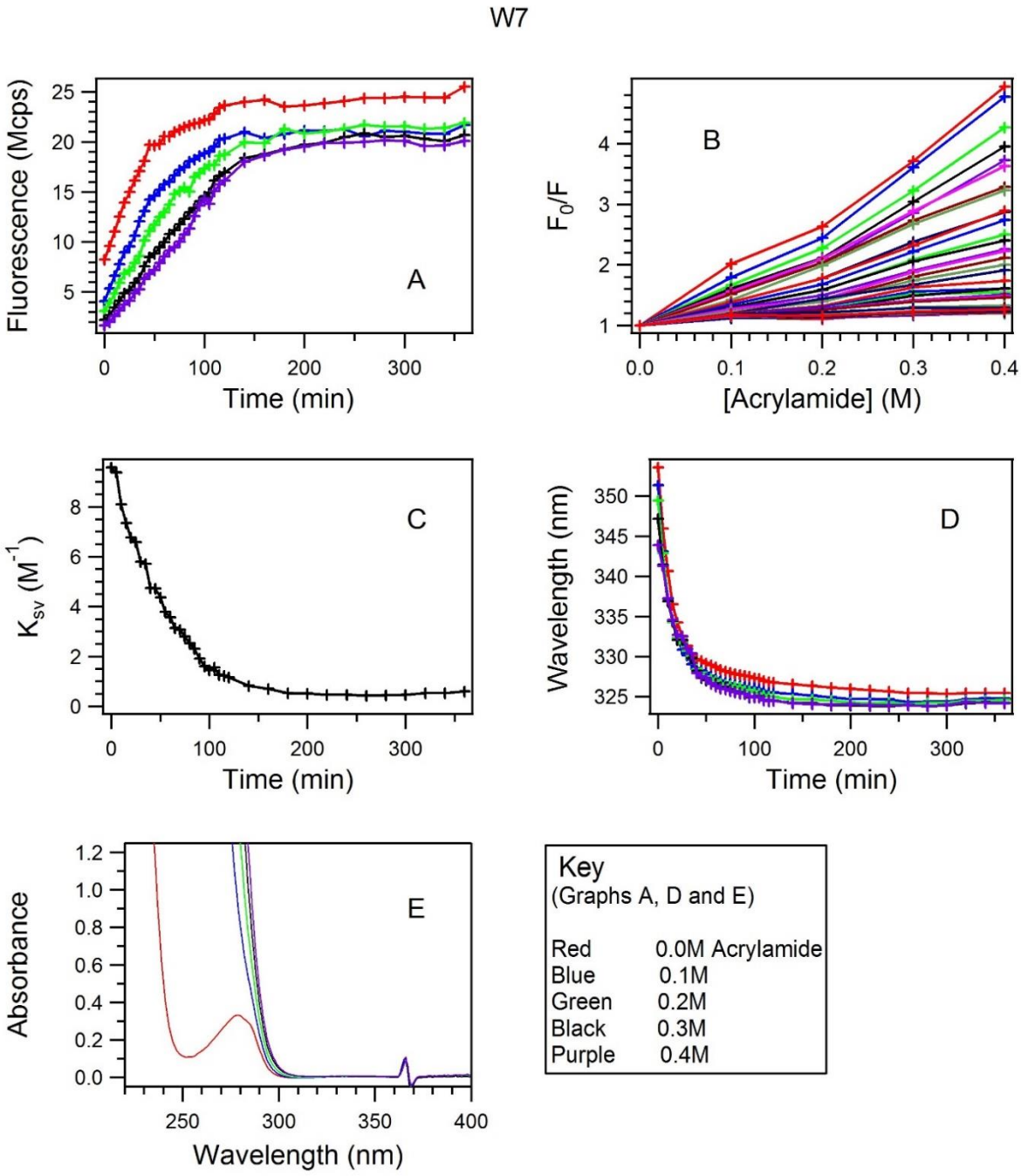

Figure S4: W7 Experiment 2 Data Workup. Panel A depicts fluorescence maxima from the gaussian fits for each sample and time point. For panels A, D and E, red corresponds to the 0.0M acrylamide sample, blue to the 0.1M sample, green to the 0.2M sample, black to the 0.3M sample and purple to the 0.4M sample. Panel B depicts Stern-Volmer plots for each time point in the experiment. Panel C depicts the linear slope (K_{SV}) of the Stern-Vomer plots in panel B over the time of the experiment. Panel D depicts the shift of maximum wavelength of emission for all samples over the time of the experiment. Panel E depicts absorbance spectra for all samples.

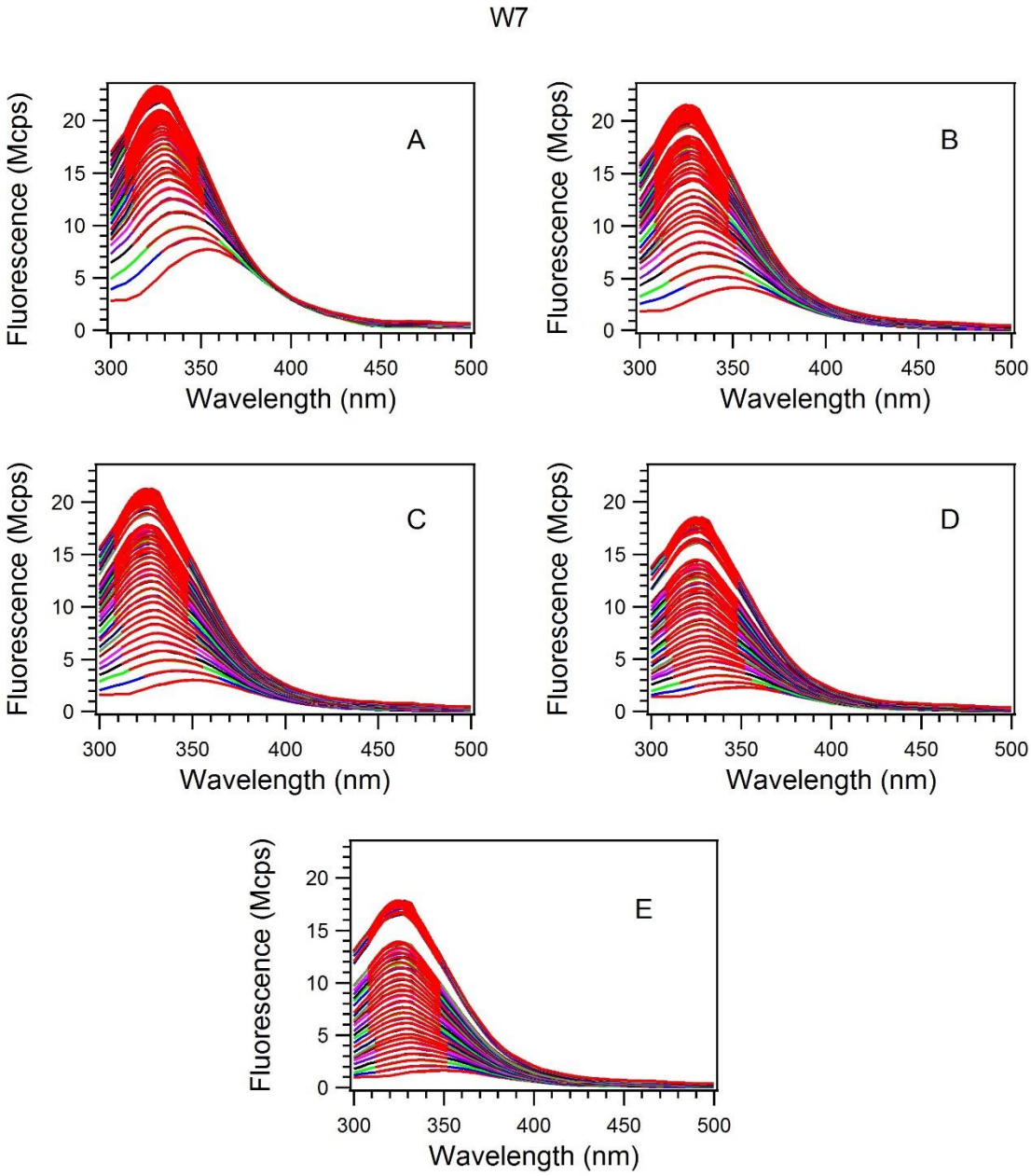

Figure S5: W7 Experiment 3 Data. Depicted are the fluorescence spectra for the 0.0M (A), 0.1M (B), 0.2M (C), 0.3M (D) and 0.4M (E) acrylamide samples for all 6 hours of the experiment. Gaussian fits are in red.

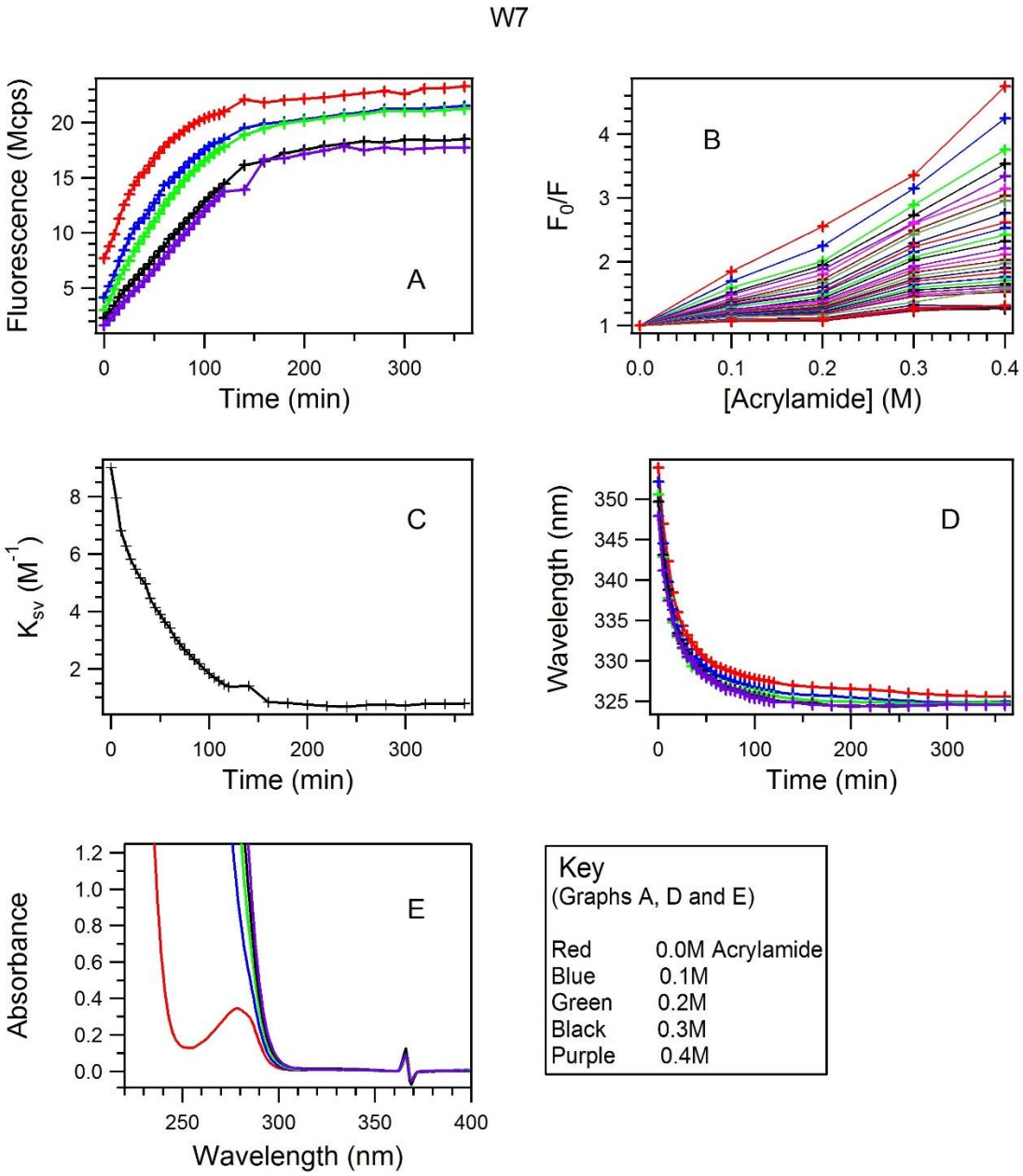

Figure S6: W7 Experiment 3 Data Workup. Panel A depicts fluorescence maxima from the gaussian fits for each sample and time point. For panels A, D and E, red corresponds to the 0.0M acrylamide sample, blue to the 0.1M sample, green to the 0.2M sample, black to the 0.3M sample and purple to the 0.4M sample. Panel B depicts Stern-Volmer plots for each time point in the experiment. Panel C depicts the linear slope (K_{SV}) of the Stern-Vomer plots in panel B over the time of the experiment. Panel D depicts the shift of maximum wavelength of emission for all samples over the time of the experiment. Panel E depicts absorbance spectra for all samples.

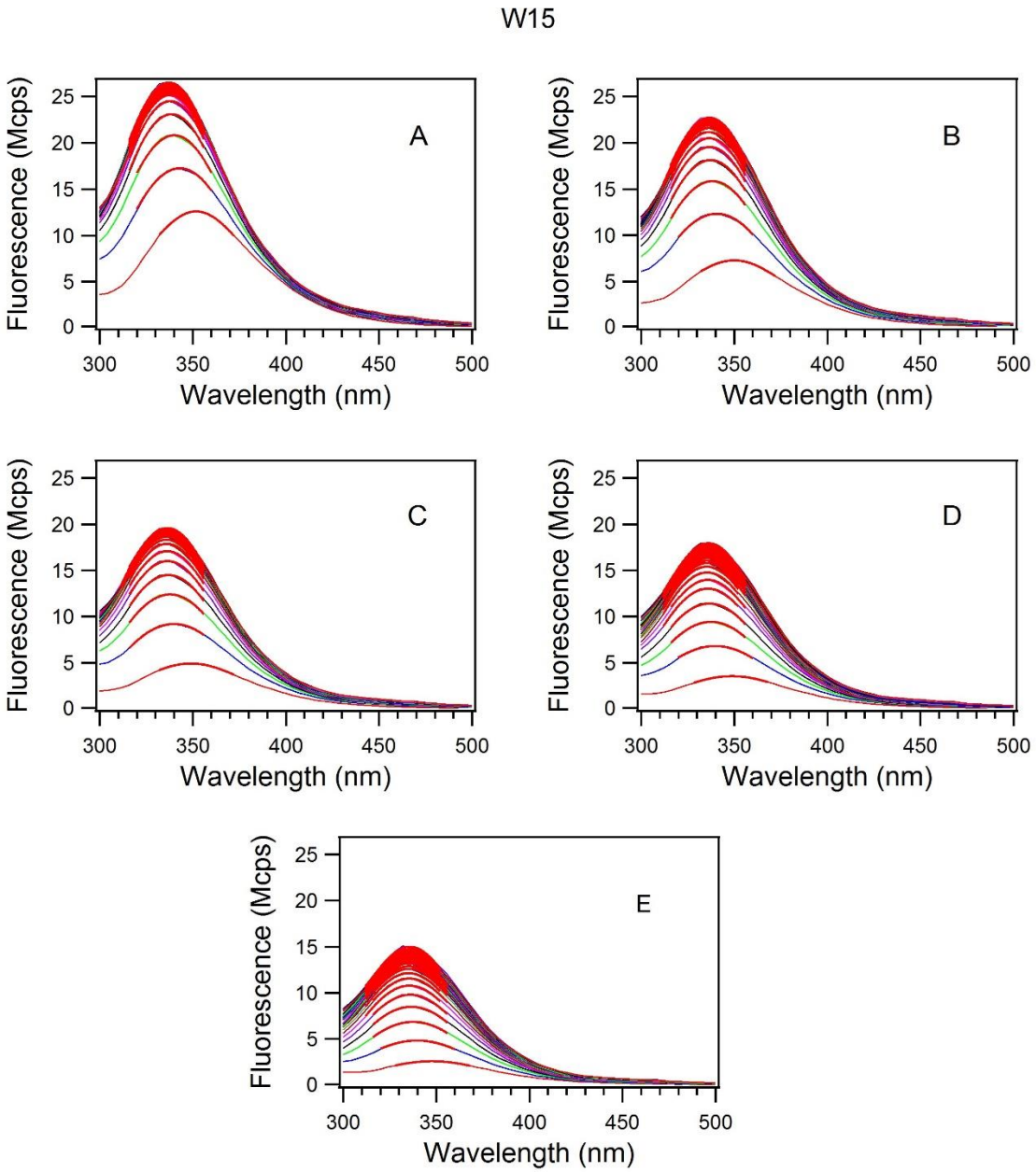

Figure S7: W15 Experiment 1 Data. Depicted are the fluorescence spectra for the 0.0M (A), 0.1M (B), 0.2M (C), 0.3M (D) and 0.4M (E) acrylamide samples for all 6 hours of the experiment. Gaussian fits are in red.

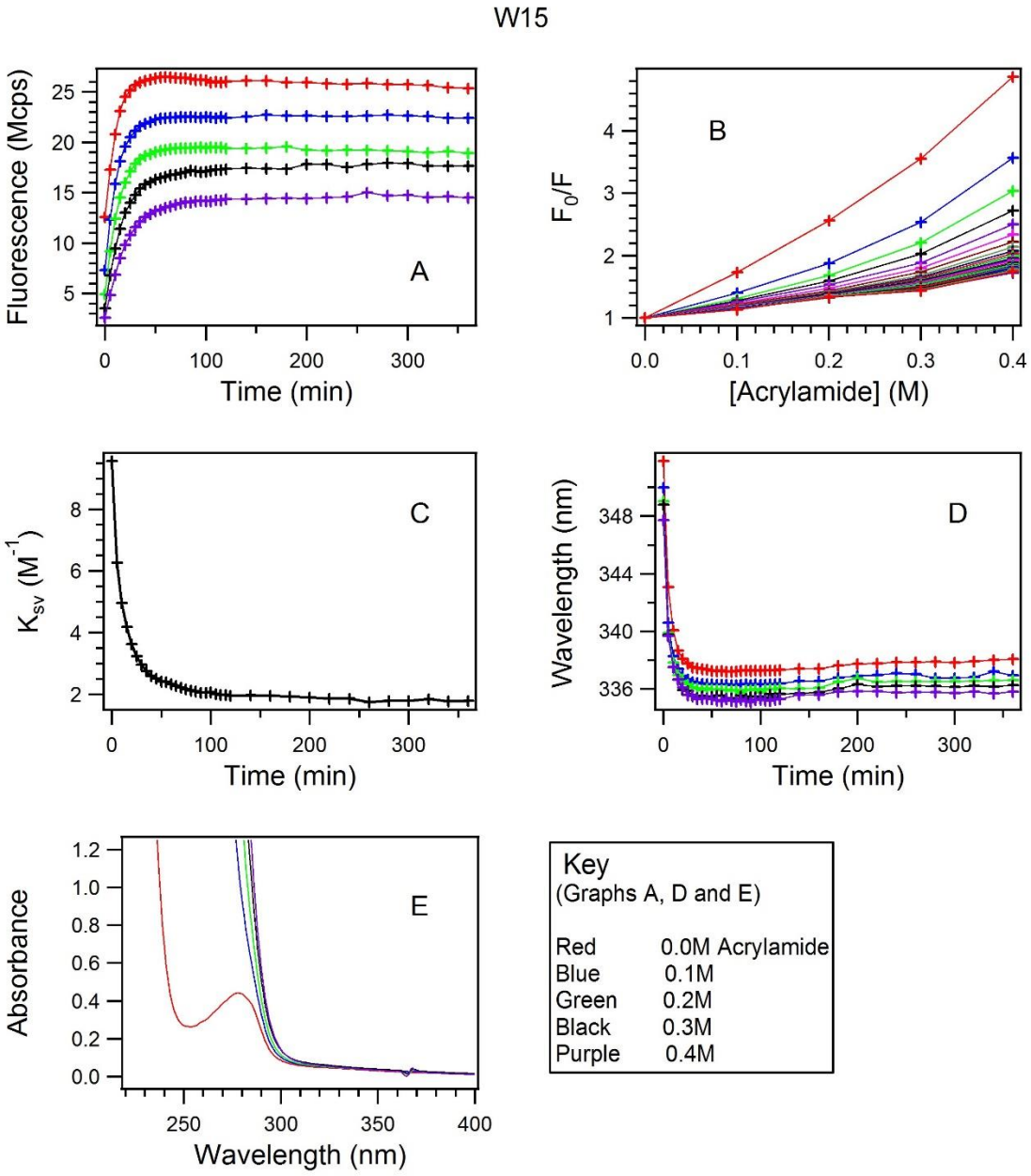

Figure S8: W15 Experiment 1 Data Workup. Panel A depicts fluorescence maxima from the gaussian fits for each sample and time point. For panels A, D and E, red corresponds to the 0.0M acrylamide sample, blue to the 0.1M sample, green to the 0.2M sample, black to the 0.3M sample and purple to the 0.4M sample. Panel B depicts Stern-Volmer plots for each time point in the experiment. Panel C depicts the linear slope (K_{SV}) of the Stern-Vomer plots in panel B over the time of the experiment. Panel D depicts the shift of maximum wavelength of emission for all samples over the time of the experiment. Panel E depicts absorbance spectra for all samples.

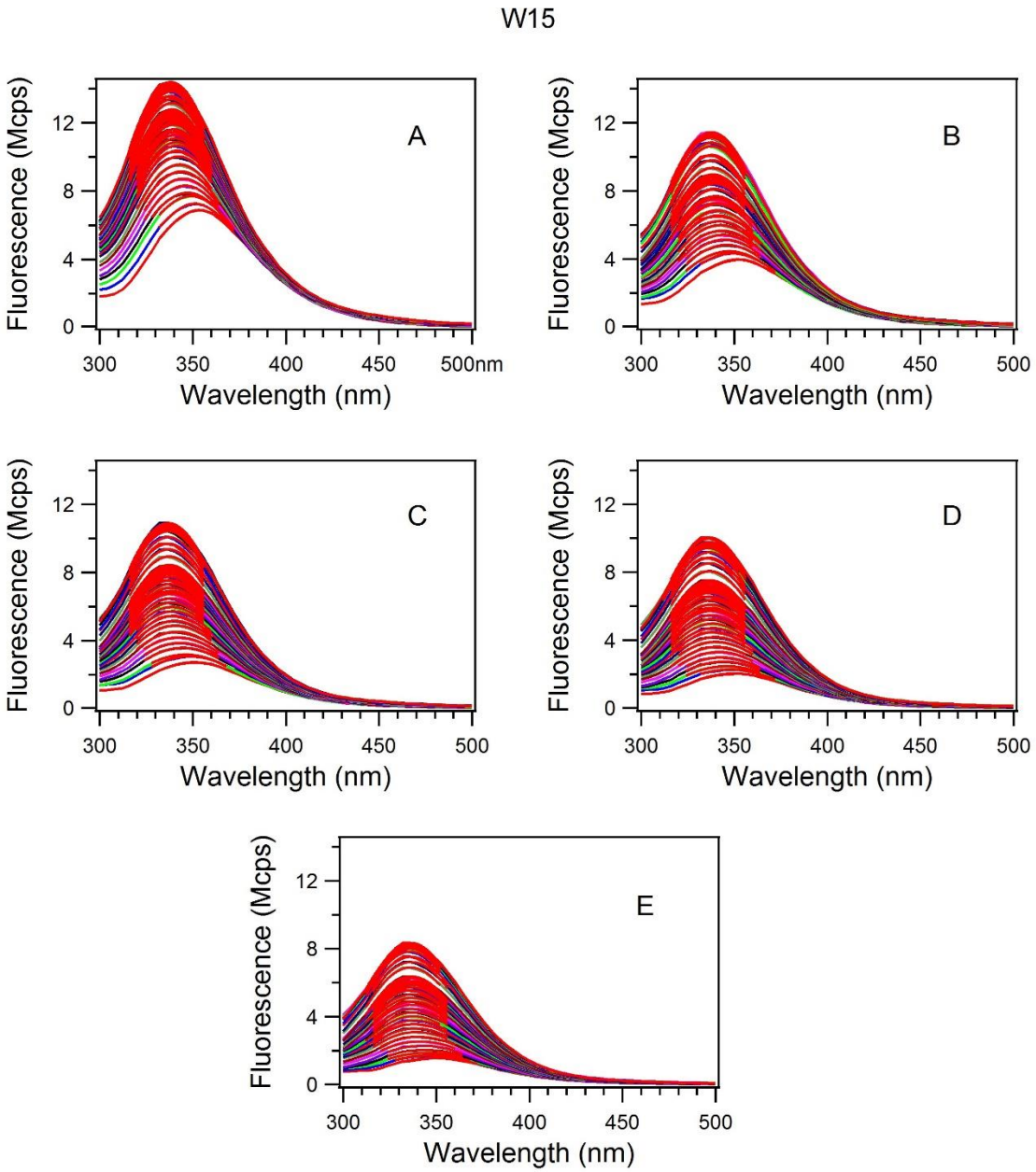

Figure S9: W15 Experiment 2 Data. Depicted are the fluorescence spectra for the 0.0M (A), 0.1M (B), 0.2M (C), 0.3M (D) and 0.4M (E) acrylamide samples for all 6 hours of the experiment. Gaussian fits are in red.

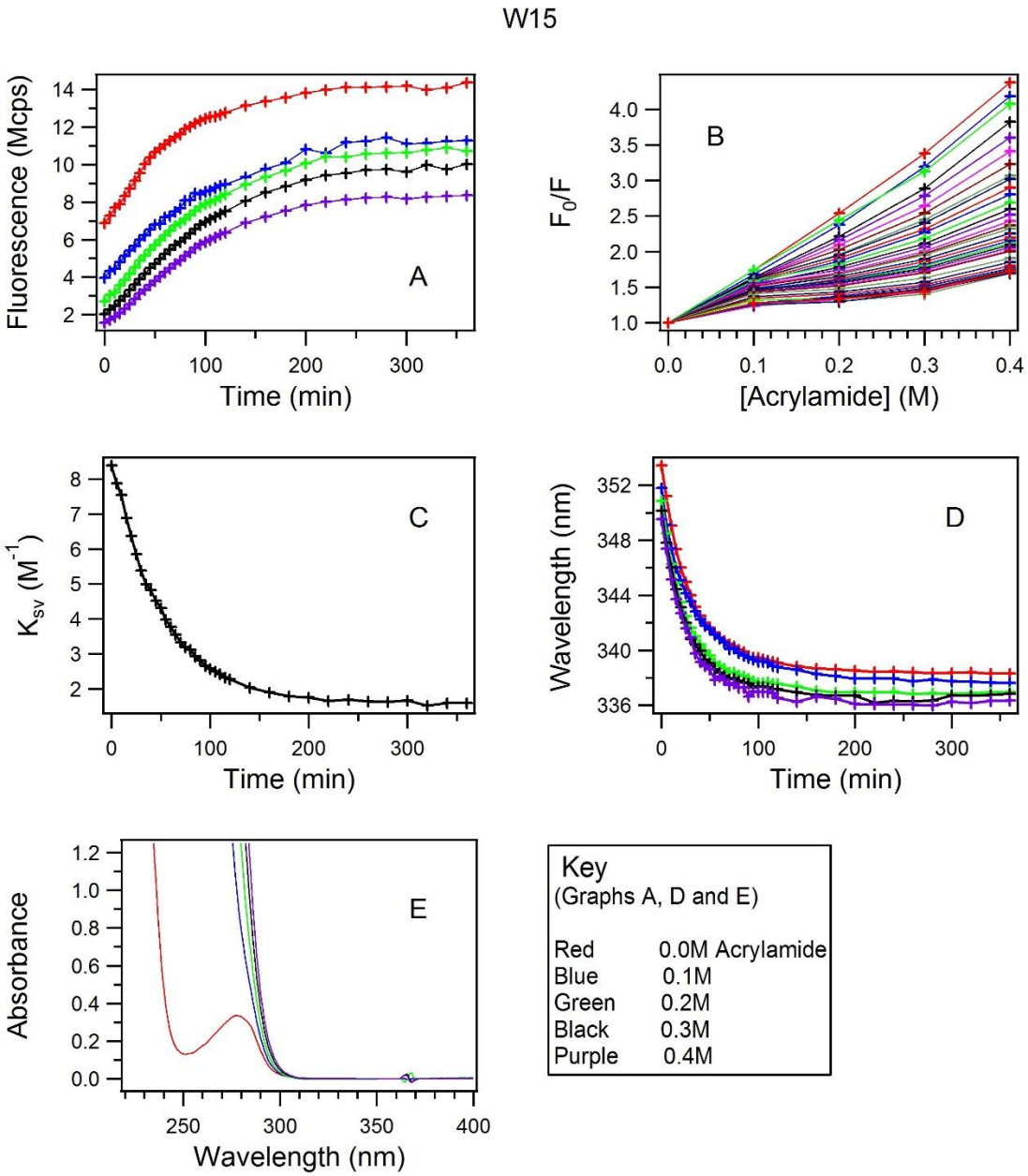

Figure S10: W15 Experiment 2 Data Workup. Panel A depicts fluorescence maxima from the gaussian fits for each sample and time point. For panels A, D and E, red corresponds to the 0.0M acrylamide sample, blue to the 0.1M sample, green to the 0.2M sample, black to the 0.3M sample and purple to the 0.4M sample. Panel B depicts Stern-Volmer plots for each time point in the experiment. Panel C depicts the linear slope (K_{SV}) of the Stern-Vomer plots in panel B over the time of the experiment. Panel D depicts the shift of maximum wavelength of emission for all samples over the time of the experiment. Panel E depicts absorbance spectra for all samples.

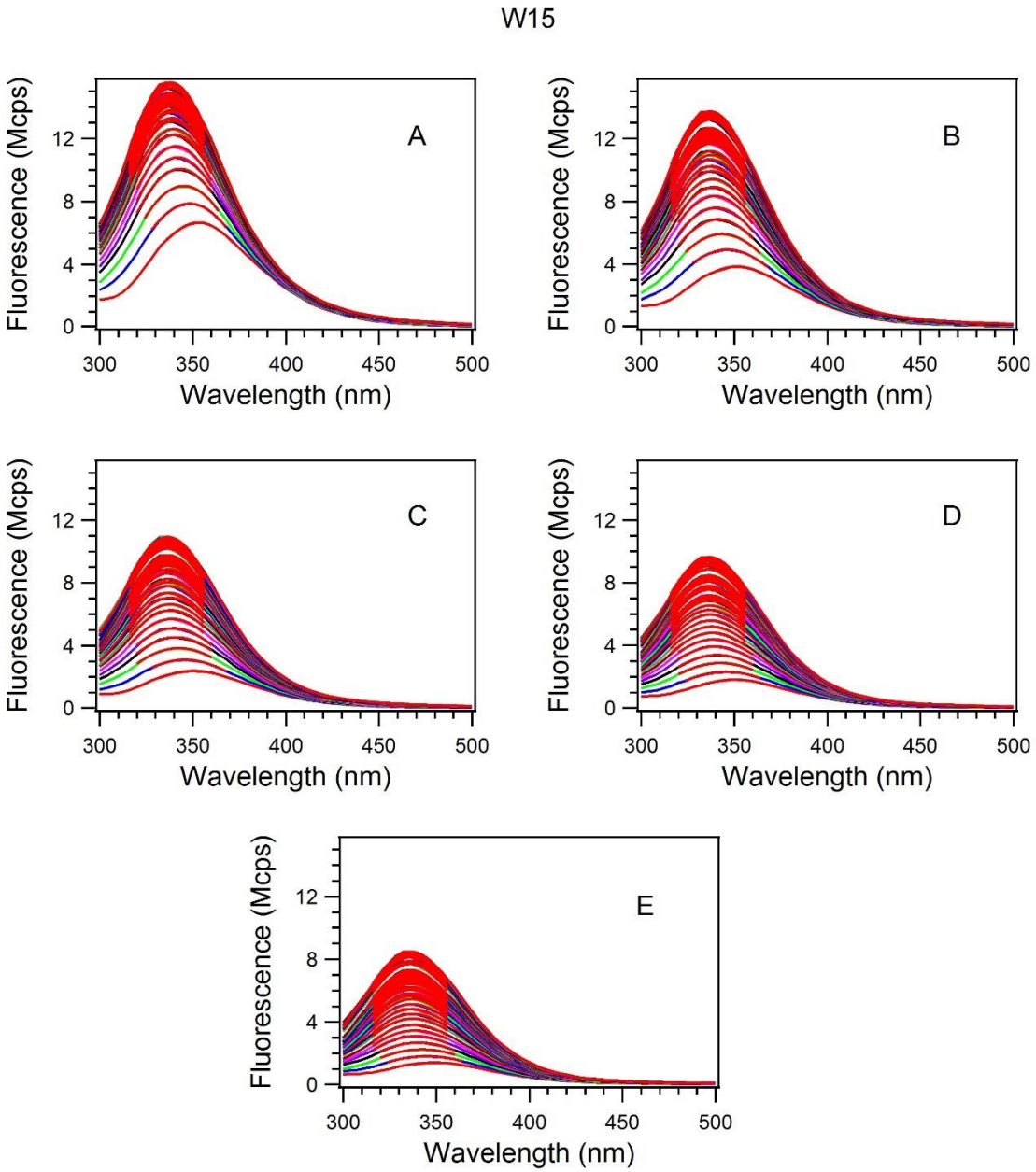

Figure S11: W15 Experiment 3 Data. Depicted are the fluorescence spectra for the 0.0M (A), 0.1M (B), 0.2M (C), 0.3M (D) and 0.4M (E) acrylamide samples for all 6 hours of the experiment. Gaussian fits are in red.

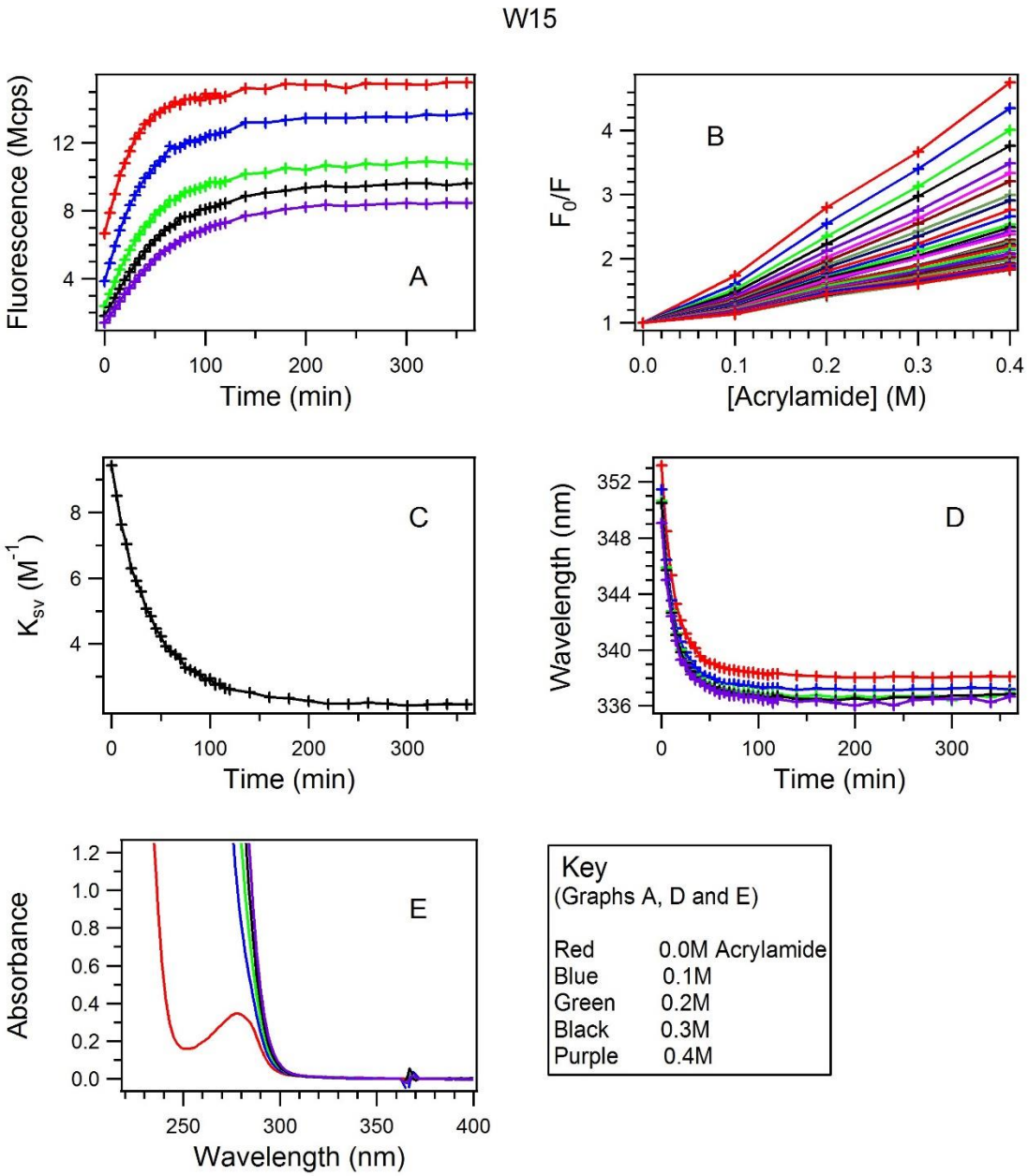

Figure S12: W15 Experiment 3 Data Workup. Panel A depicts fluorescence maxima from the gaussian fits for each sample and time point. For panels A, D and E, red corresponds to the 0.0M acrylamide sample, blue to the 0.1M sample, green to the 0.2M sample, black to the 0.3M sample and purple to the 0.4M sample. Panel B depicts Stern-Volmer plots for each time point in the experiment. Panel C depicts the linear slope (K_{SV}) of the Stern-Vomer plots in panel B over the time of the experiment. Panel D depicts the shift of maximum wavelength of emission for all samples over the time of the experiment. Panel E depicts absorbance spectra for all samples.

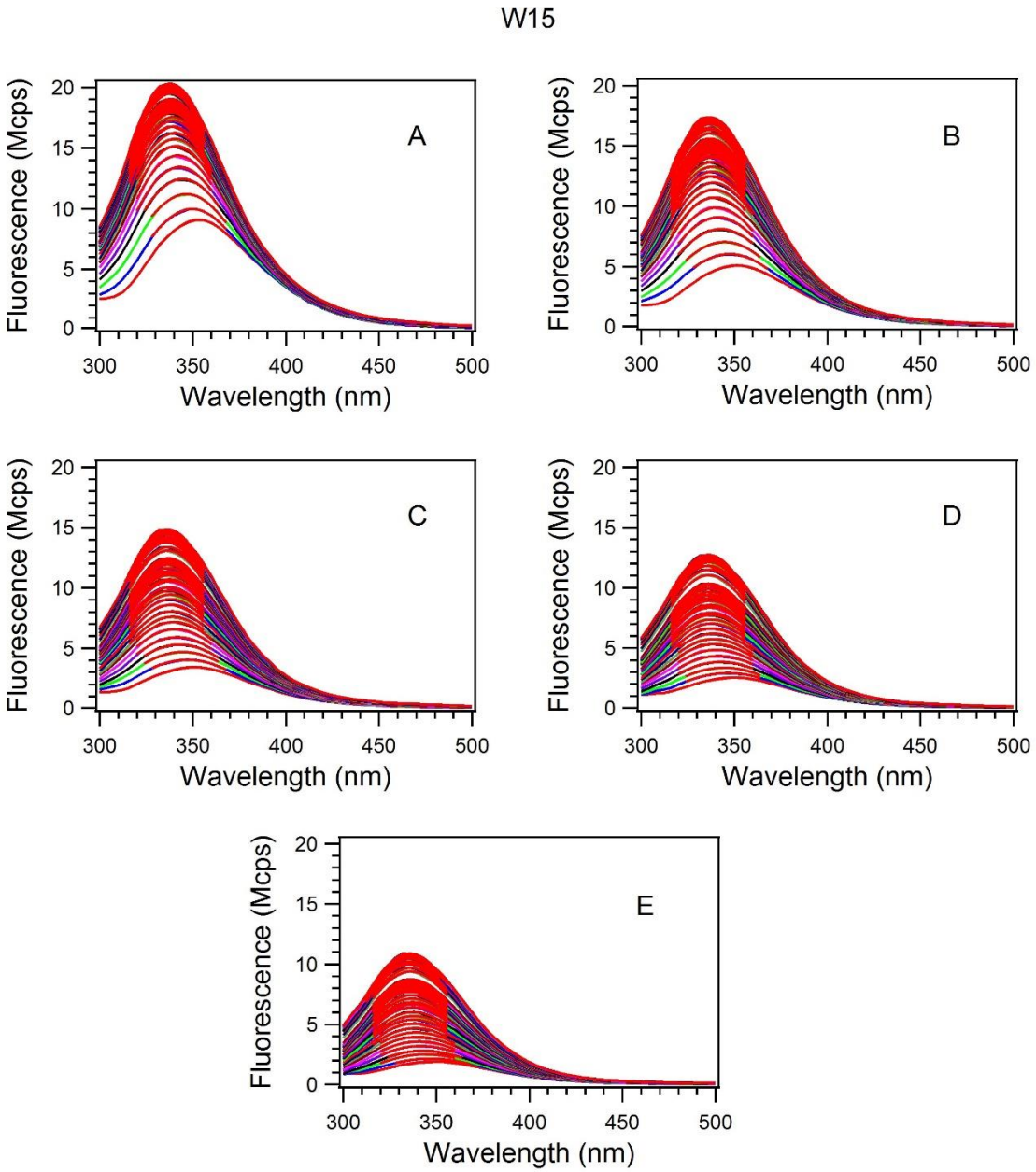

Figure S13: W15 Experiment 4 Data. Depicted are the fluorescence spectra for the 0.0M (A), 0.1M (B), 0.2M (C), 0.3M (D) and 0.4M (E) acrylamide samples for all 6 hours of the experiment. Gaussian fits are in red.

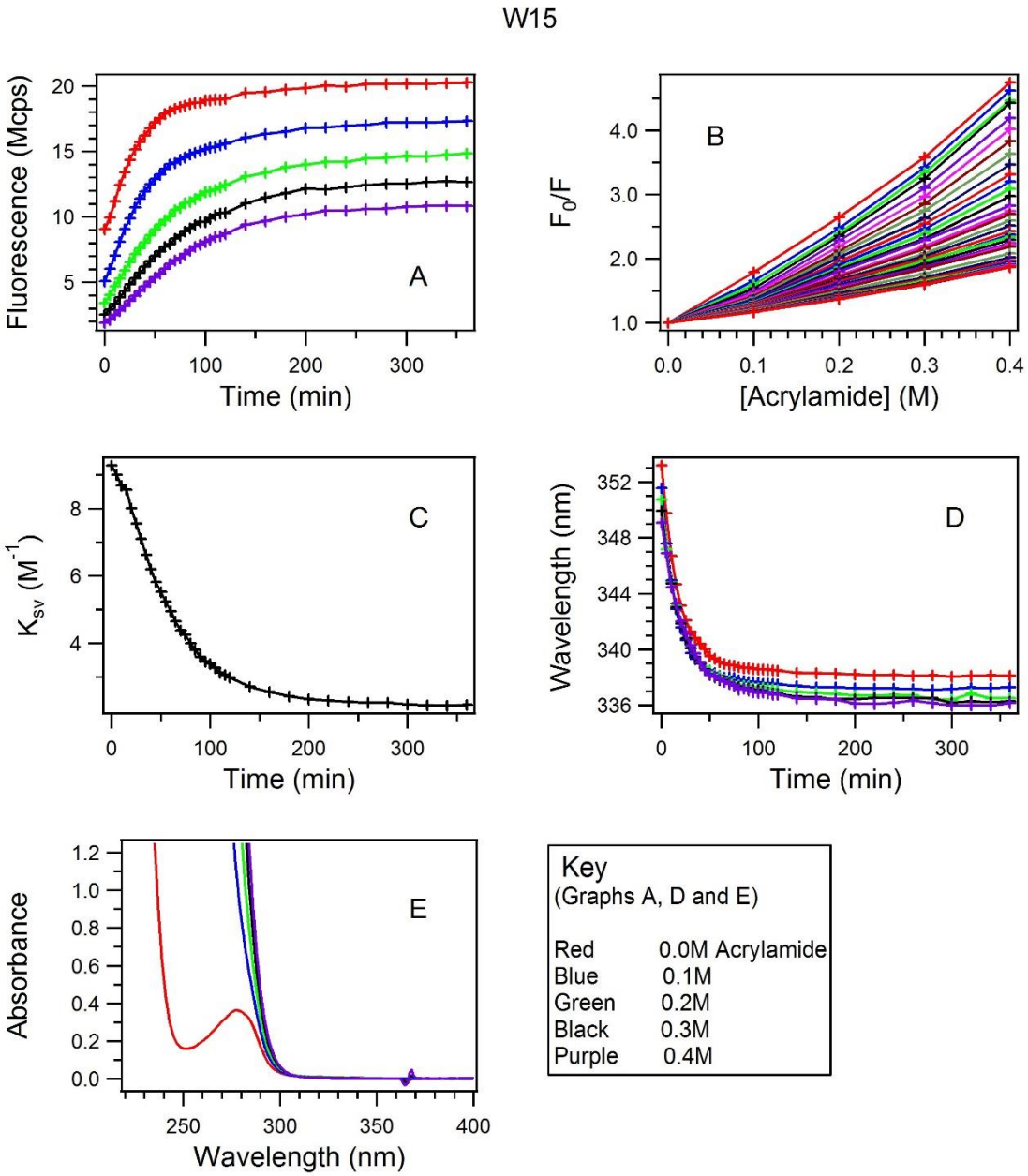

Figure S14: W15 Experiment 4 Data Workup. Panel A depicts fluorescence maxima from the gaussian fits for each sample and time point. For panels A, D and E, red corresponds to the 0.0M acrylamide sample, blue to the 0.1M sample, green to the 0.2M sample, black to the 0.3M sample and purple to the 0.4M sample. Panel B depicts Stern-Volmer plots for each time point in the experiment. Panel C depicts the linear slope (K_{SV}) of the Stern-Vomer plots in panel B over the time of the experiment. Panel D depicts the shift of maximum wavelength of emission for all samples over the time of the experiment. Panel E depicts absorbance spectra for all samples.

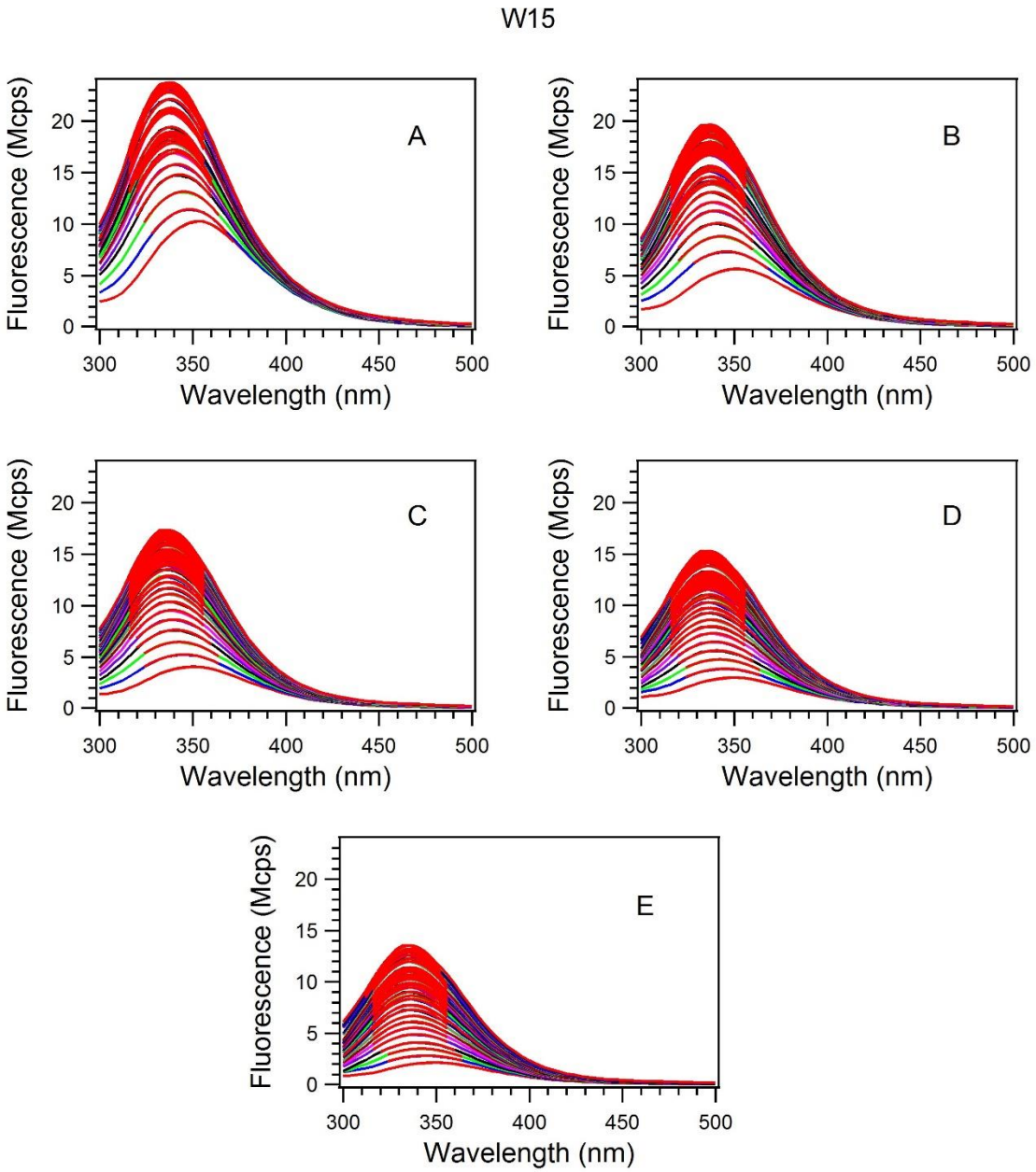

Figure S15: W15 Experiment 5 Data. Depicted are the fluorescence spectra for the 0.0M (A), 0.1M (B), 0.2M (C), 0.3M (D) and 0.4M (E) acrylamide samples for all 6 hours of the experiment. Gaussian fits are in red.

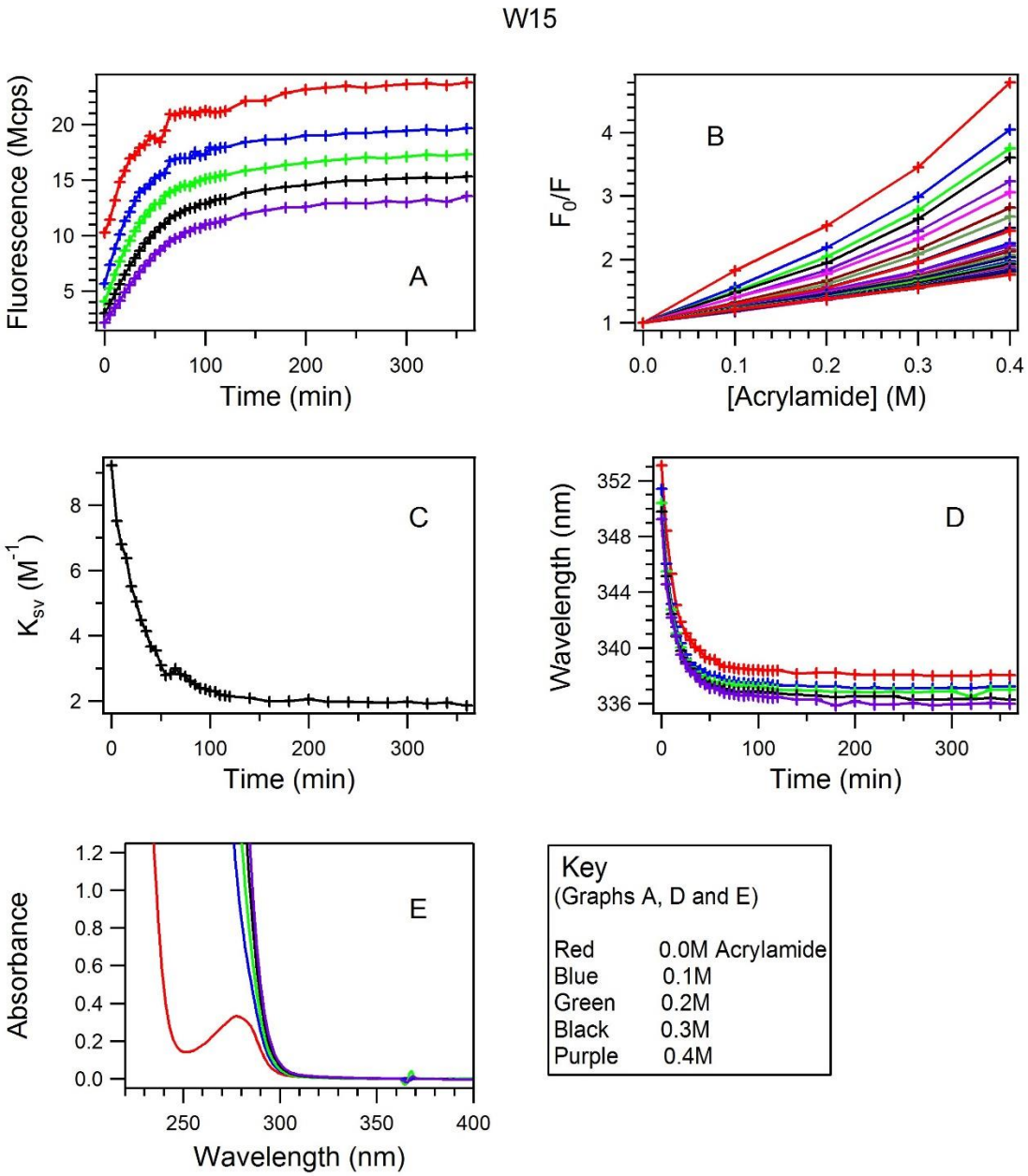

Figure S16: W15 Experiment 5 Data Workup. Panel A depicts fluorescence maxima from the gaussian fits for each sample and time point. For panels A, D and E, red corresponds to the 0.0M acrylamide sample, blue to the 0.1M sample, green to the 0.2M sample, black to the 0.3M sample and purple to the 0.4M sample. Panel B depicts Stern-Volmer plots for each time point in the experiment. Panel C depicts the linear slope (K_{SV}) of the Stern-Vomer plots in panel B over the time of the experiment. Panel D depicts the shift of maximum wavelength of emission for all samples over the time of the experiment. Panel E depicts absorbance spectra for all samples.

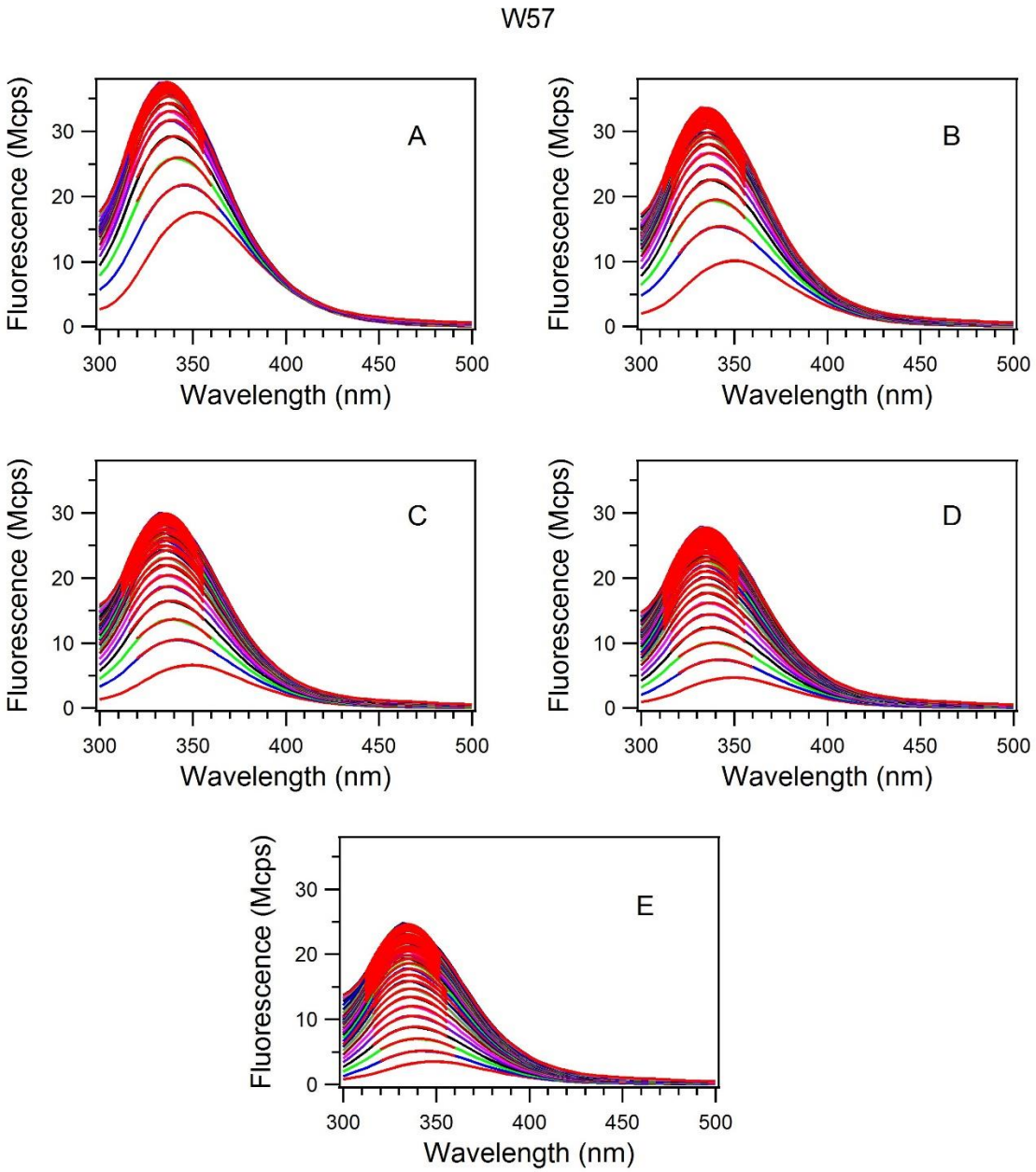

Figure S17: W57 Experiment 1 Data. Depicted are the fluorescence spectra for the 0.0M (A), 0.1M (B), 0.2M (C), 0.3M (D) and 0.4M (E) acrylamide samples for all 6 hours of the experiment. Gaussian fits are in red.

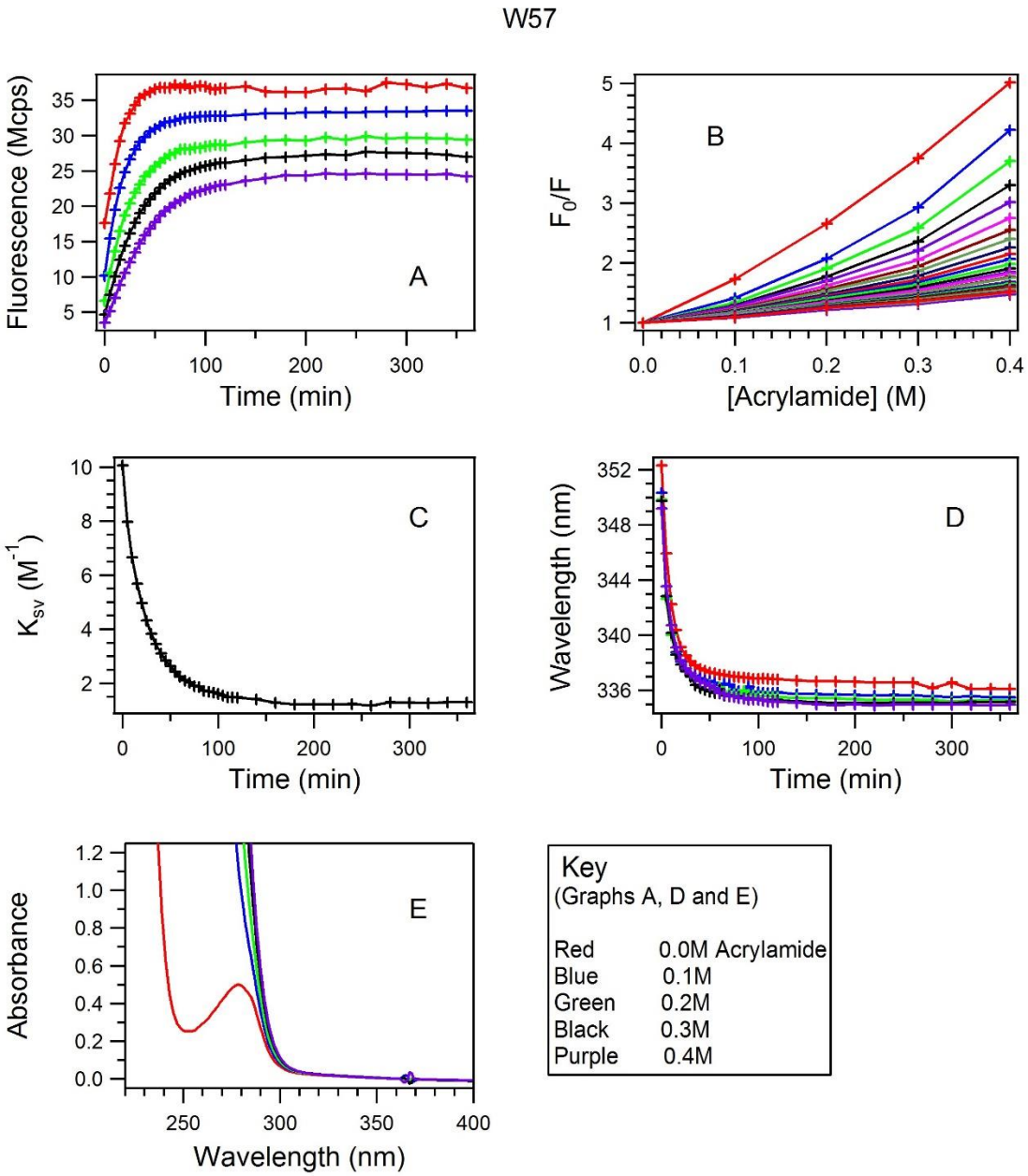

Figure S18: W57 Experiment 1 Data Workup. Panel A depicts fluorescence maxima from the gaussian fits for each sample and time point. For panels A, D and E, red corresponds to the 0.0M acrylamide sample, blue to the 0.1M sample, green to the 0.2M sample, black to the 0.3M sample and purple to the 0.4M sample. Panel B depicts Stern-Volmer plots for each time point in the experiment. Panel C depicts the linear slope (K_{SV}) of the Stern-Vomer plots in panel B over the time of the experiment. Panel D depicts the shift of maximum wavelength of emission for all samples over the time of the experiment. Panel E depicts absorbance spectra for all samples.

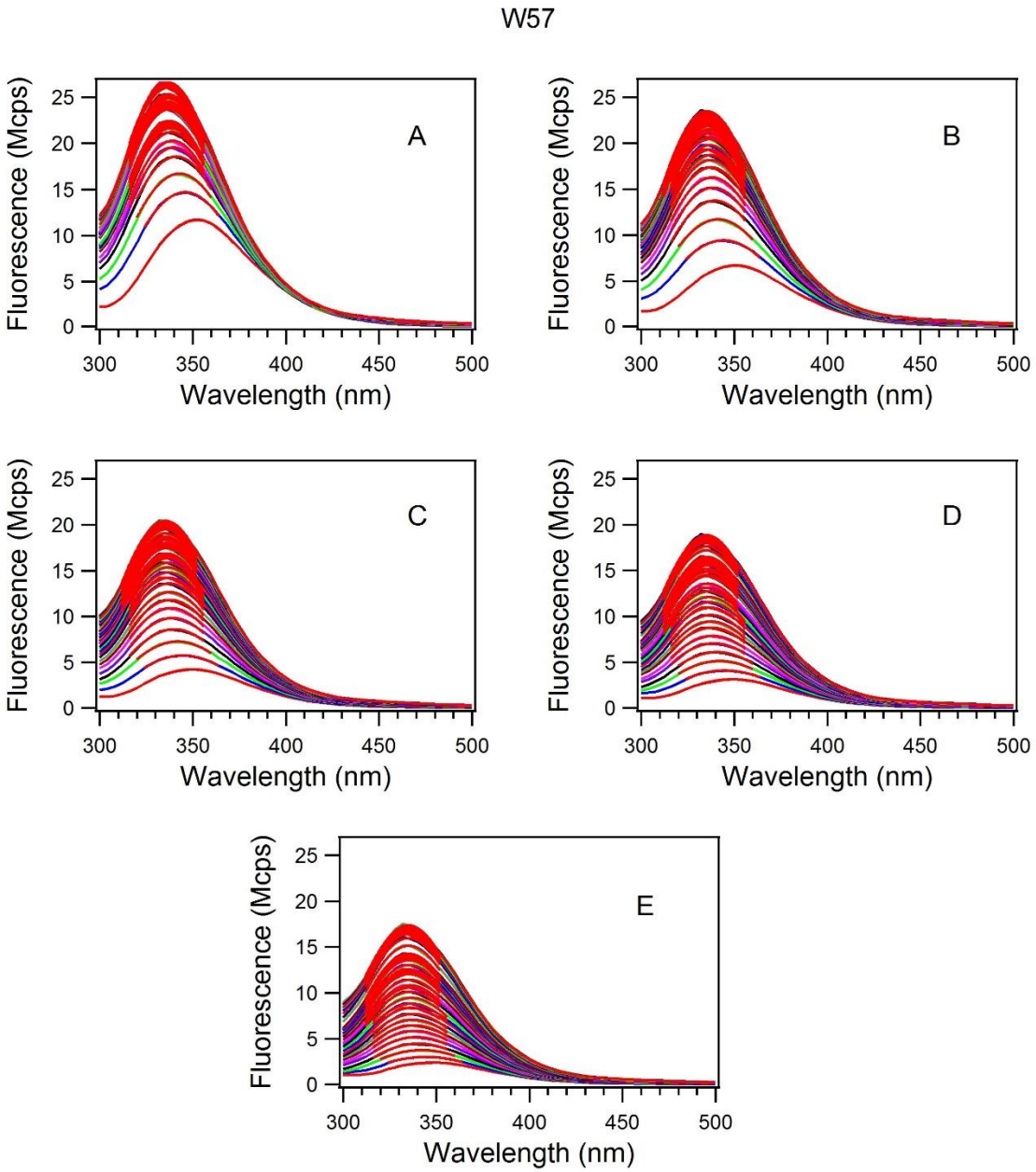

Figure S19: W57 Experiment 2 Data. Depicted are the fluorescence spectra for the 0.0M (A), 0.1M (B), 0.2M (C), 0.3M (D) and 0.4M (E) acrylamide samples for all 6 hours of the experiment. Gaussian fits are in red.

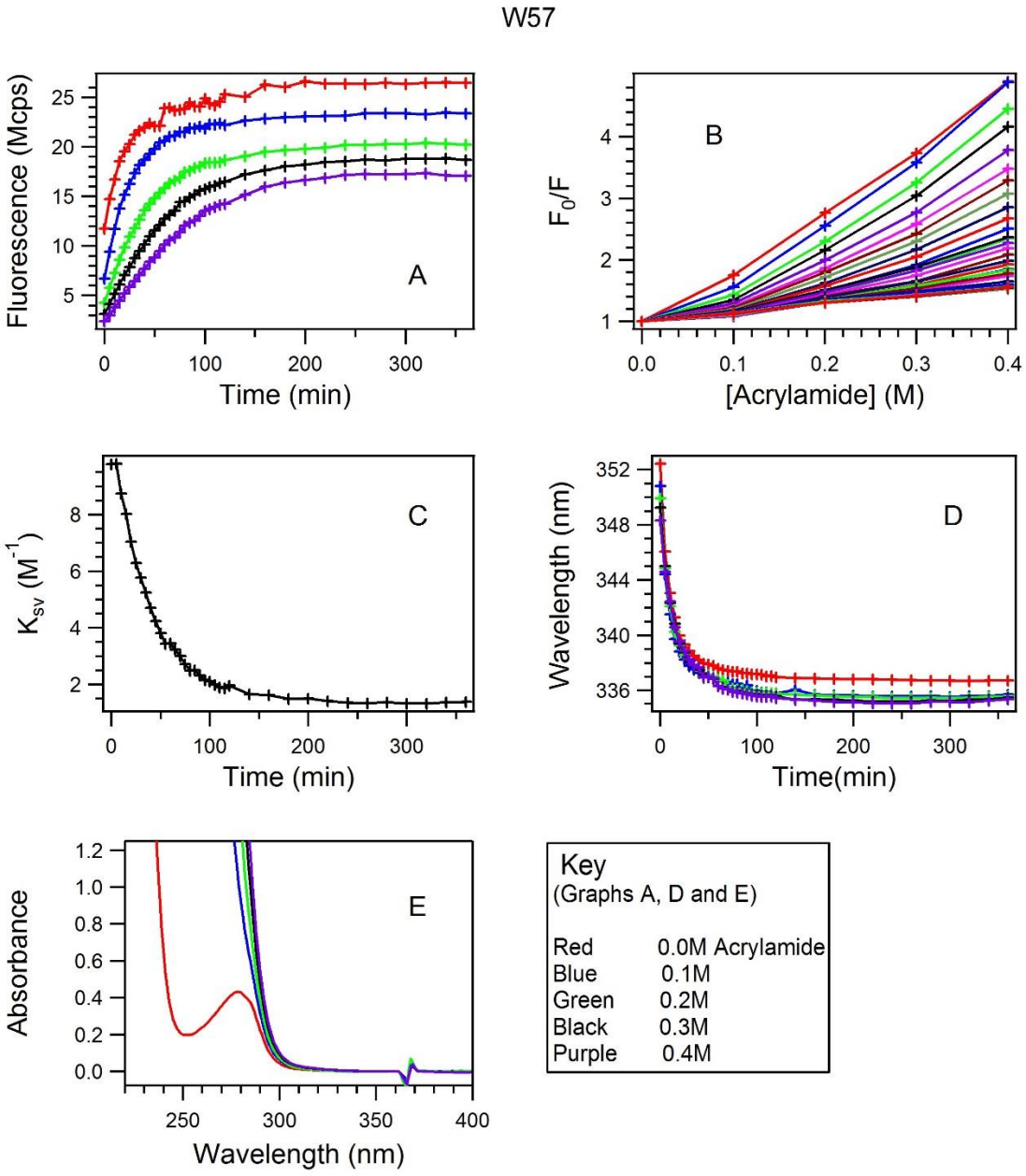

Figure S20: W57 Experiment 2 Data Workup. Panel A depicts fluorescence maxima from the gaussian fits for each sample and time point. For panels A, D and E, red corresponds to the 0.0M acrylamide sample, blue to the 0.1M sample, green to the 0.2M sample, black to the 0.3M sample and purple to the 0.4M sample. Panel B depicts Stern-Volmer plots for each time point in the experiment. Panel C depicts the linear slope (K_{SV}) of the Stern-Vomer plots in panel B over the time of the experiment. Panel D depicts the shift of maximum wavelength of emission for all samples over the time of the experiment. Panel E depicts absorbance spectra for all samples.

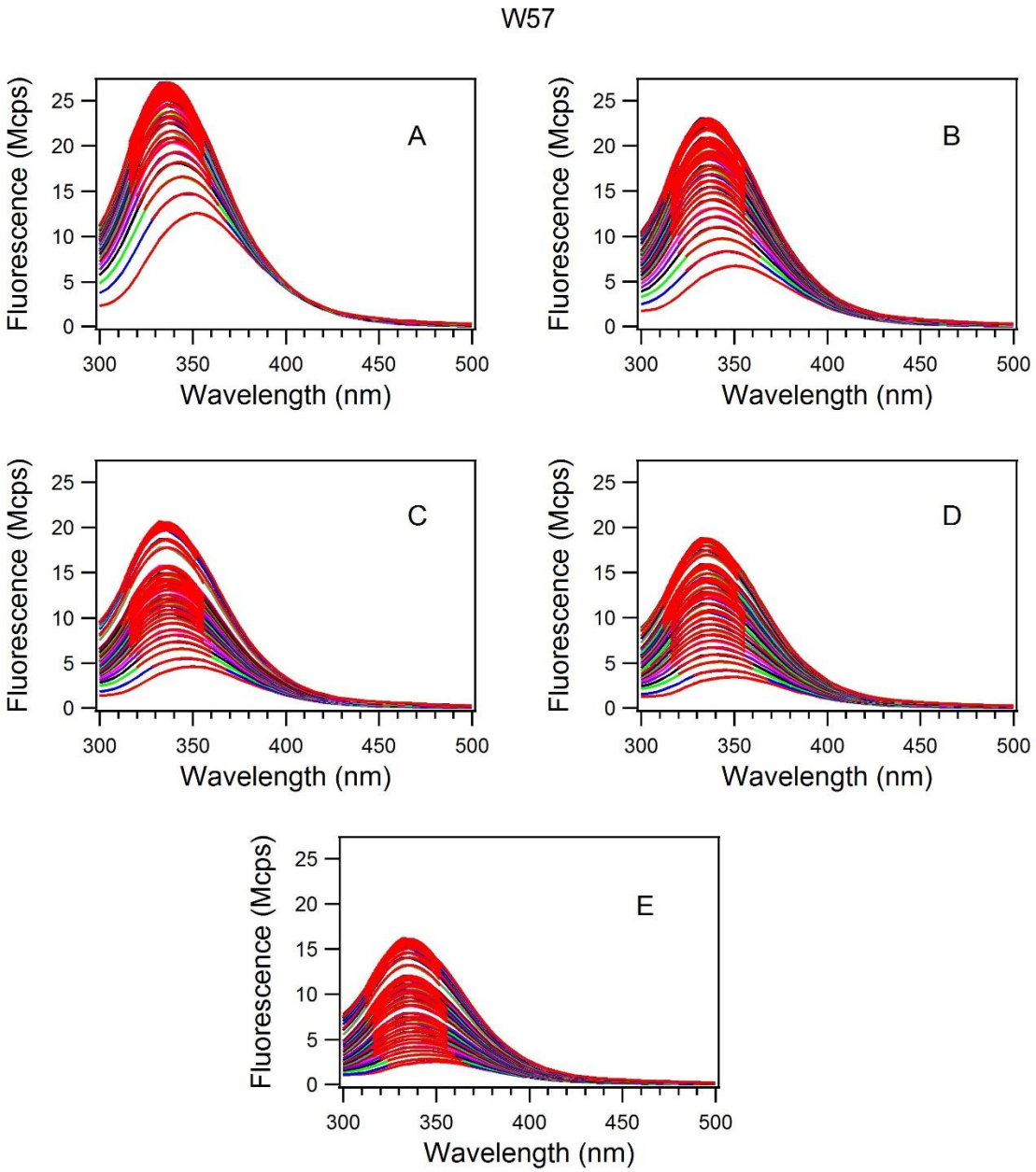

Figure S21: W57 Experiment 3 Data. Depicted are the fluorescence spectra for the 0.0M (A), 0.1M (B), 0.2M (C), 0.3M (D) and 0.4M (E) acrylamide samples for all 6 hours of the experiment. Gaussian fits are in red.

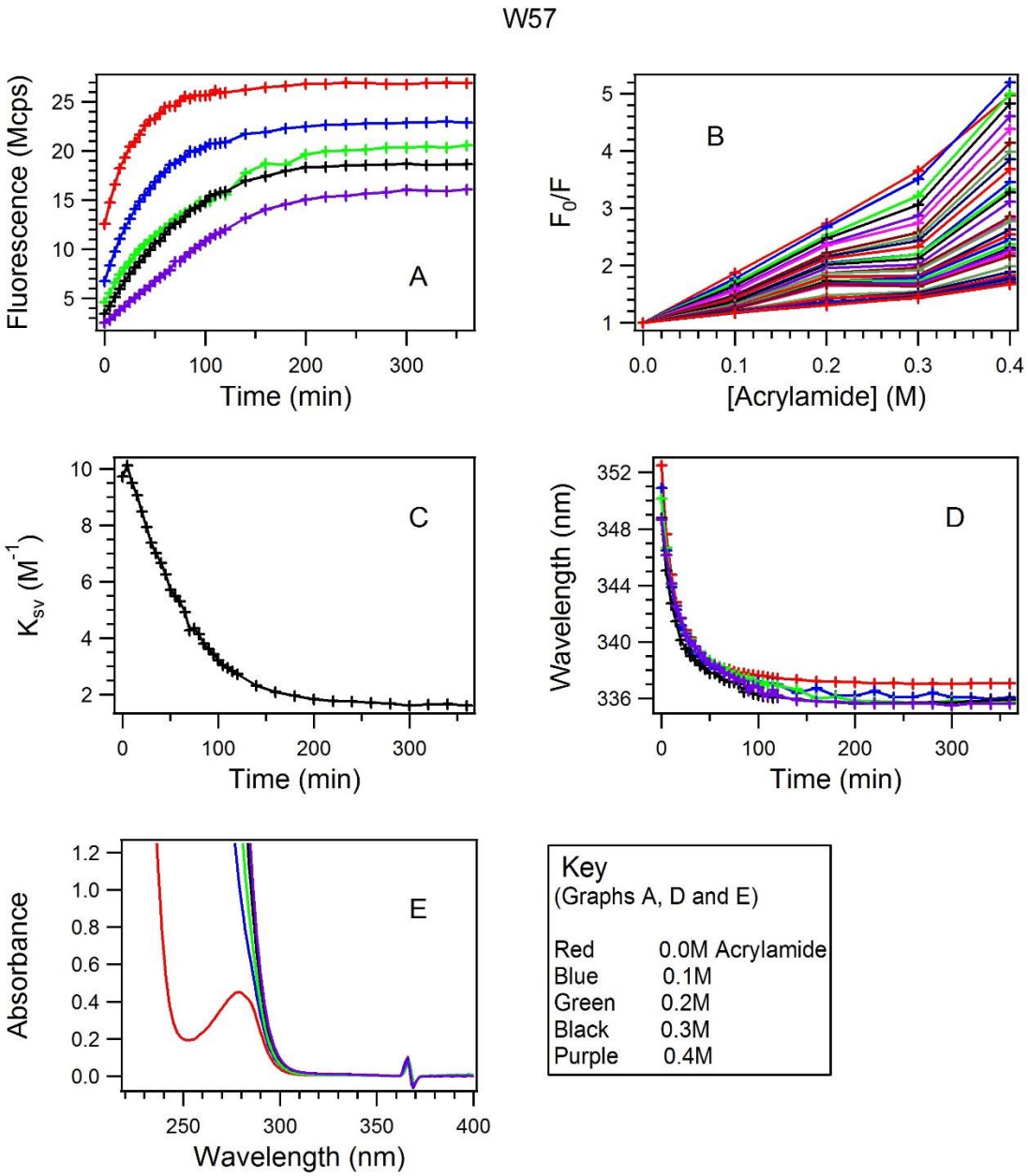

Figure S22: W57 Experiment 3 Data Workup. Panel A depicts fluorescence maxima from the gaussian fits for each sample and time point. For panels A, D and E, red corresponds to the 0.0M acrylamide sample, blue to the 0.1M sample, green to the 0.2M sample, black to the 0.3M sample and purple to the 0.4M sample. Panel B depicts Stern-Volmer plots for each time point in the experiment. Panel C depicts the linear slope (K_{SV}) of the Stern-Vomer plots in panel B over the time of the experiment. Panel D depicts the shift of maximum wavelength of emission for all samples over the time of the experiment. Panel E depicts absorbance spectra for all samples.

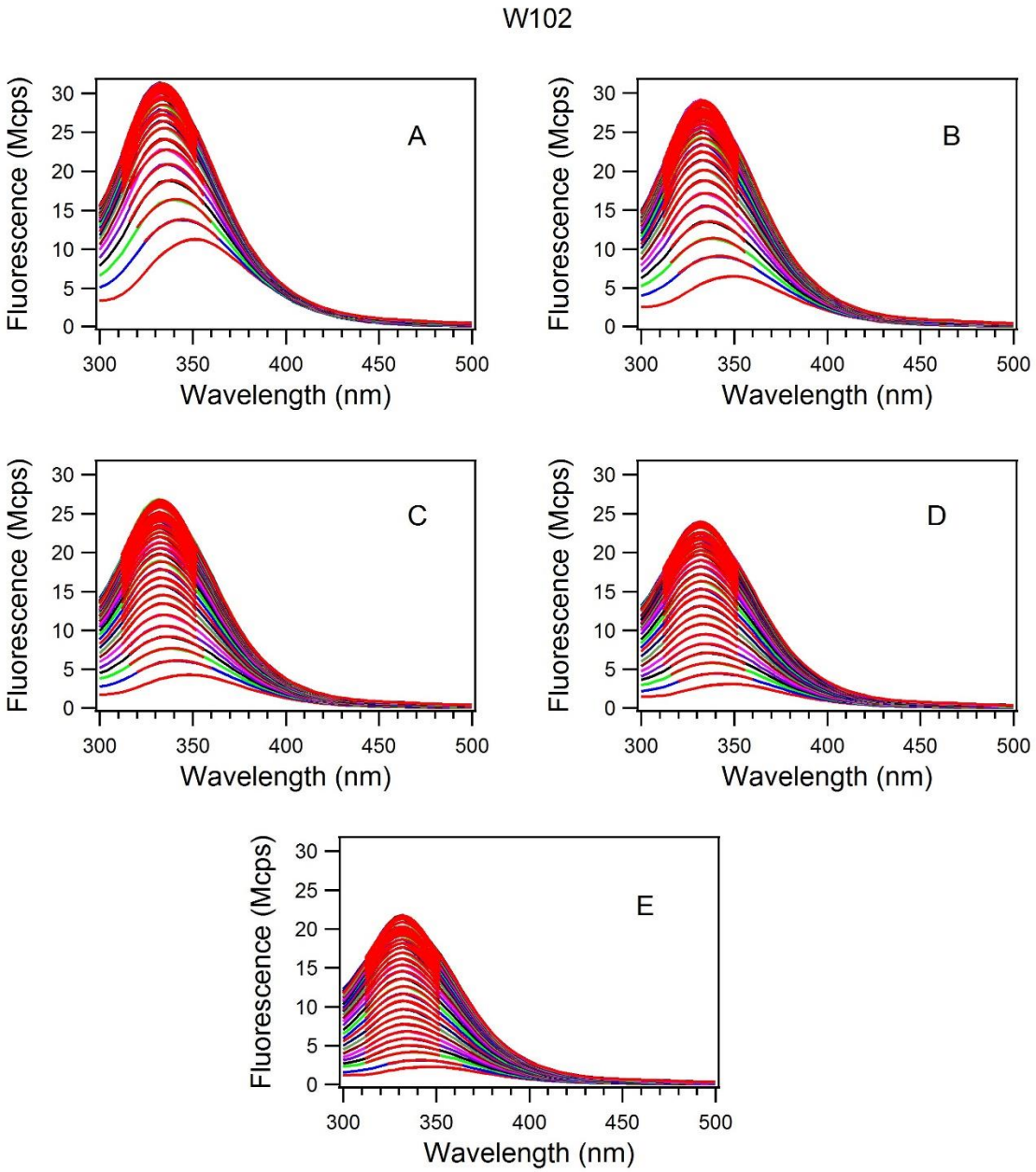

Figure S23: W102 Experiment 1 Data. Depicted are the fluorescence spectra for the 0.0M (A), 0.1M (B), 0.2M (C), 0.3M (D) and 0.4M (E) acrylamide samples for all 6 hours of the experiment. Gaussian fits are in red.

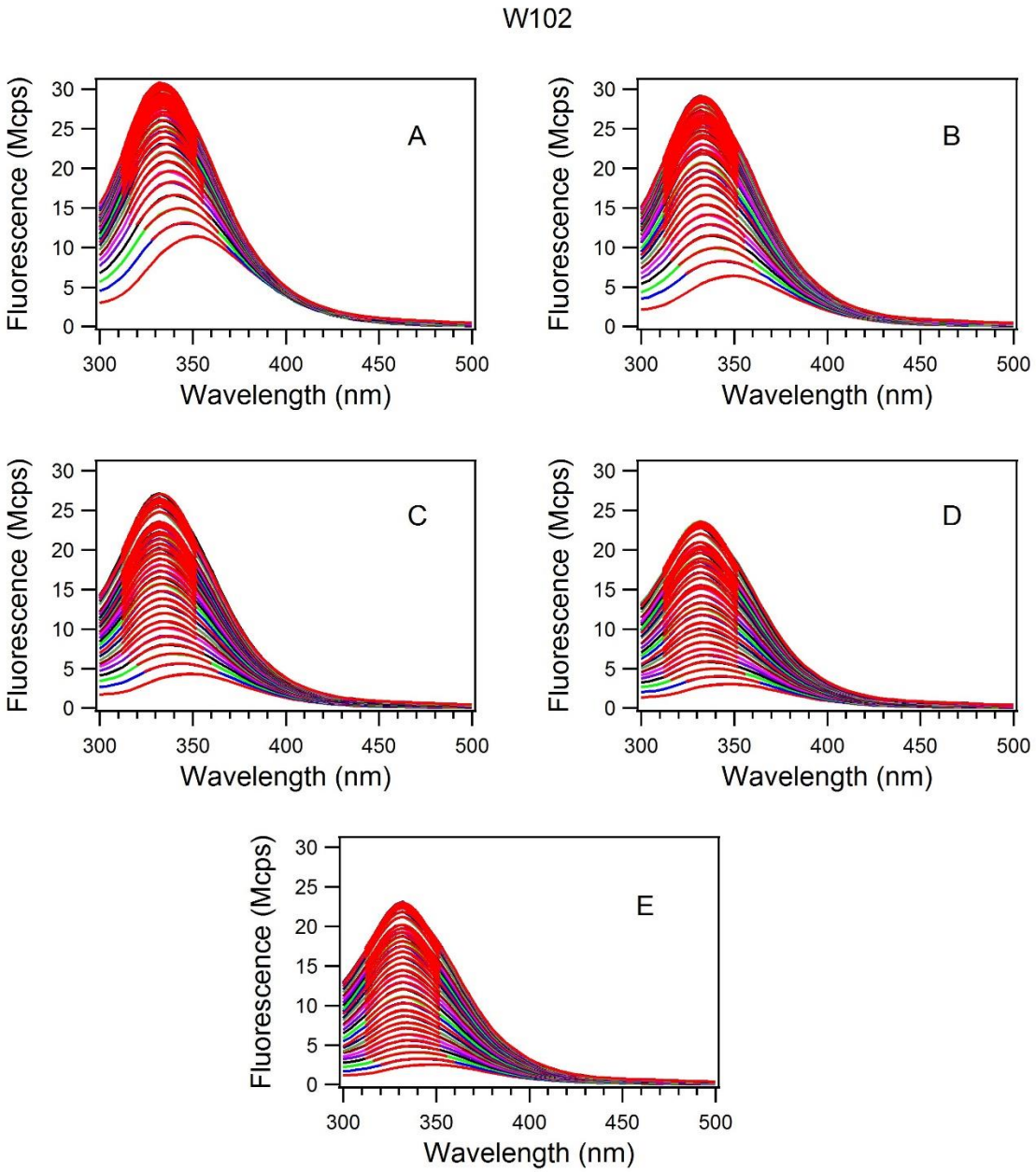

Figure S24: W102 Experiment 2 Data. Depicted are the fluorescence spectra for the 0.0M (A), 0.1M (B), 0.2M (C), 0.3M (D) and 0.4M (E) acrylamide samples for all 6 hours of the experiment. Gaussian fits are in red.

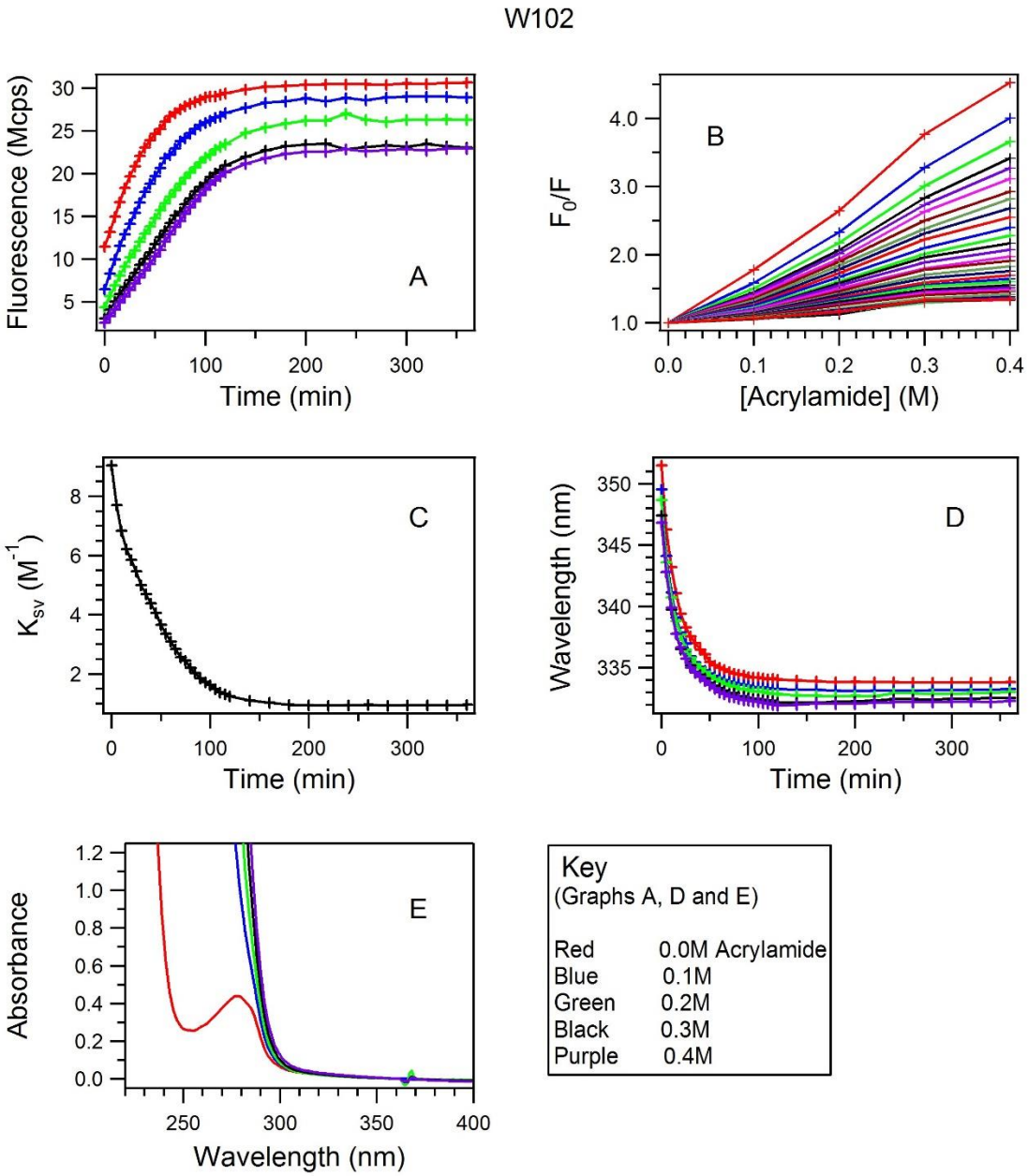

Figure S25: W102 Experiment 2 Data Workup. Panel A depicts fluorescence maxima from the gaussian fits for each sample and time point. For panels A, D and E, red corresponds to the 0.0M acrylamide sample, blue to the 0.1M sample, green to the 0.2M sample, black to the 0.3M sample and purple to the 0.4M sample. Panel B depicts Stern-Volmer plots for each time point in the experiment. Panel C depicts the linear slope (K_{SV}) of the Stern-Vomer plots in panel B over the time of the experiment. Panel D depicts the shift of maximum wavelength of emission for all samples over the time of the experiment. Panel E depicts absorbance spectra for all samples.

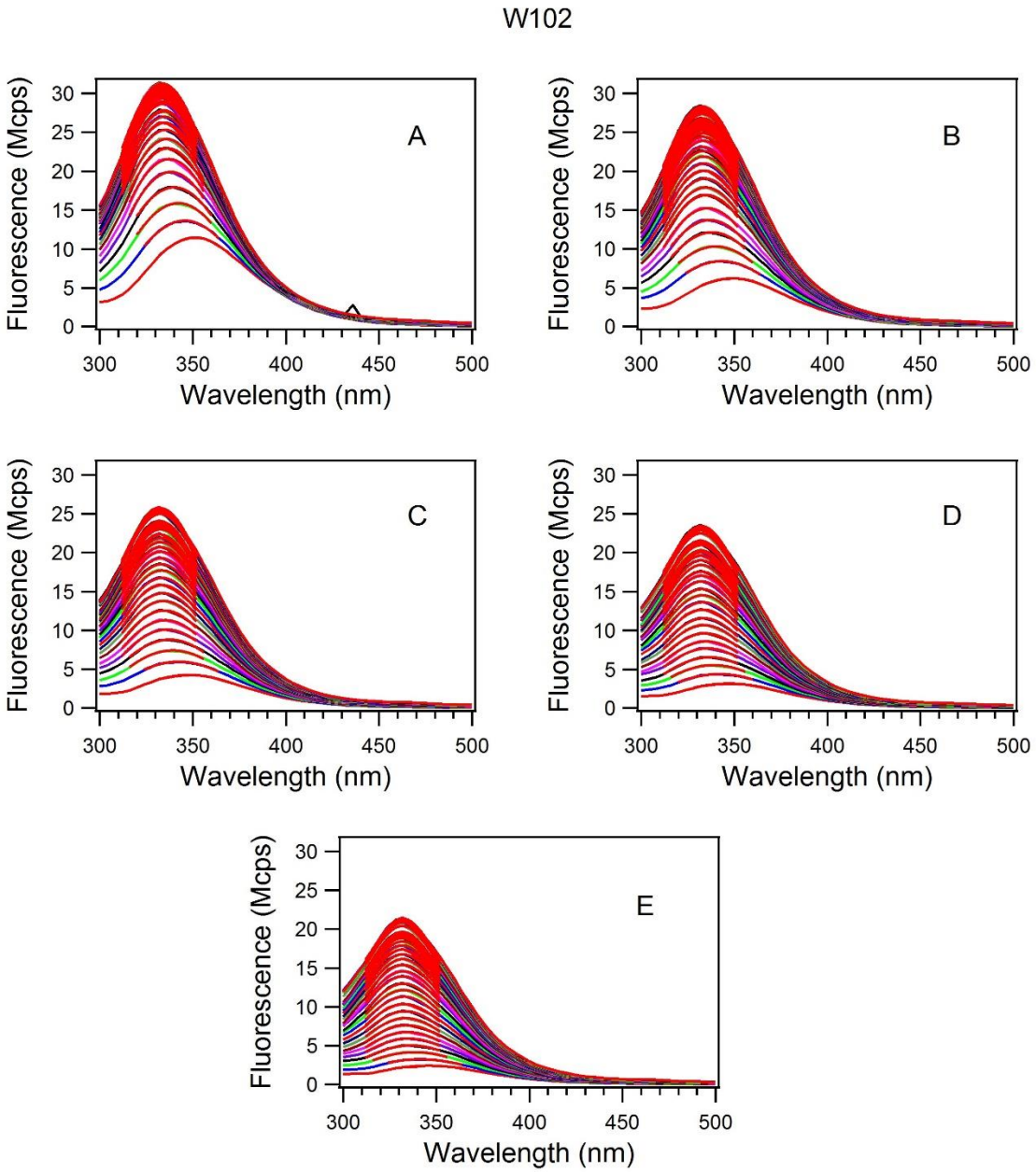

Figure S26: W102 Experiment 3 Data. Depicted are the fluorescence spectra for the 0.0M (A), 0.1M (B), 0.2M (C), 0.3M (D) and 0.4M (E) acrylamide samples for all 6 hours of the experiment. Gaussian fits are in red.

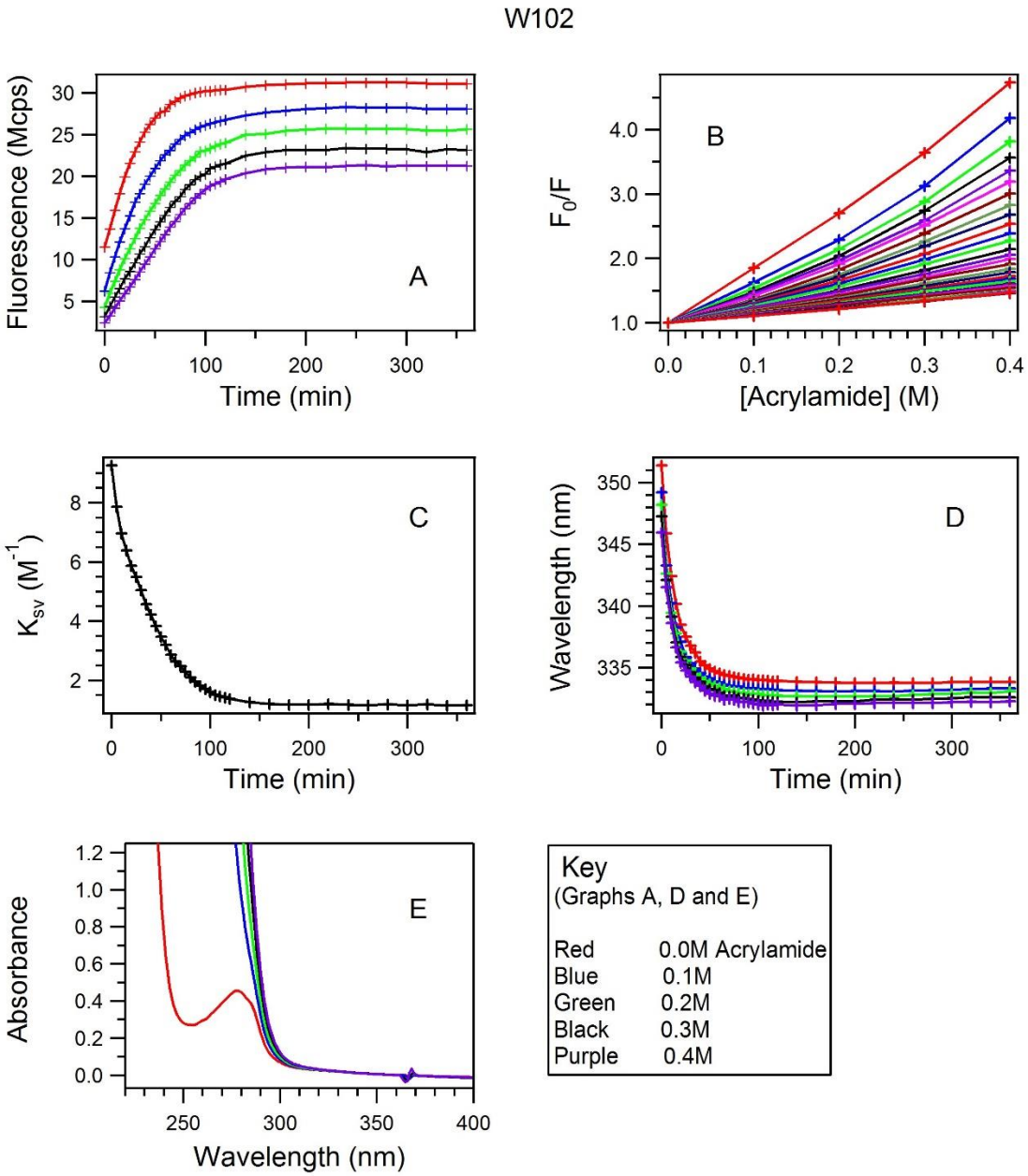

Figure S27: W102 Experiment 3 Data Workup. Panel A depicts fluorescence maxima from the gaussian fits for each sample and time point. For panels A, D and E, red corresponds to the 0.0M acrylamide sample, blue to the 0.1M sample, green to the 0.2M sample, black to the 0.3M sample and purple to the 0.4M sample. Panel B depicts Stern-Volmer plots for each time point in the experiment. Panel C depicts the linear slope (K_{SV}) of the Stern-Vomer plots in panel B over the time of the experiment. Panel D depicts the shift of maximum wavelength of emission for all samples over the time of the experiment. Panel E depicts absorbance spectra for all samples.

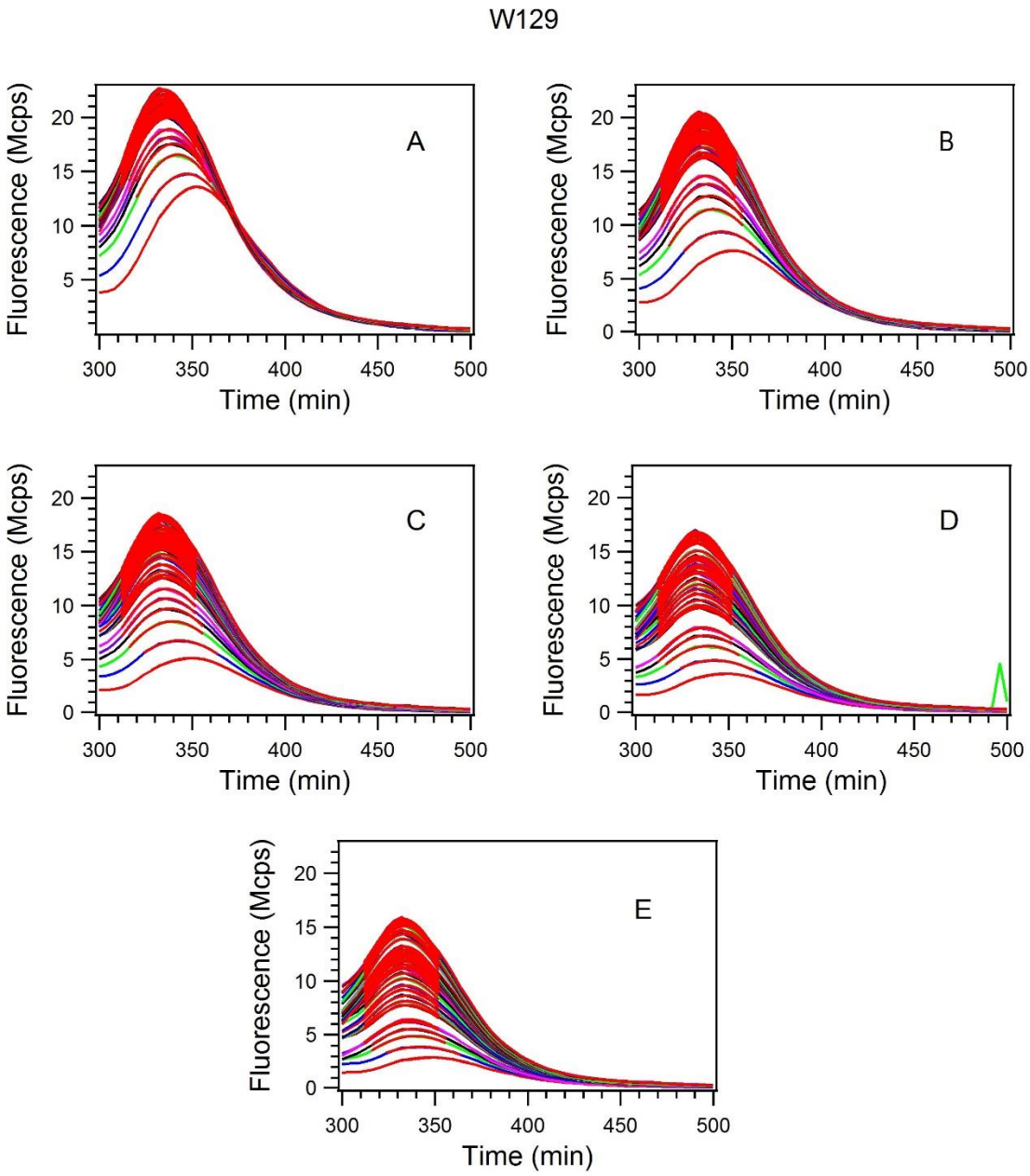

Figure S28: W129 Experiment 1 Data. Depicted are the fluorescence spectra for the 0.0M (A), 0.1M (B), 0.2M (C), 0.3M (D) and 0.4M (E) acrylamide samples for all 6 hours of the experiment. Gaussian fits are in red.

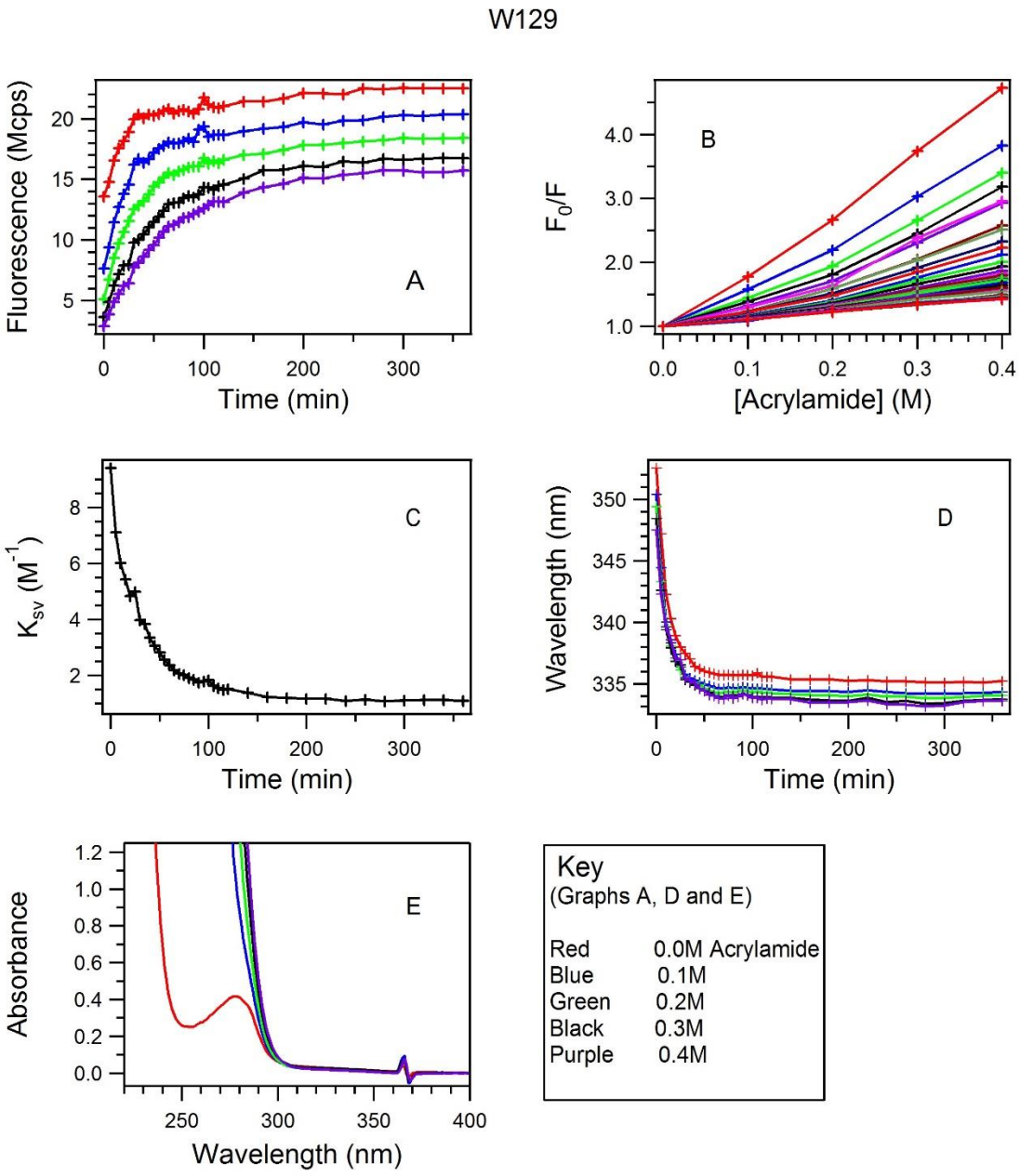

Figure S29: W129 Experiment 1 Data Workup. Panel A depicts fluorescence maxima from the gaussian fits for each sample and time point. For panels A, D and E, red corresponds to the 0.0M acrylamide sample, blue to the 0.1M sample, green to the 0.2M sample, black to the 0.3M sample and purple to the 0.4M sample. Panel B depicts Stern-Volmer plots for each time point in the experiment. Panel C depicts the linear slope (K_{SV}) of the Stern-Vomer plots in panel B over the time of the experiment. Panel D depicts the shift of maximum wavelength of emission for all samples over the time of the experiment. Panel E depicts absorbance spectra for all samples.

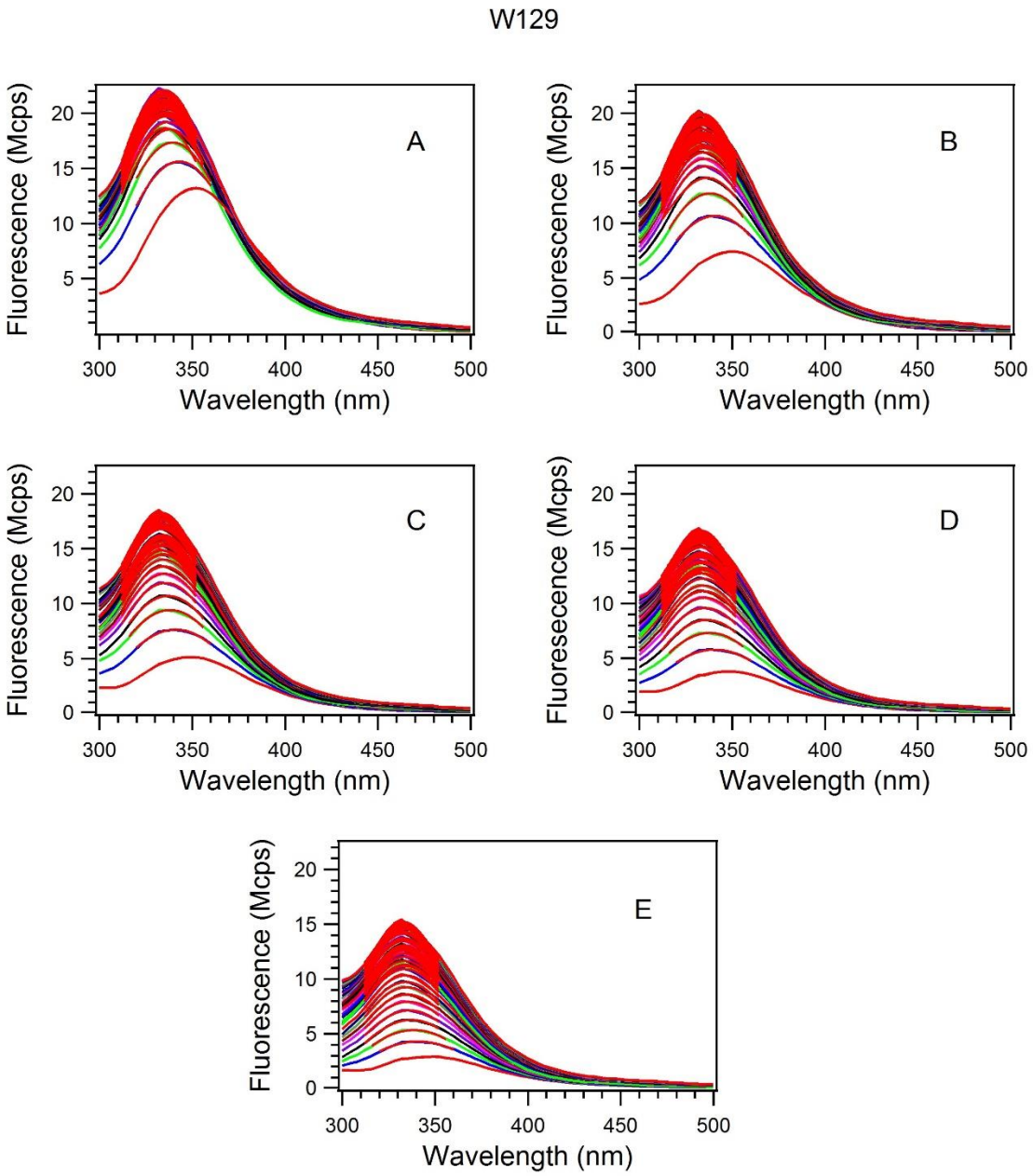

Figure S30: W129 Experiment 2 Data. Depicted are the fluorescence spectra for the 0.0M (A), 0.1M (B), 0.2M (C), 0.3M (D) and 0.4M (E) acrylamide samples for all 6 hours of the experiment. Gaussian fits are in red.

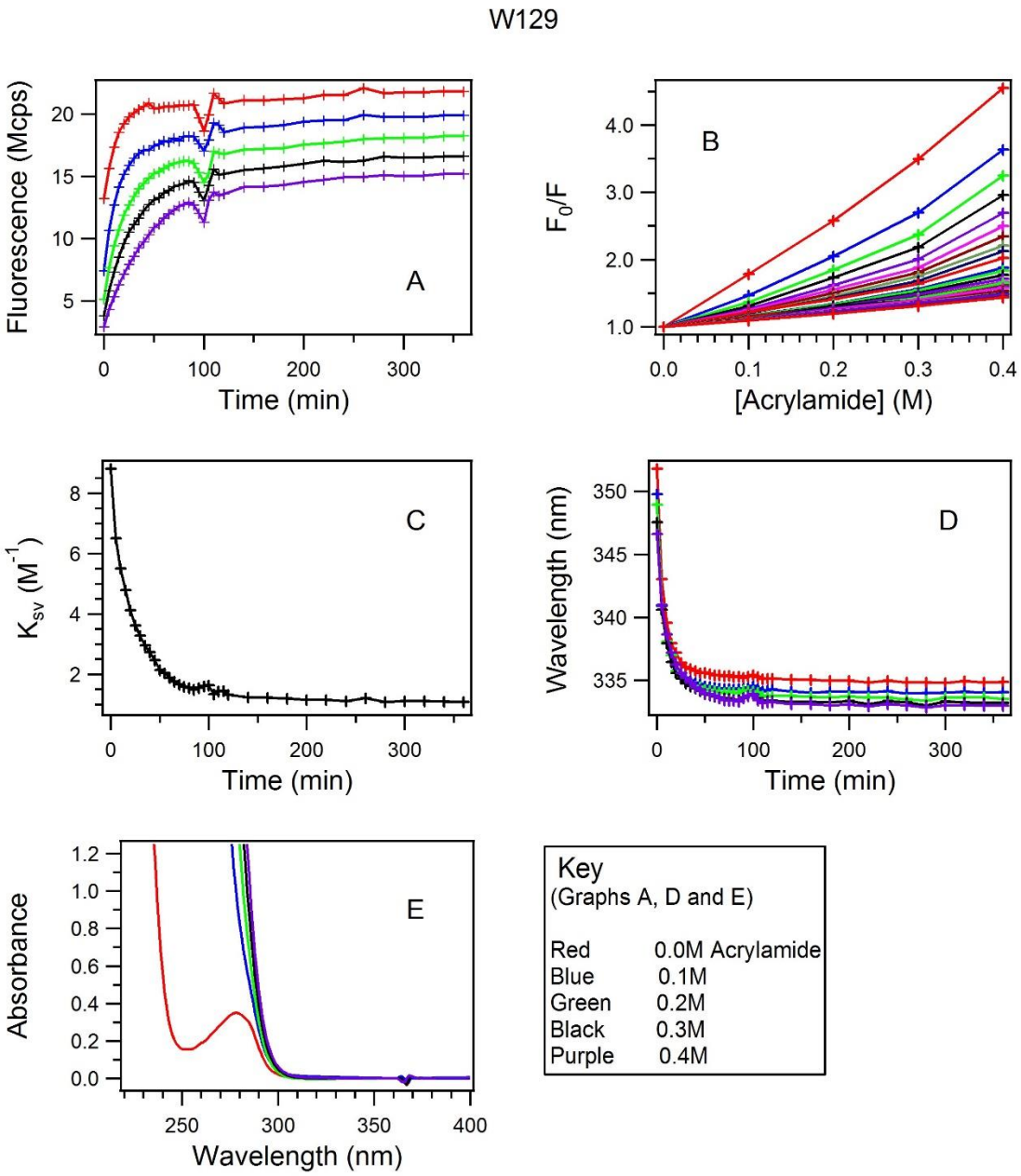

Figure S31: W129 Experiment 2 Data Workup. Panel A depicts fluorescence maxima from the gaussian fits for each sample and time point. The, unanimous and anomalous drop in fluorescence intensity may have been caused by a faulty power supply, resulting in the observed fluctuations K_{SV} values remained unchanged. For panels A, D and E, red corresponds to the 0.0M acrylamide sample, blue to the 0.1M sample, green to the 0.2M sample, black to the 0.3M sample and purple to the 0.4M sample. Panel B depicts Stern-Volmer plots for each time point in the experiment. Panel C depicts the linear slope (K_{SV}) of the Stern-Vomer plots in panel B over the time of the experiment. Panel D depicts the shift of maximum wavelength of emission for all samples over the time of the experiment. Panel E depicts absorbance spectra for all samples.

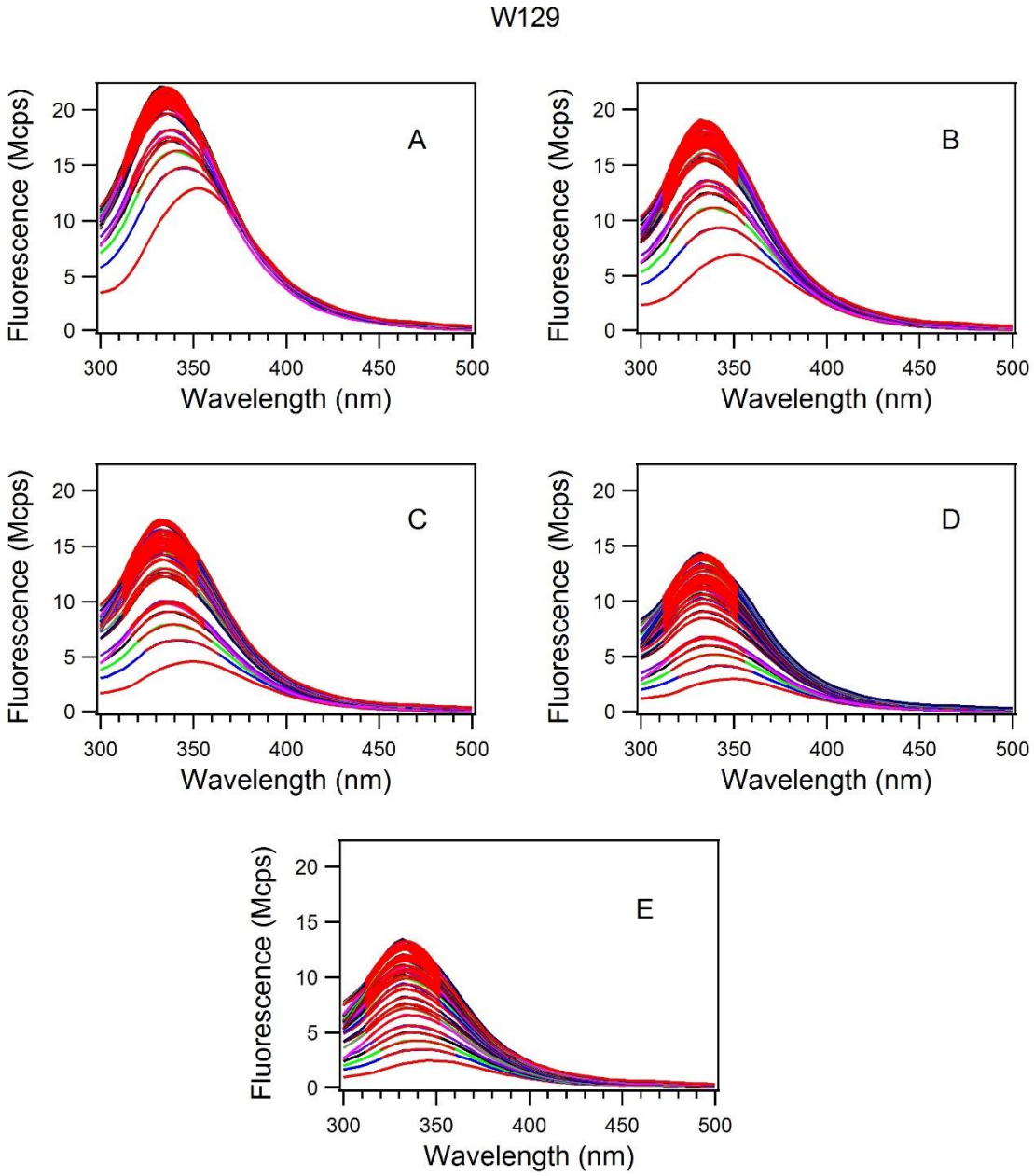

Figure S32: W129 Experiment 3 Data. Depicted are the fluorescence spectra for the 0.0M (A), 0.1M (B), 0.2M (C), 0.3M (D) and 0.4M (E) acrylamide samples for all 6 hours of the experiment. Gaussian fits are in red.

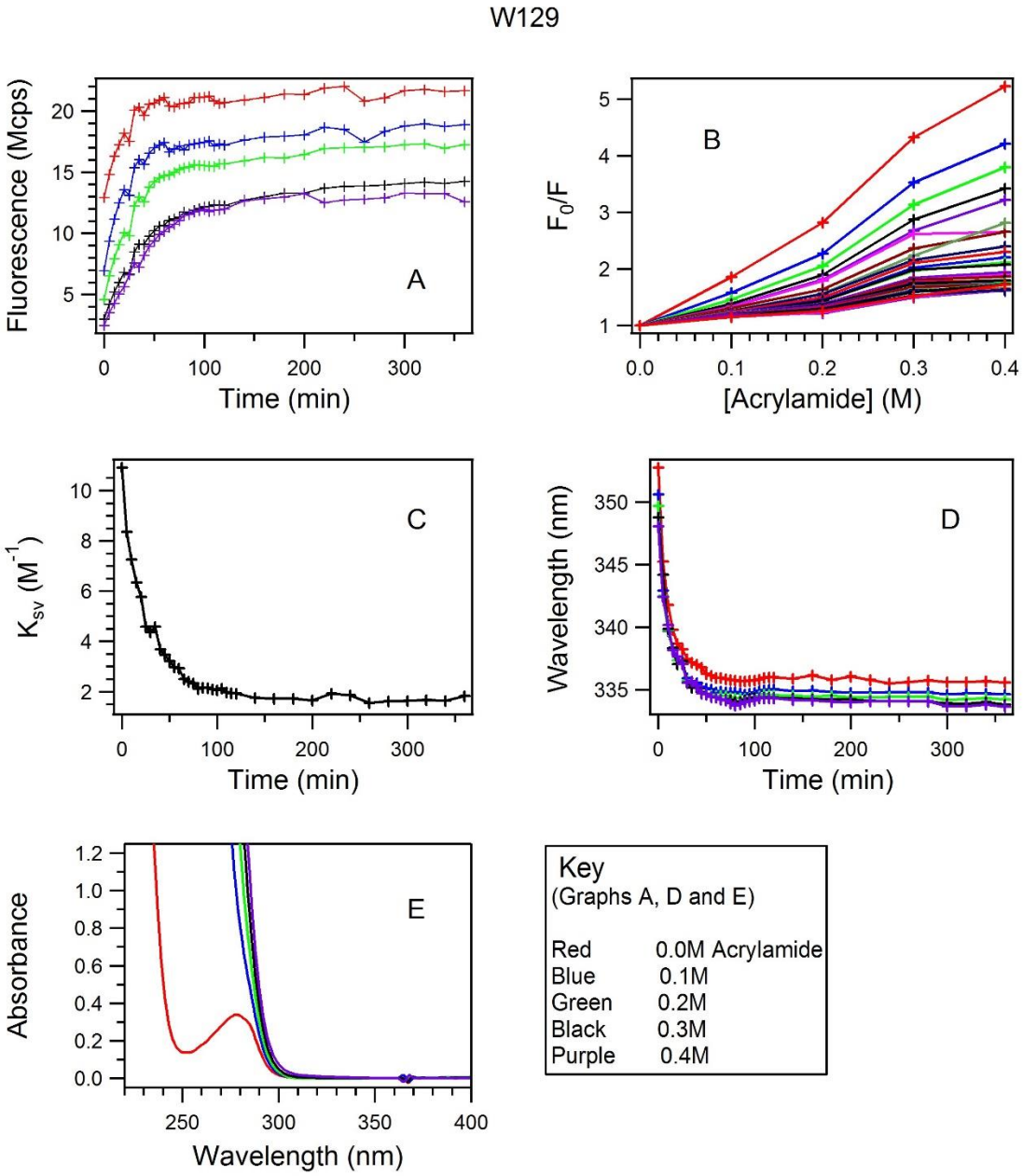

Figure S33: W129 Experiment 3 Data Workup. Panel A depicts fluorescence maxima from the gaussian fits for each sample and time point. For panels A, D and E, red corresponds to the 0.0M acrylamide sample, blue to the 0.1M sample, green to the 0.2M sample, black to the 0.3M sample and purple to the 0.4M sample. Panel B depicts Stern-Volmer plots for each time point in the experiment. Panel C depicts the linear slope (K_{SV}) of the Stern-Vomer plots in panel B over the time of the experiment. Panel D depicts the shift of maximum wavelength of emission for all samples over the time of the experiment. Panel E depicts absorbance spectra for all samples.

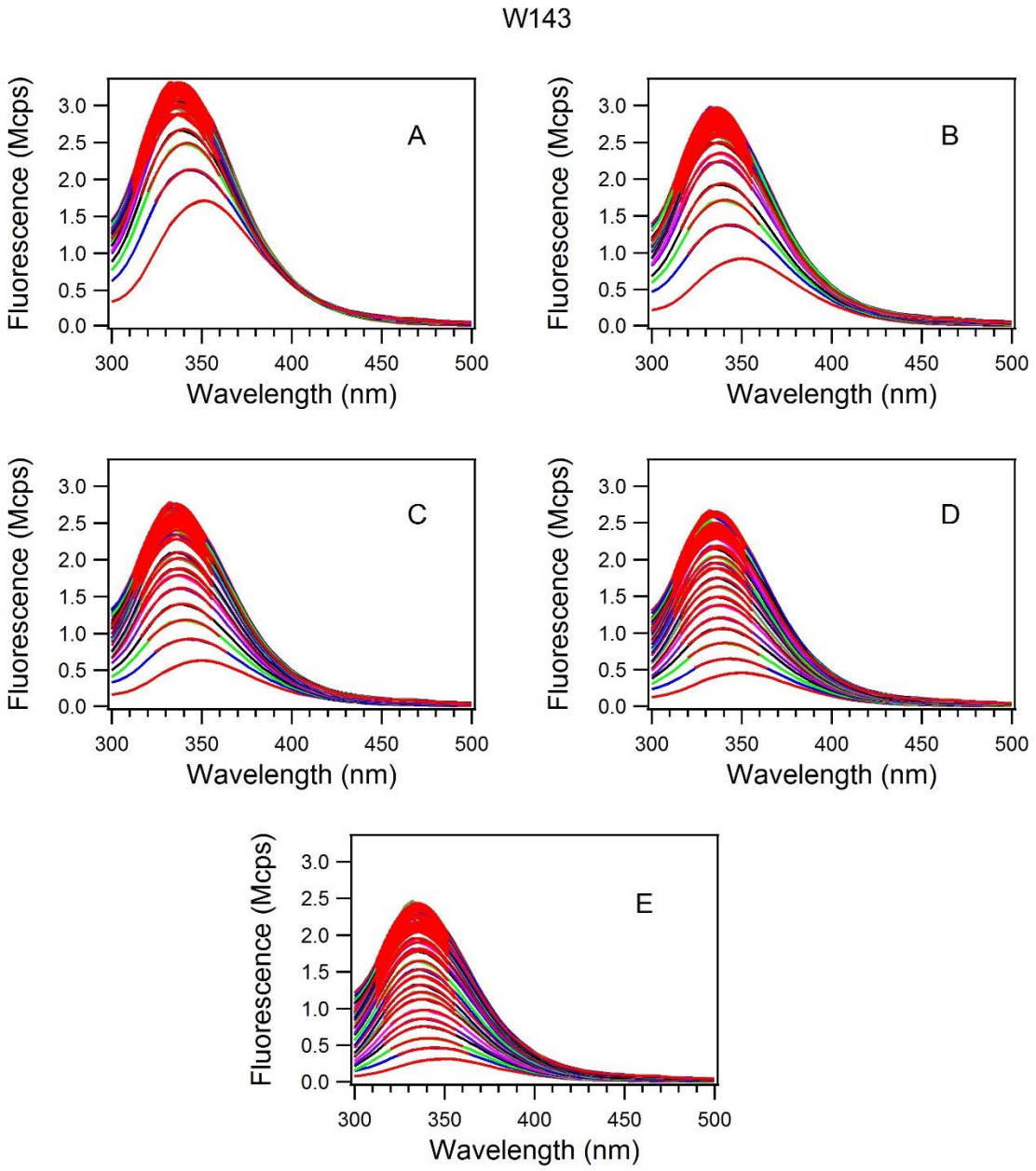

Figure S34: W143 Experiment 1 Data. Depicted are the fluorescence spectra for the 0.0M (A), 0.1M (B), 0.2M (C), 0.3M (D) and 0.4M (E) acrylamide samples for all 6 hours of the experiment. Gaussian fits are in red.

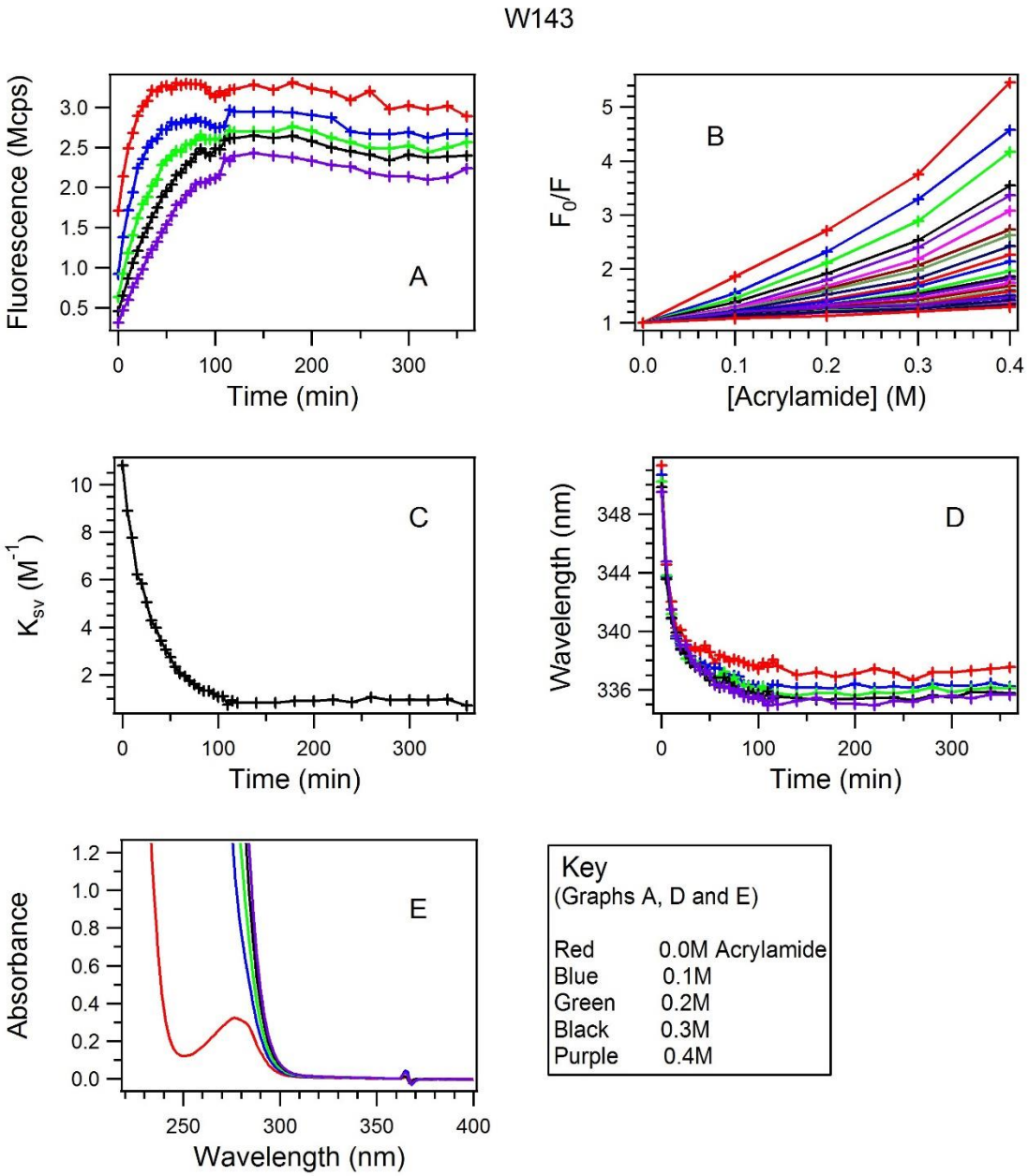

Figure S35: W143 Experiment 1 Data Workup. Panel A depicts fluorescence maxima from the gaussian fits for each sample and time point. For panels A, D and E, red corresponds to the 0.0M acrylamide sample, blue to the 0.1M sample, green to the 0.2M sample, black to the 0.3M sample and purple to the 0.4M sample. Panel B depicts Stern-Volmer plots for each time point in the experiment. Panel C depicts the linear slope (K_{SV}) of the Stern-Vomer plots in panel B over the time of the experiment. Panel D depicts the shift of maximum wavelength of emission for all samples over the time of the experiment. Panel E depicts absorbance spectra for all samples.

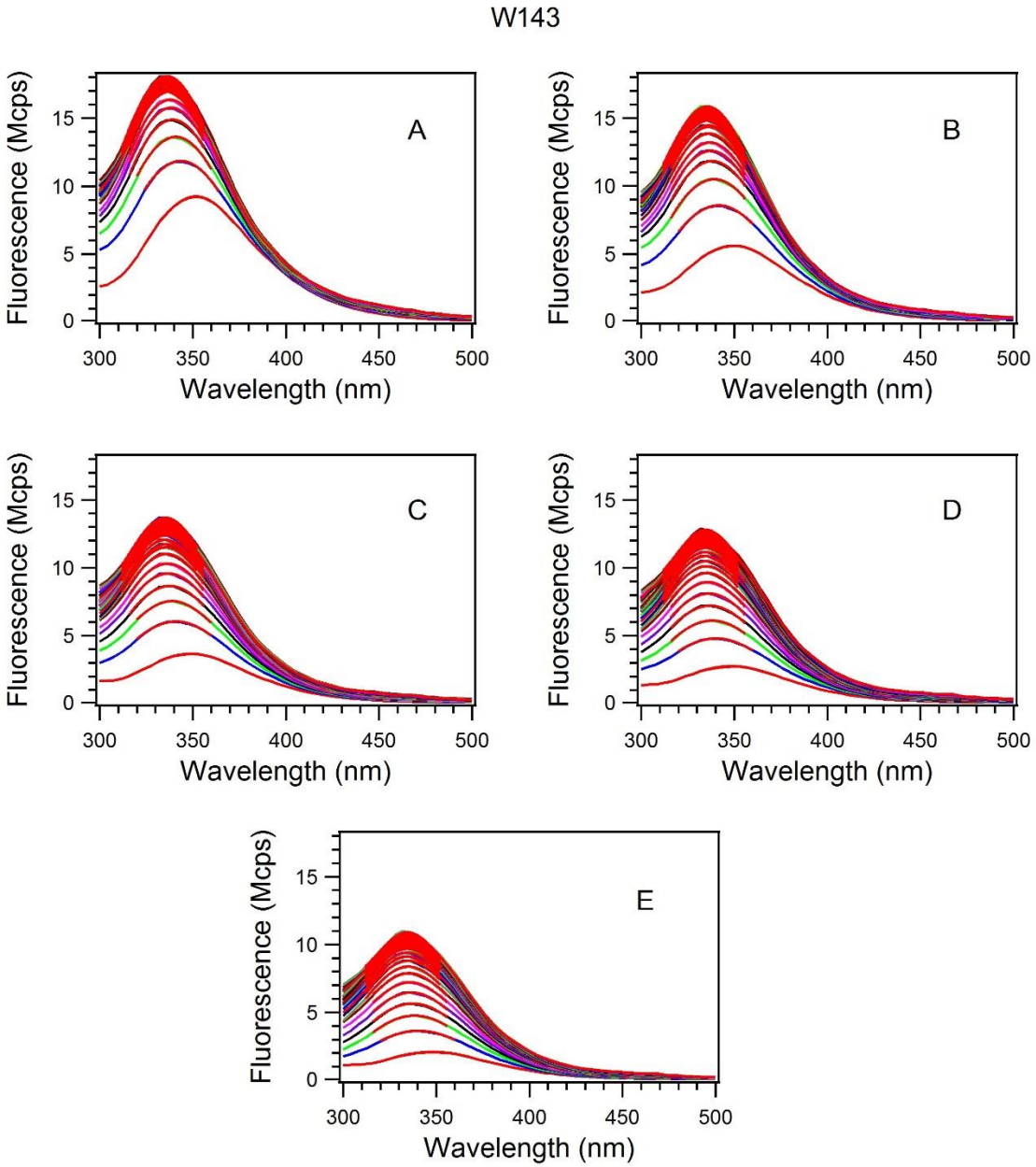

Figure S36: W143 Experiment 2 Data. Depicted are the fluorescence spectra for the 0.0M (A), 0.1M (B), 0.2M (C), 0.3M (D) and 0.4M (E) acrylamide samples for all 6 hours of the experiment. Gaussian fits are in red.

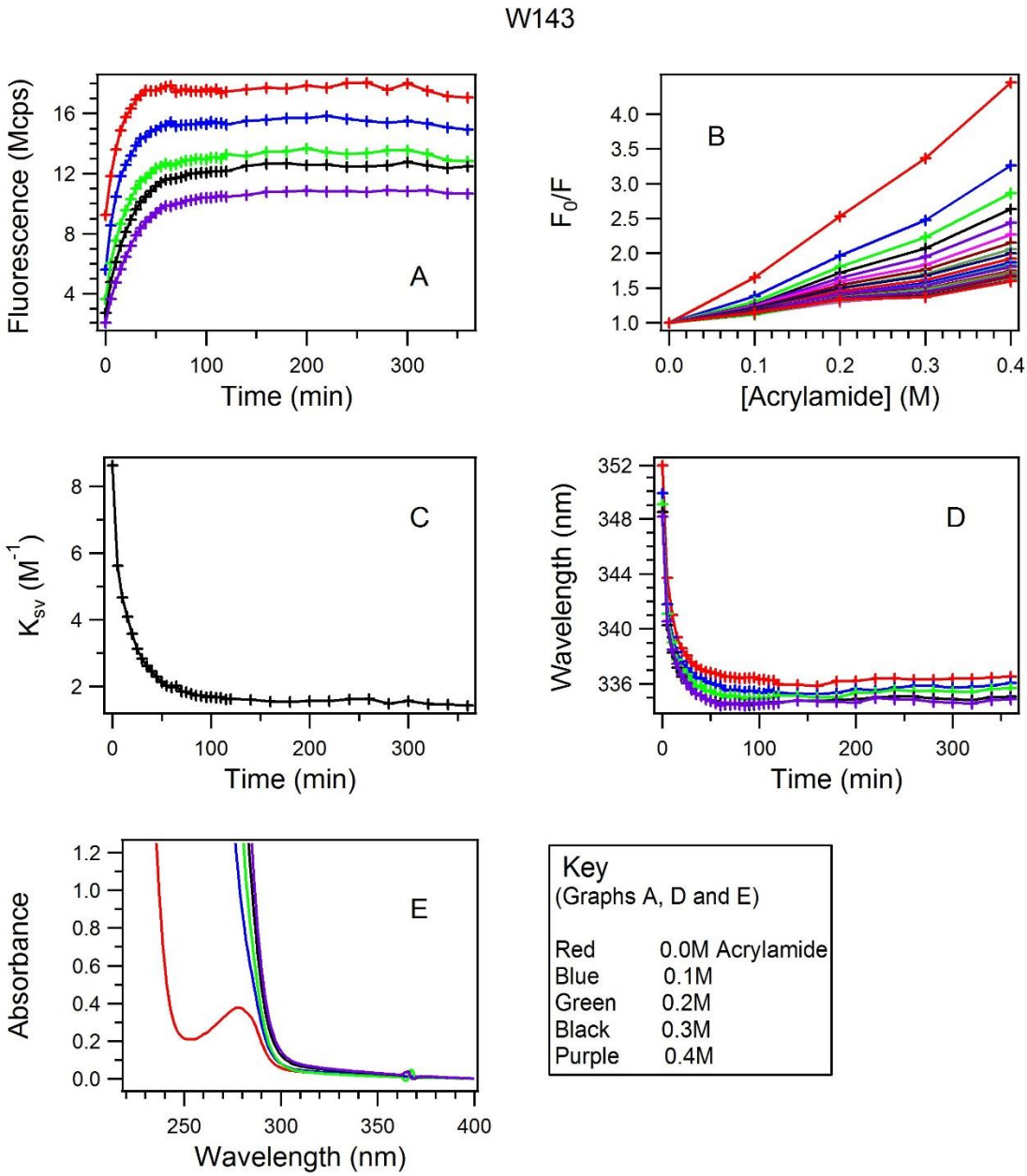

Figure S37: W143 Experiment 2 Data Workup. Panel A depicts fluorescence maxima from the gaussian fits for each sample and time point. For panels A, D and E, red corresponds to the 0.0M acrylamide sample, blue to the 0.1M sample, green to the 0.2M sample, black to the 0.3M sample and purple to the 0.4M sample. Panel B depicts Stern-Volmer plots for each time point in the experiment. Panel C depicts the linear slope (K_{SV}) of the Stern-Vomer plots in panel B over the time of the experiment. Panel D depicts the shift of maximum wavelength of emission for all samples over the time of the experiment. Panel E depicts absorbance spectra for all samples.

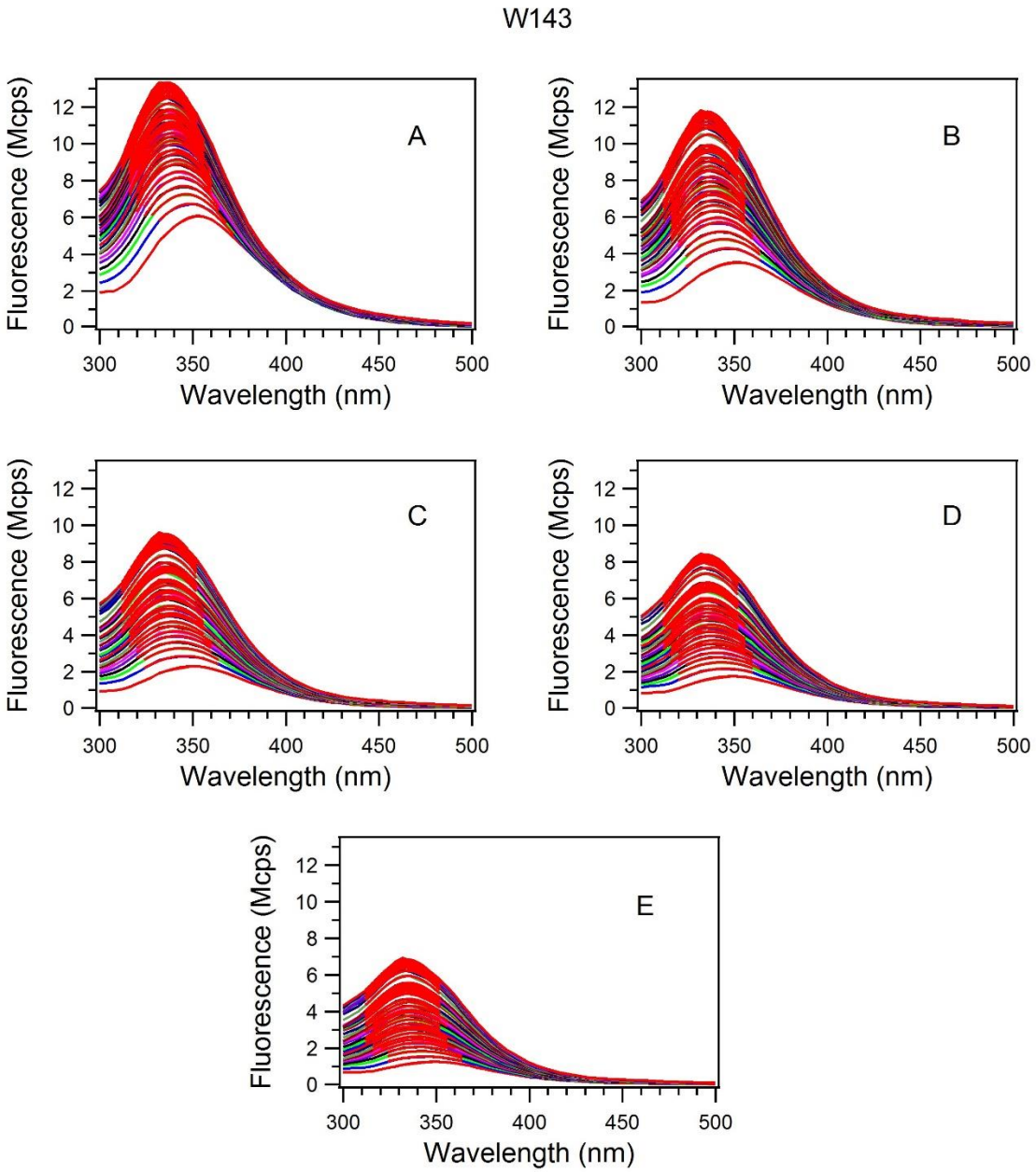

Figure S38: W143 Experiment 3 Data. Depicted are the fluorescence spectra for the 0.0M (A), 0.1M (B), 0.2M (C), 0.3M (D) and 0.4M (E) acrylamide samples for all 6 hours of the experiment. Gaussian fits are in red.

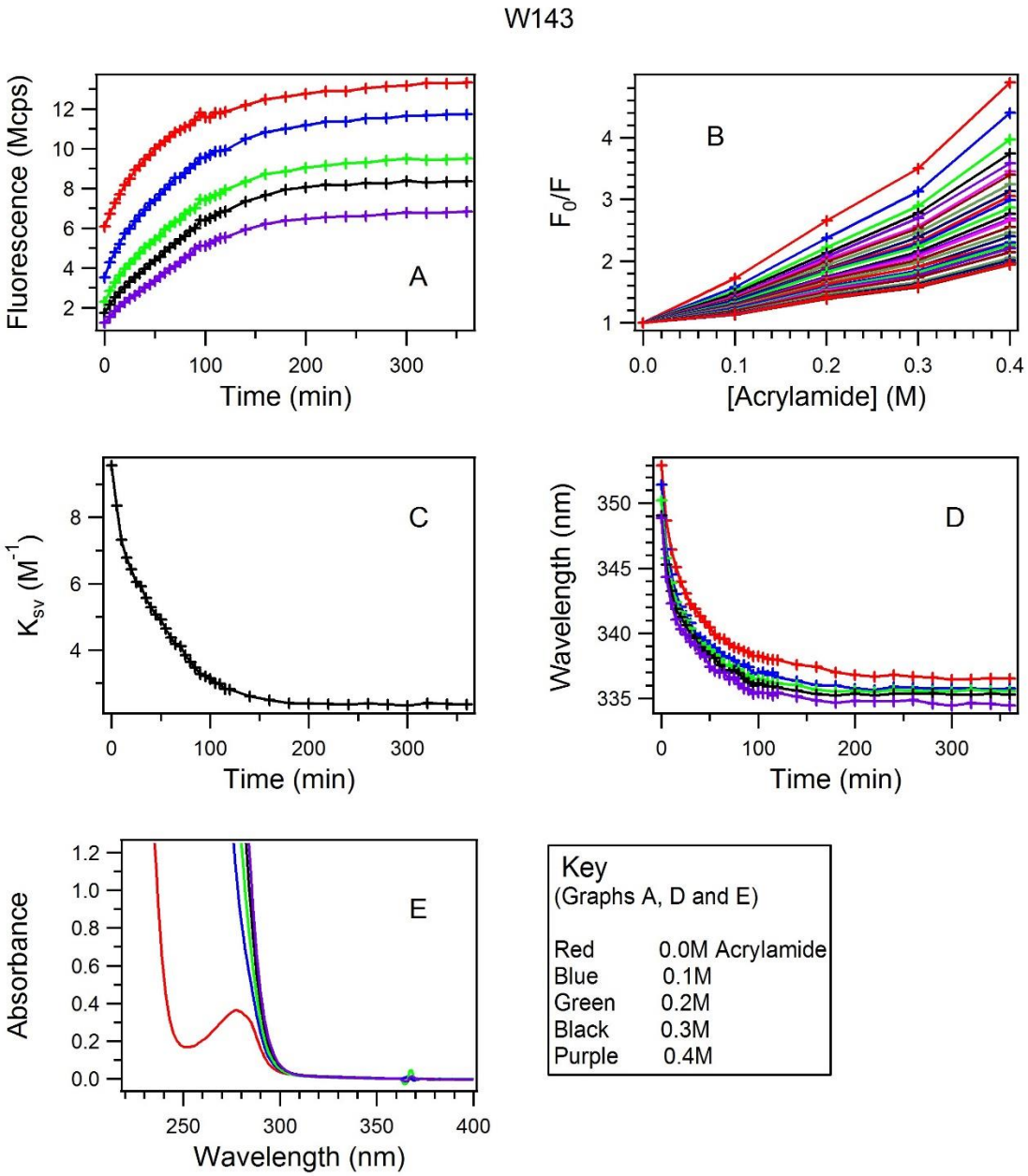

Figure S39: W143 Experiment 3 Data Workup. Panel A depicts fluorescence maxima from the gaussian fits for each sample and time point. For panels A, D and E, red corresponds to the 0.0M acrylamide sample, blue to the 0.1M sample, green to the 0.2M sample, black to the 0.3M sample and purple to the 0.4M sample. Panel B depicts Stern-Volmer plots for each time point in the experiment. Panel C depicts the linear slope (K_{SV}) of the Stern-Vomer plots in panel B over the time of the experiment. Panel D depicts the shift of maximum wavelength of emission for all samples over the time of the experiment. Panel E depicts absorbance spectra for all samples.

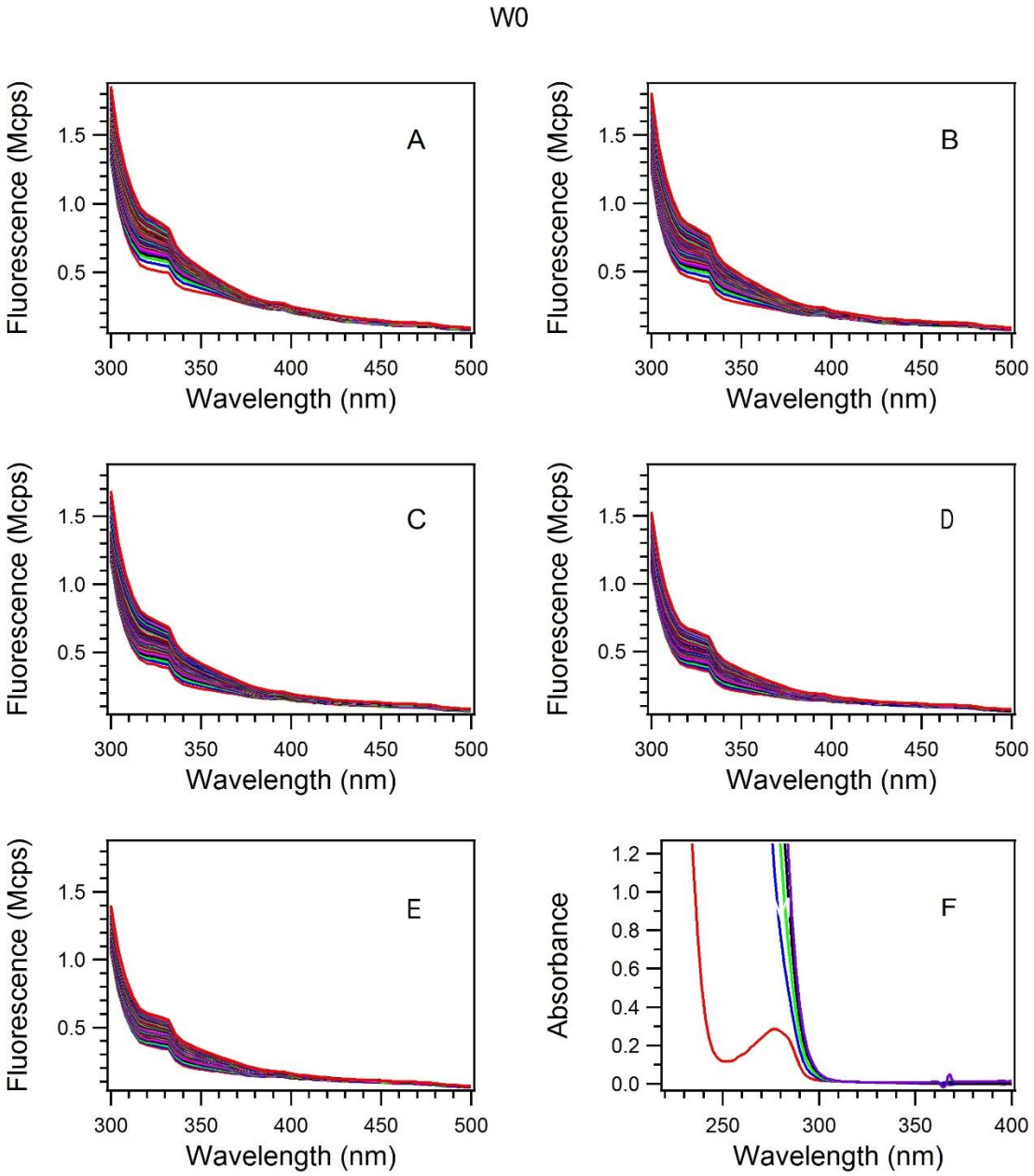

Figure S40: W0 Experiment. A folding experiment was conducted with the W0 mutant of OmpA. In W0, all native trp residues have been mutated to phenylalanine. Depicted are the fluorescence spectra for the 0.0M (A), 0.1M (B), 0.2M (C), 0.3M (D) and 0.4M (E) acrylamide samples for all 6 hours of the experiment. These spectra have not been corrected by subtraction of vesicle scattering. Rather, they were used as tyrosine and vesicle scatter blank spectra to be subtracted out of a single trp OmpA mutant experiment to observe the effects of fluorescence on the K_{SV} vs time data.

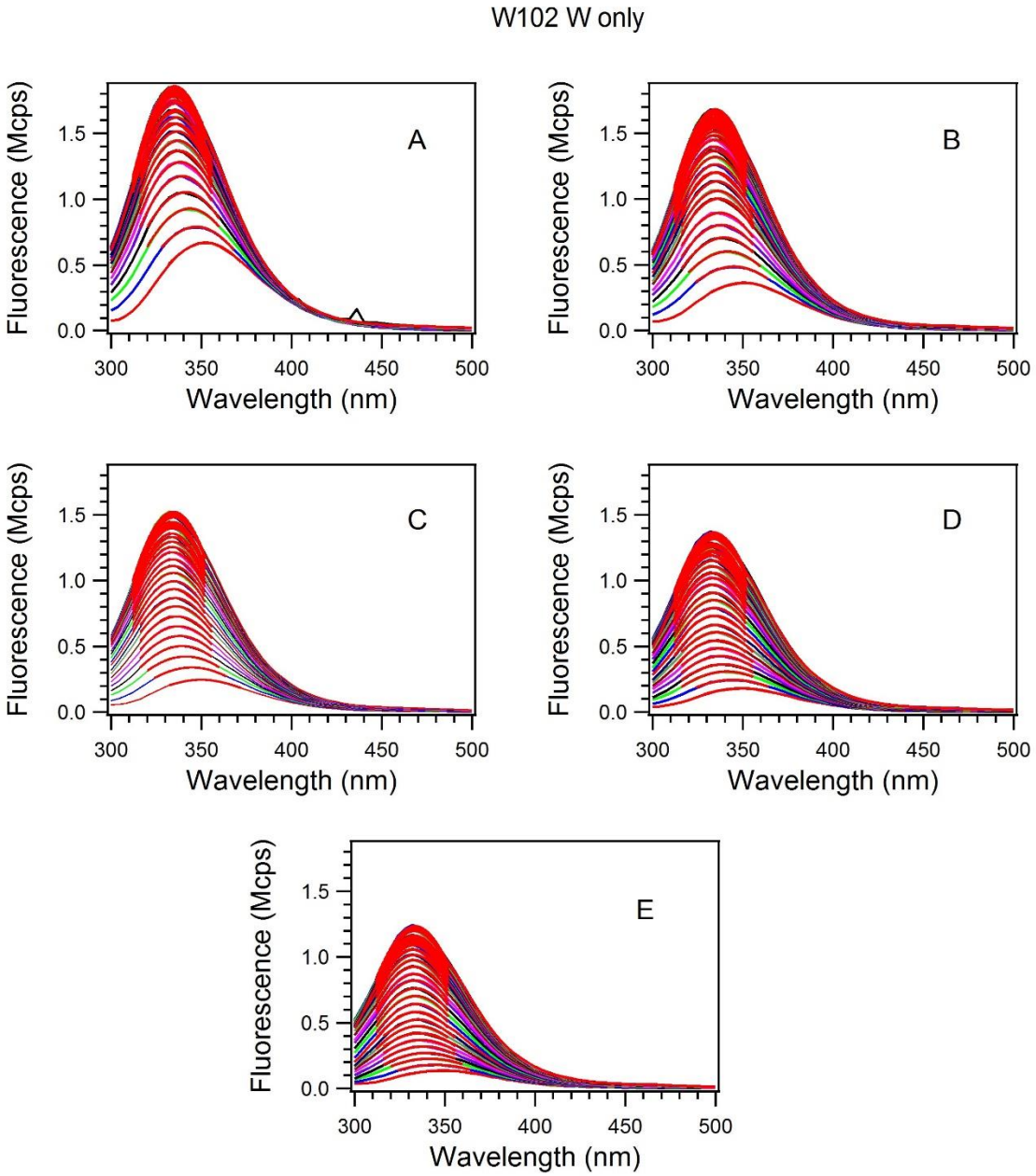

Figure S41: W102 trp only experiment. Depicted are the fluorescence spectra for the 0.0M (A), 0.1M (B), 0.2M (C), 0.3M (D) and 0.4M (E) acrylamide samples for all 6 hours of the experiment. These spectra have been subtracted of OmpA W0 tyrosine emission and vesicle scattter blanks that are shown in Figure S40. Gaussian fits are in red

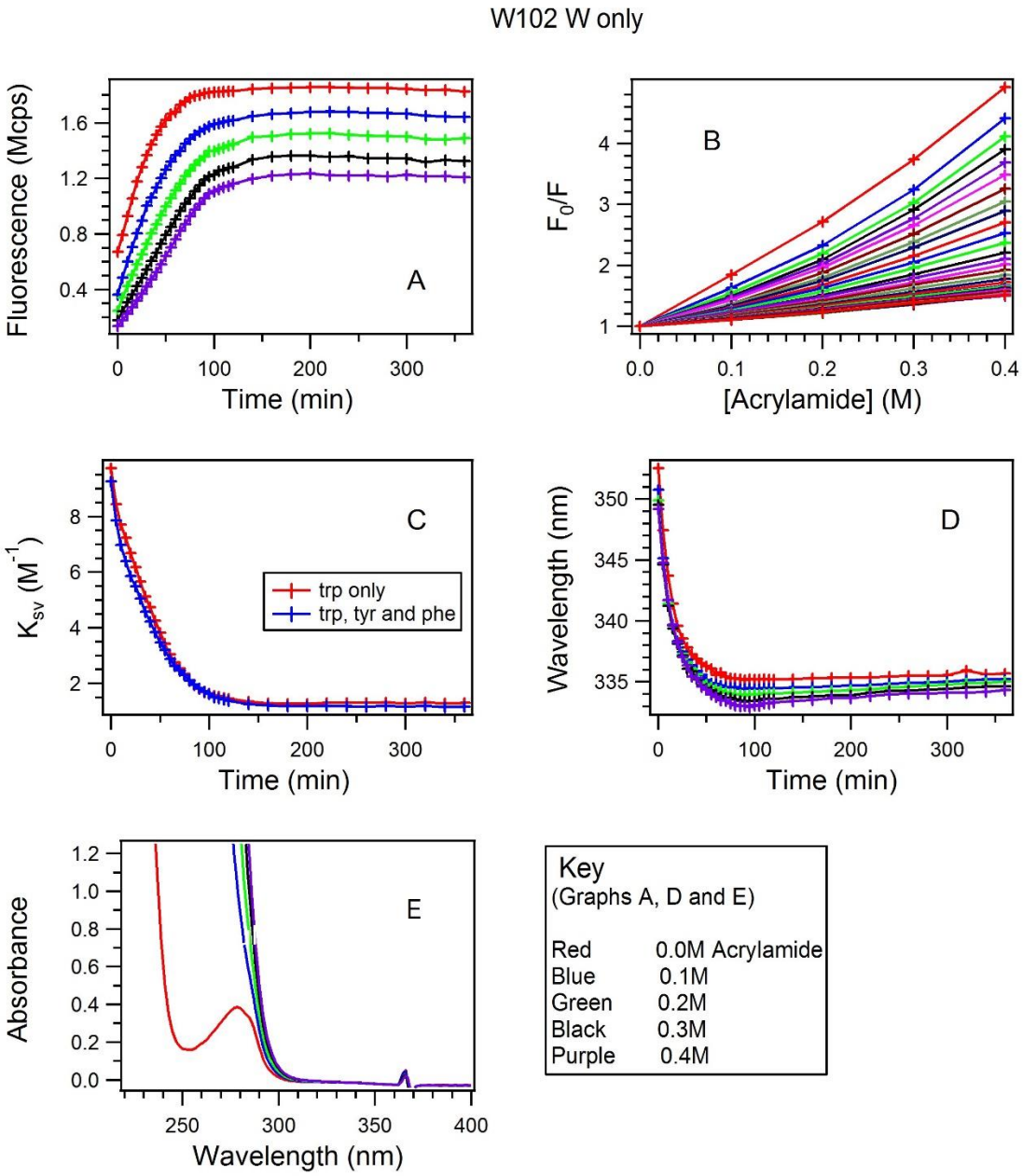

Figure S42: W102 trp only Experiment Data Workup. Panel A depicts fluorescence maxima from the gaussian fits for each sample and time point. For panels A, D and E, red corresponds to the 0.0M acrylamide sample, blue to the 0.1M sample, green to the 0.2M sample, black to the 0.3M sample and purple to the 0.4M sample. Panel B depicts Stern-Volmer plots for each time point in the experiment. Panel C depicts the linear slope (K_{SV}) of the Stern-Vomer plots in panel B (red) over the time of the experiment. Also included in panel C is the K_{SV} data for the same W102 experiment but without subtraction of the tyrosine signal (blue). Panel D depicts the shift of maximum wavelength of emission for all samples over the time of the experiment. Panel E depicts absorbance spectra for all samples.

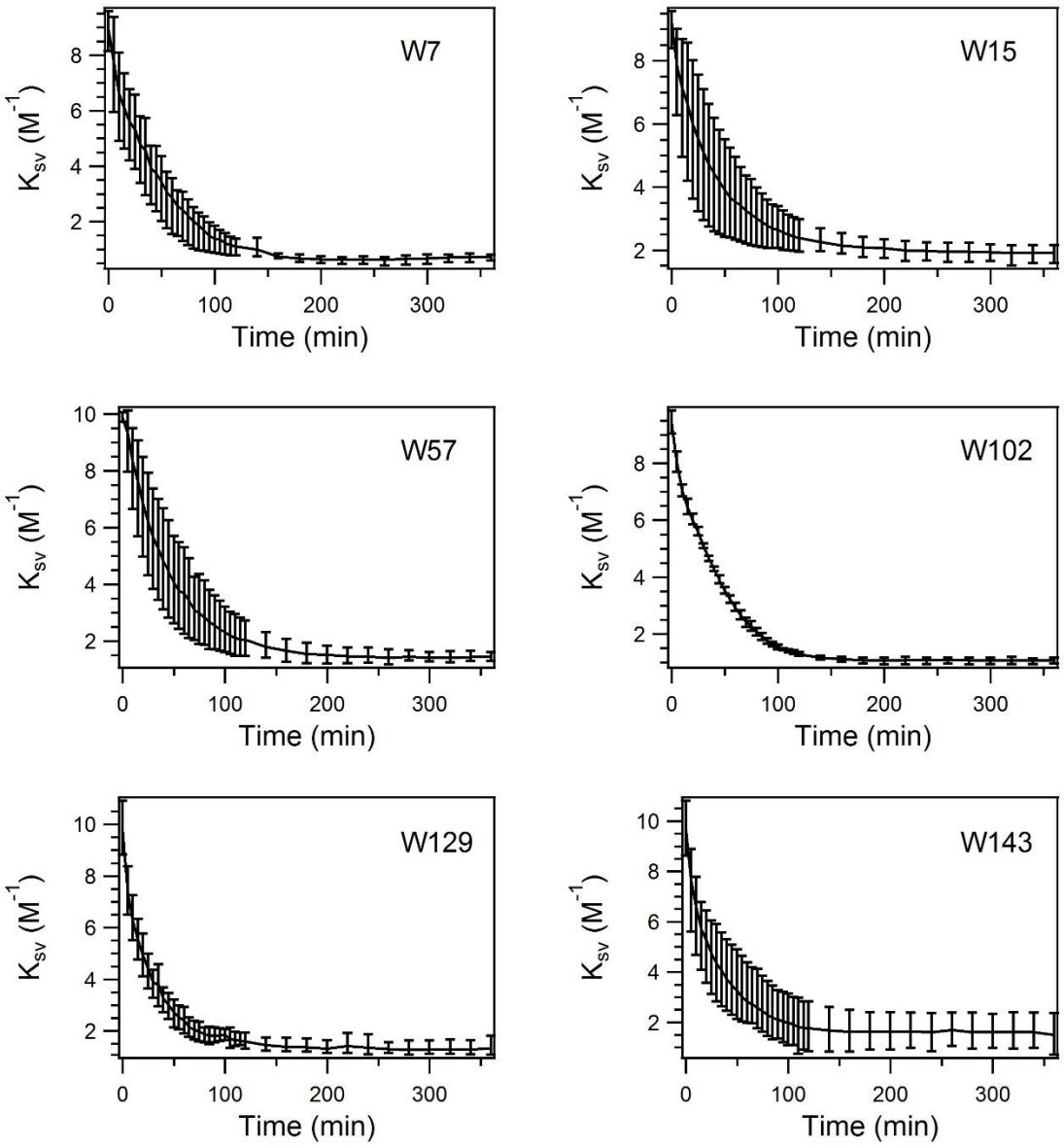

Figure S43: K_{sv} Error Bars. Shown here are the average K_{SV} versus time plots for all one trp mutants with error bars. These error bars indicate the upper and lower bounds of experimentally determined K_{SV} versus time data for each mutant.

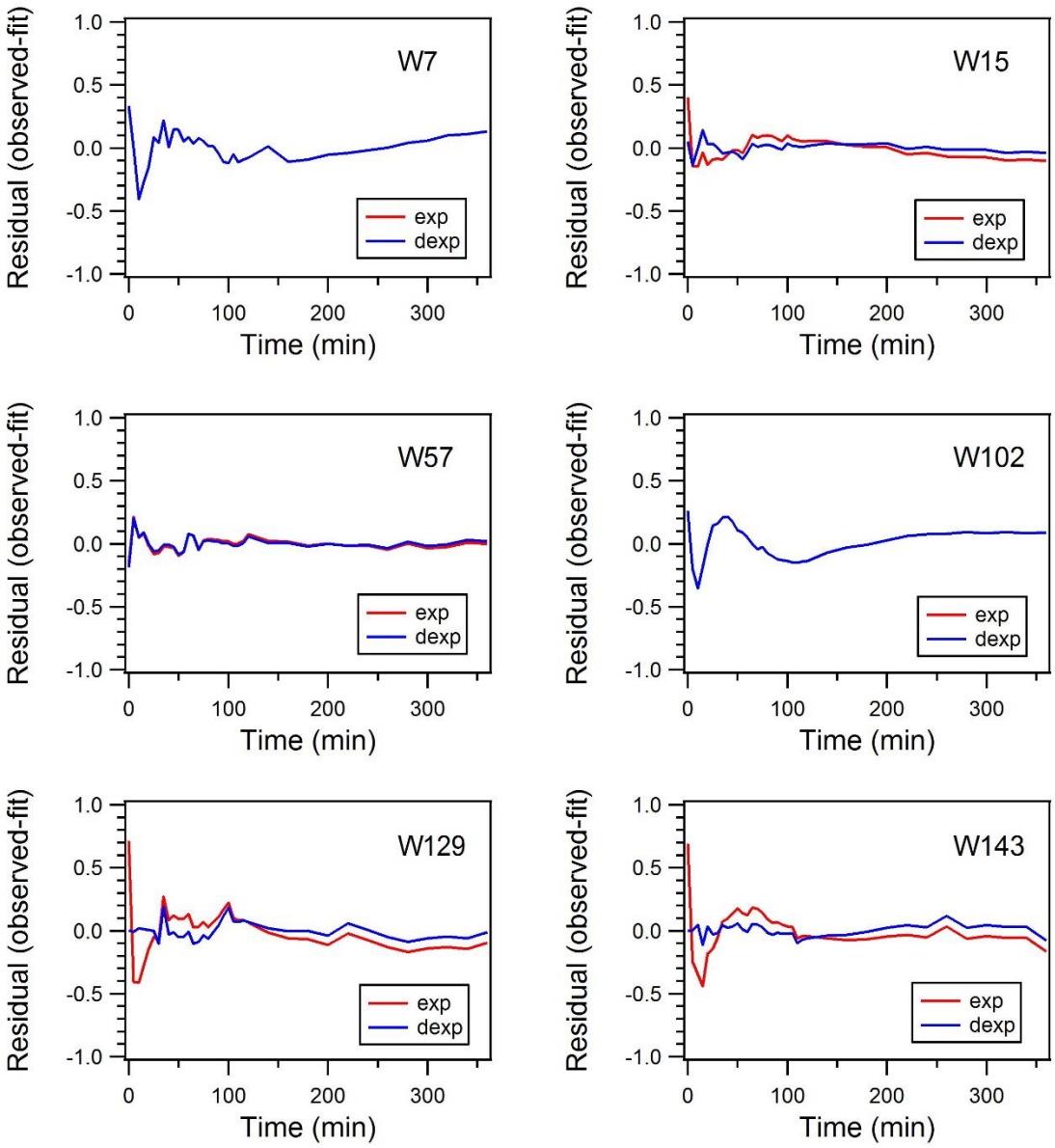

Figure S44: K_{SV} Residual plots. Shown here are residual plots for the exponential and double exponential fits to the average K_{SV} versus time data in figure 12. The residual was calculated as the difference between the experimental data (observed) and the fit equation.

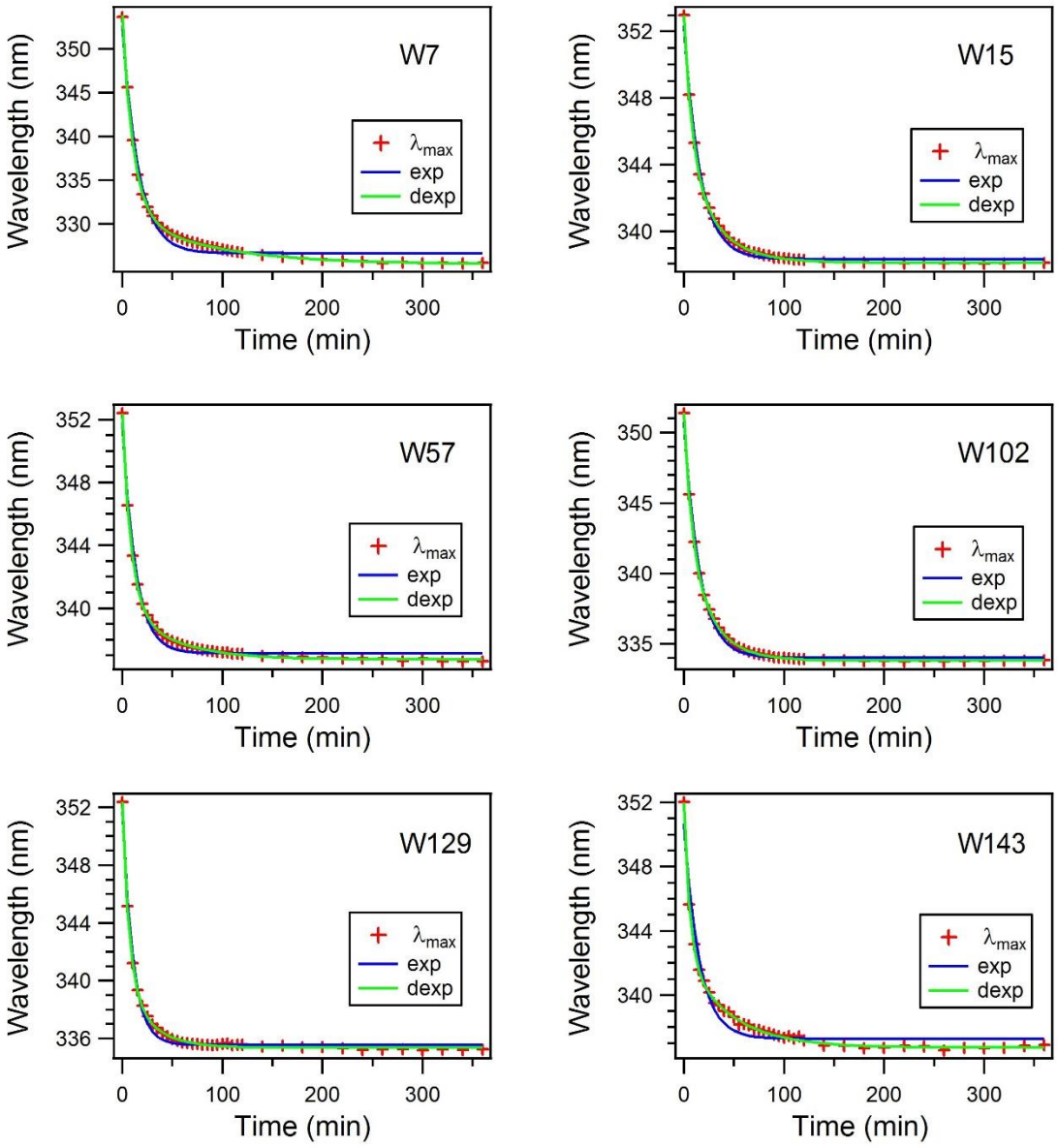

Figure S45. λ_{max} versus time. Displayed here are the average λ_{max} versus time curves for the 0.0 M acrylamide samples of each single trp mutant (red crosses). Overlaid on the plots are the exponential and double-exponential fit curves. Residual plots for each of these graphs are included in Figure S65. The fit parameters are included in Table 4.

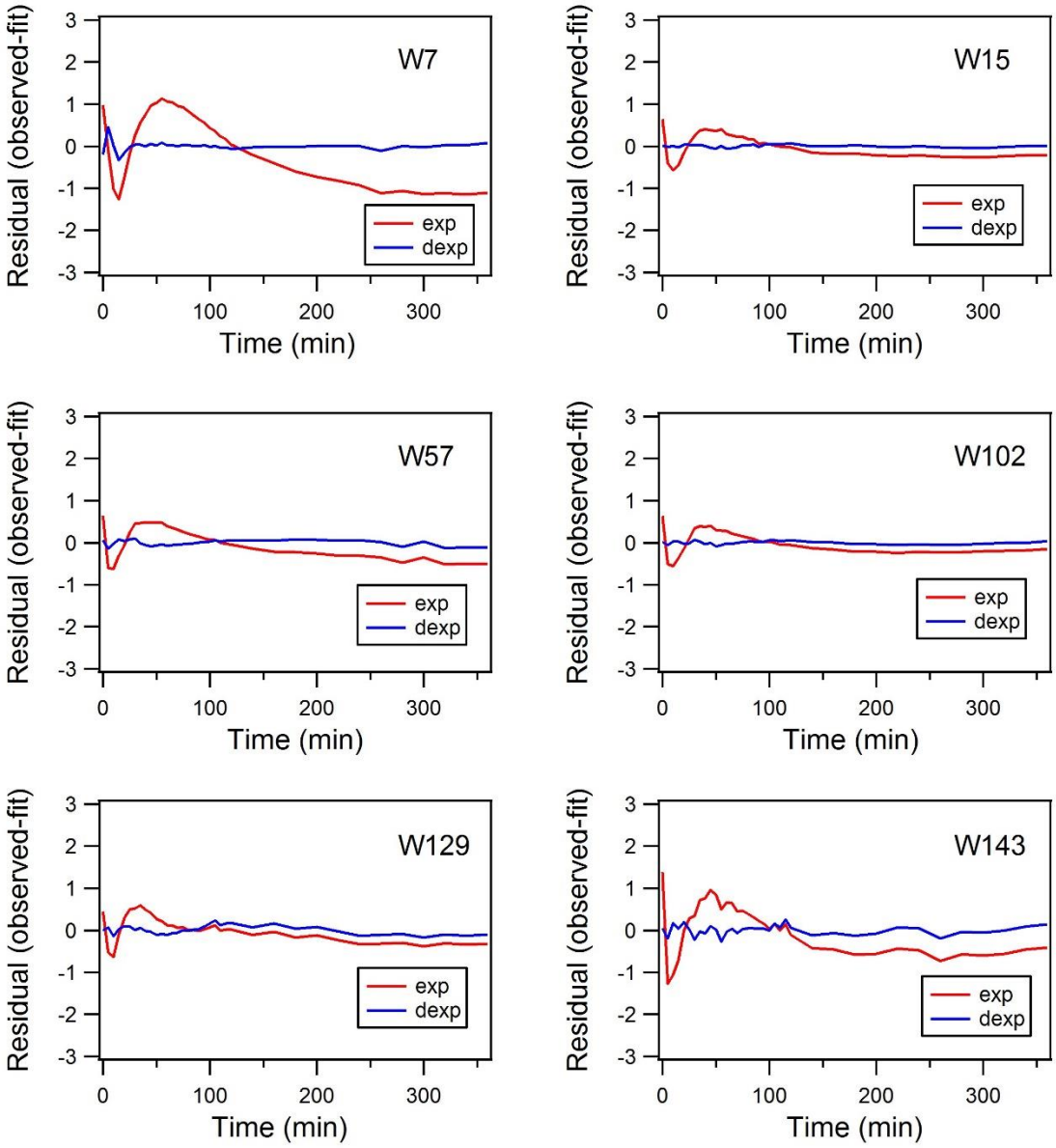

Figure S46. λ_{max} versus time residuals. Displayed here are the resiual plots for the exponential and double exponential fits to the λ_{max} vs time curves in Figure S64. The residuals were calculated as the experimentally determined λ_{max} values less the fit value.

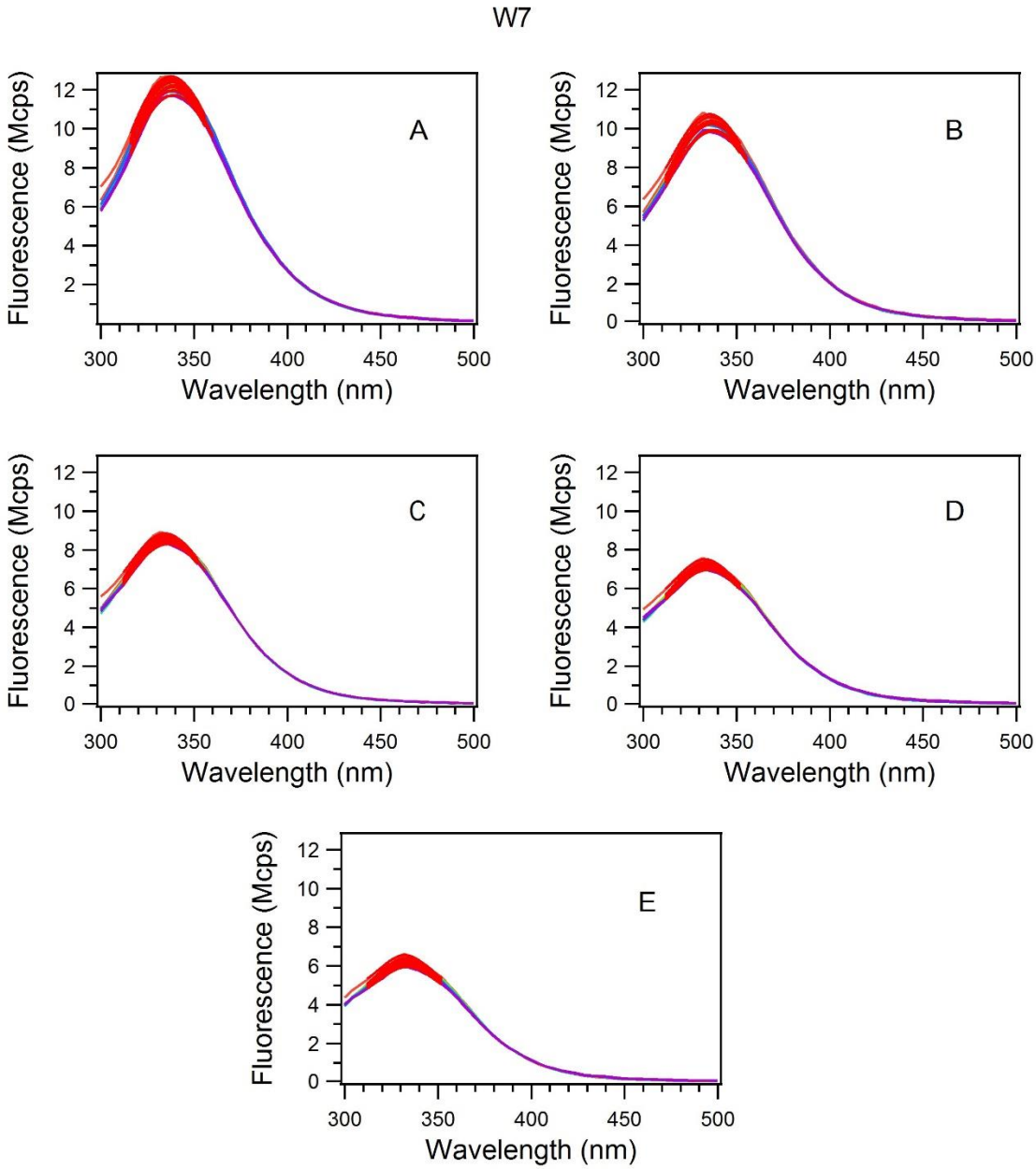

Figure S47: W7 DPPC Experiment Data. Depicted are the fluorescence spectra for the 0.0M (A), 0.1M (B), 0.2M (C), 0.3M (D) and 0.4M (E) acrylamide samples for all 60 min of the experiment. Gaussian fits are in red.

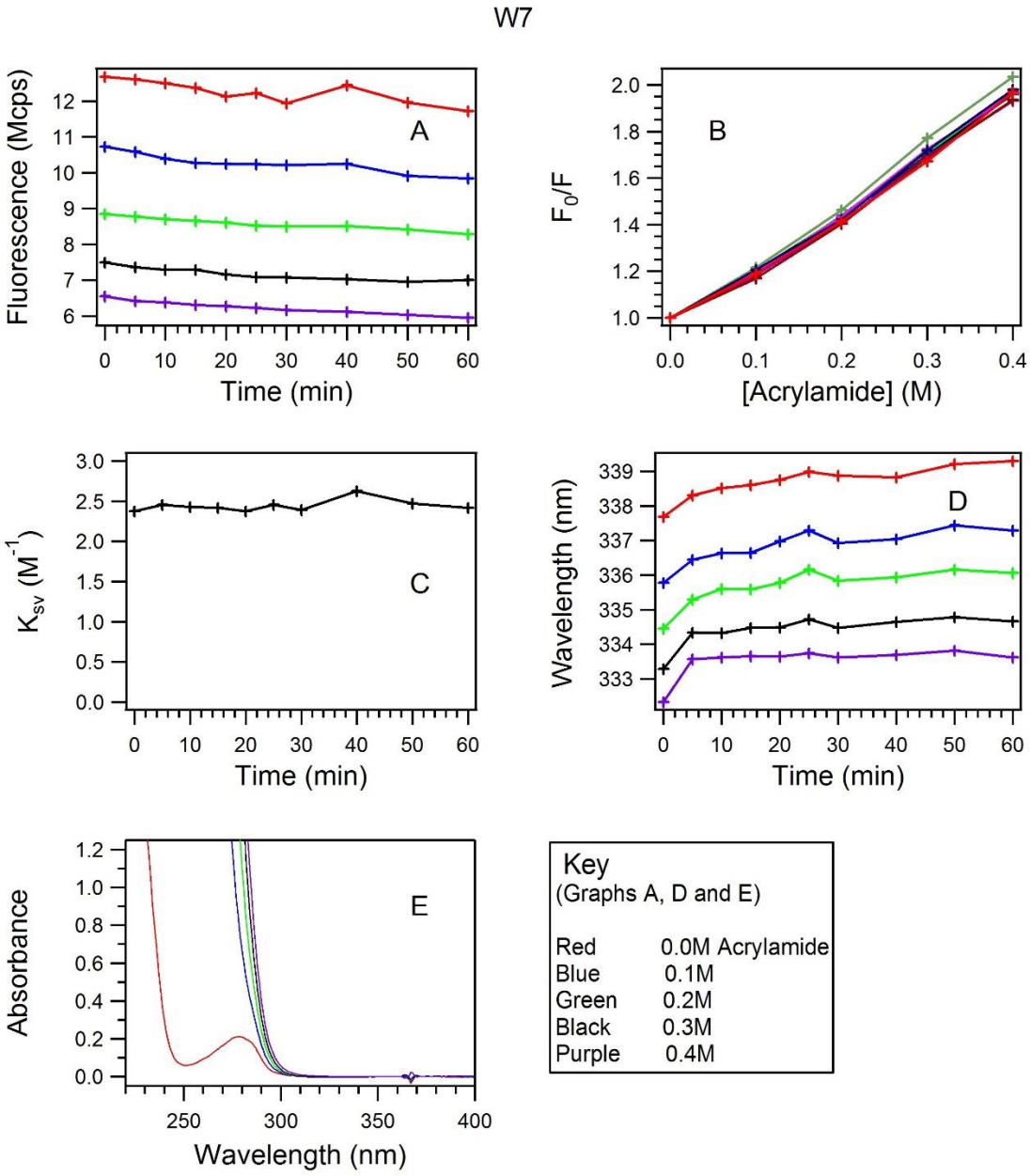

Figure S48: W7 DPPC Experiment Data Workup. Panel A depicts fluorescence maxima from the gaussian fits for each sample and time point. For panels A, D and E, red corresponds to the 0.0M acrylamide sample, blue to the 0.1M sample, green to the 0.2M sample, black to the 0.3M sample and purple to the 0.4M sample. Panel B depicts Stern-Volmer plots for each time point in the experiment. Panel C depicts the linear slope (K_{SV}) of the Stern-Vomer plots in panel B over the time of the experiment. Panel D depicts the shift of maximum wavelength of emission for all samples over the time of the experiment. Panel E depicts absorbance spectra for all samples.

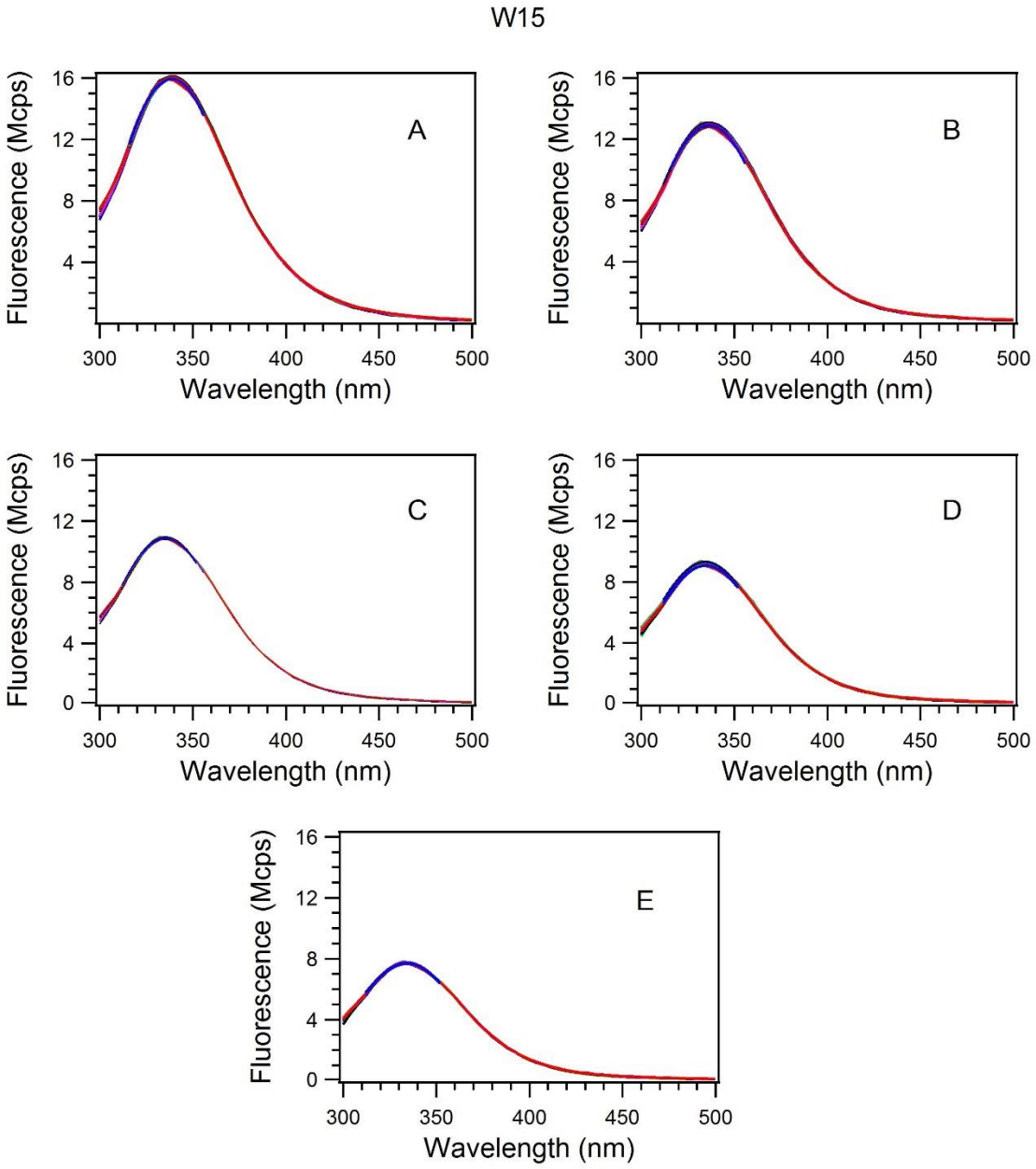

Figure S49: W15 DPPC Experiment Data. Depicted are the fluorescence spectra for the 0.0M (A), 0.1M (B), 0.2M (C), 0.3M (D) and 0.4M (E) acrylamide samples for all 60 min of the experiment. Gaussian fits are in red.

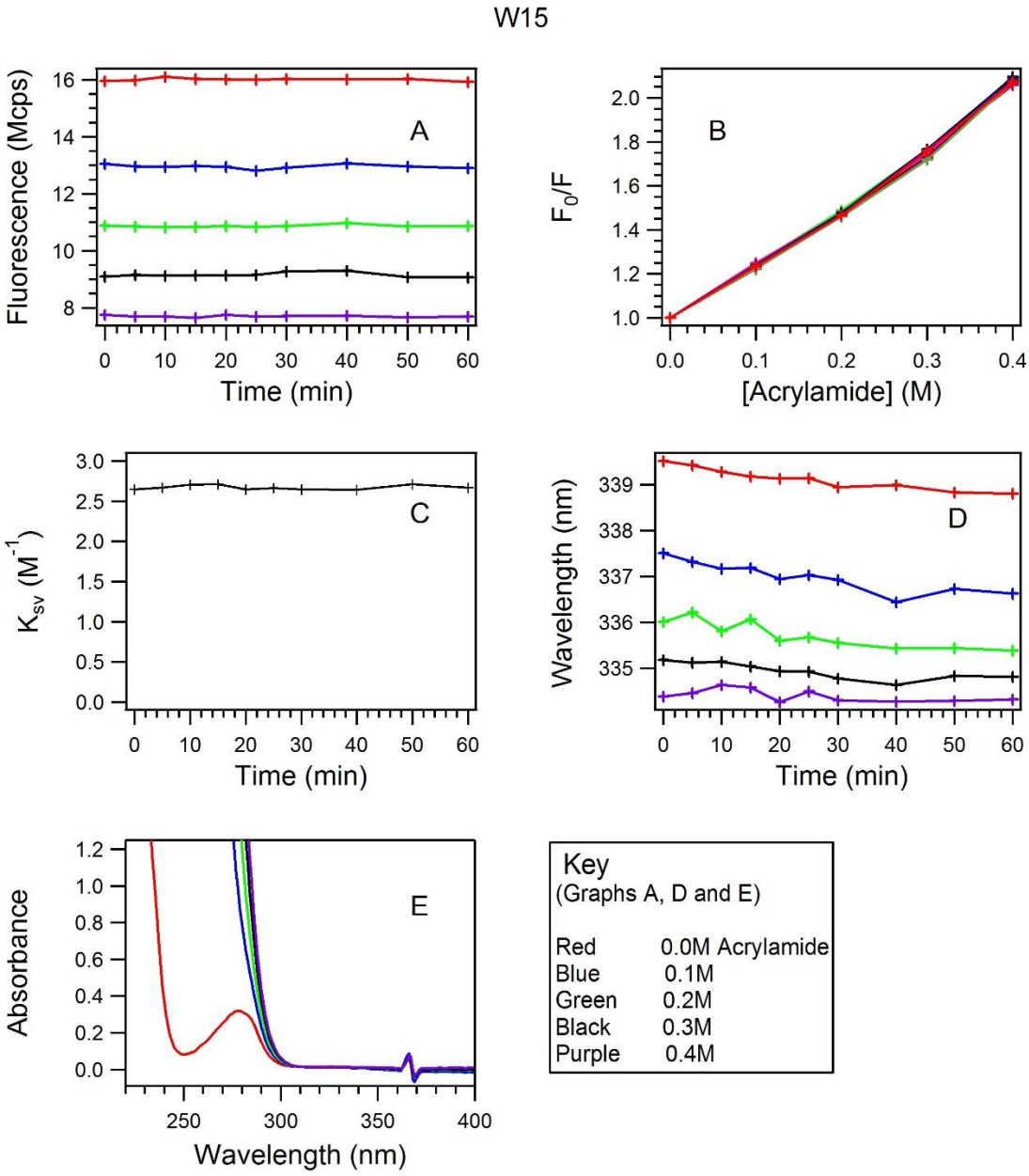

Figure S50: W15 DPPC Experiment Data Workup. Panel A depicts fluorescence maxima from the gaussian fits for each sample and time point. For panels A, D and E, red corresponds to the 0.0M acrylamide sample, blue to the 0.1M sample, green to the 0.2M sample, black to the 0.3M sample and purple to the 0.4M sample. Panel B depicts Stern-Volmer plots for each time point in the experiment. Panel C depicts the linear slope (K_{SV}) of the Stern-Vomer plots in panel B over the time of the experiment. Panel D depicts the shift of maximum wavelength of emission for all samples over the time of the experiment. Panel E depicts absorbance spectra for all samples.

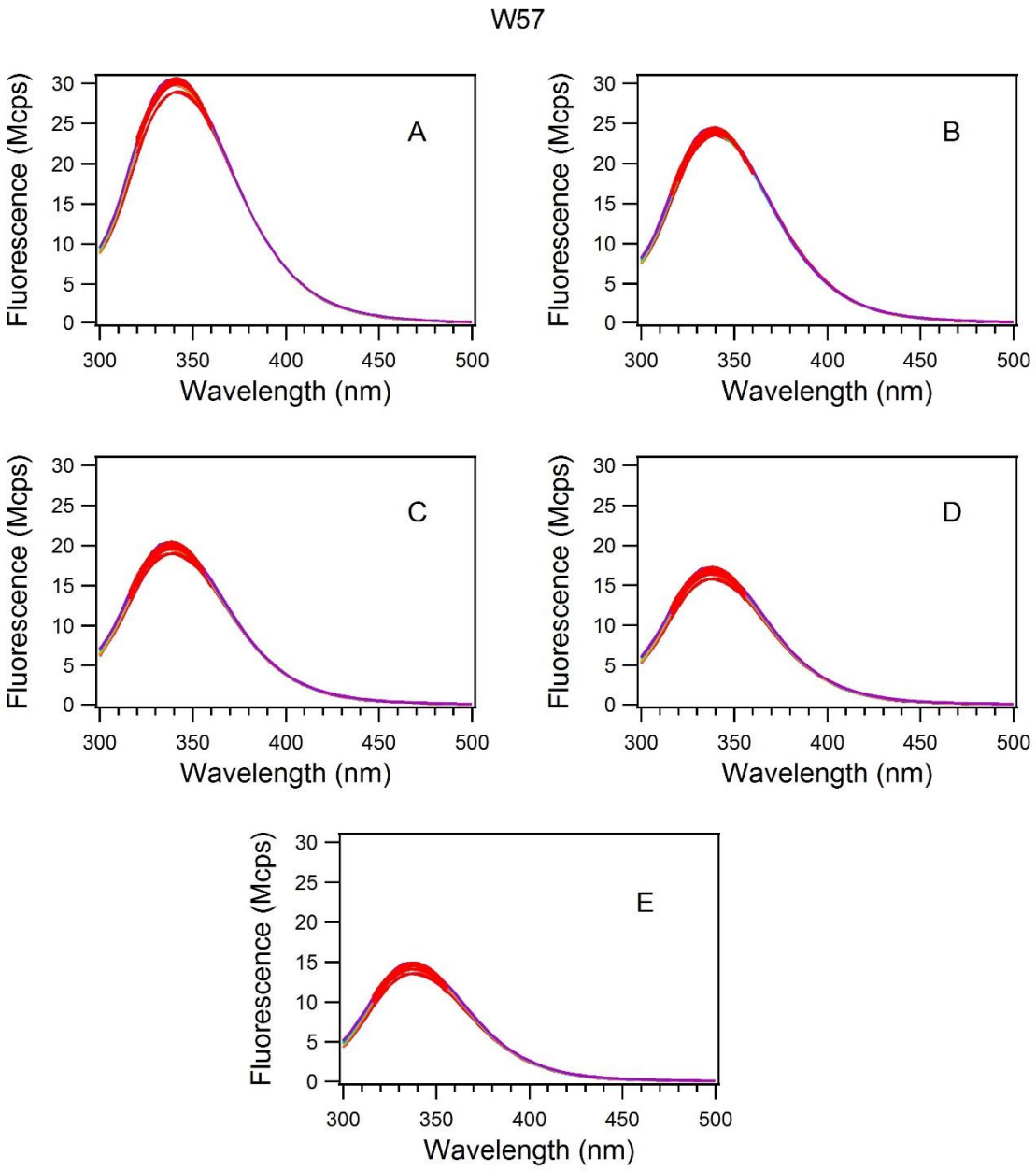

Figure S51: W57 DPPC Experiment Data. Depicted are the fluorescence spectra for the 0.0M (A), 0.1M (B), 0.2M (C), 0.3M (D) and 0.4M (E) acrylamide samples for all 60 min of the experiment. Gaussian fits are in red.

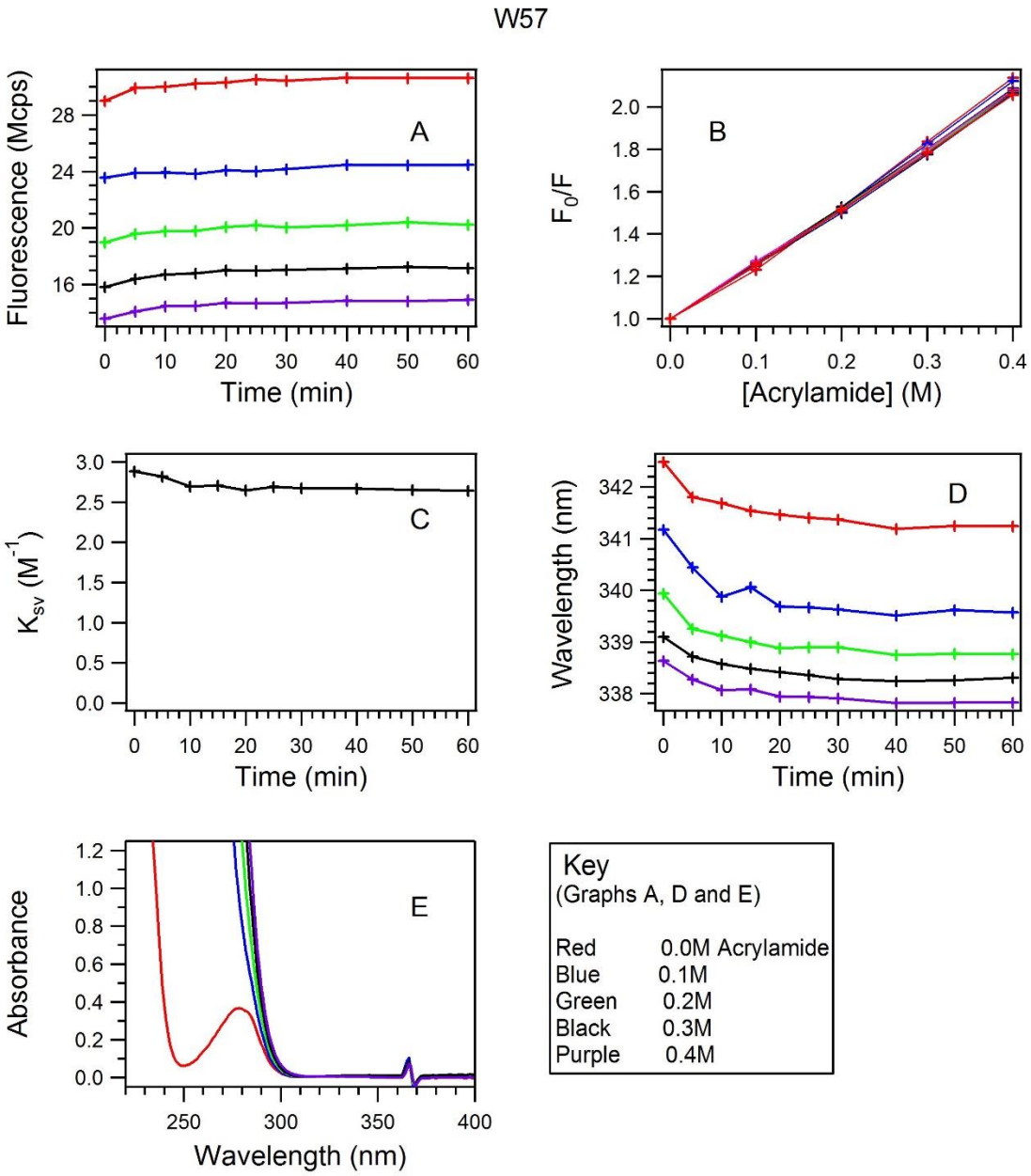

Figure S52: W57 DPPC Experiment Data Workup. Panel A depicts fluorescence maxima from the gaussian fits for each sample and time point. For panels A, D and E, red corresponds to the 0.0M acrylamide sample, blue to the 0.1M sample, green to the 0.2M sample, black to the 0.3M sample and purple to the 0.4M sample. Panel B depicts Stern-Volmer plots for each time point in the experiment. Panel C depicts the linear slope (K_{SV}) of the Stern-Vomer plots in panel B over the time of the experiment. Panel D depicts the shift of maximum wavelength of emission for all samples over the time of the experiment. Panel E depicts absorbance spectra for all samples.

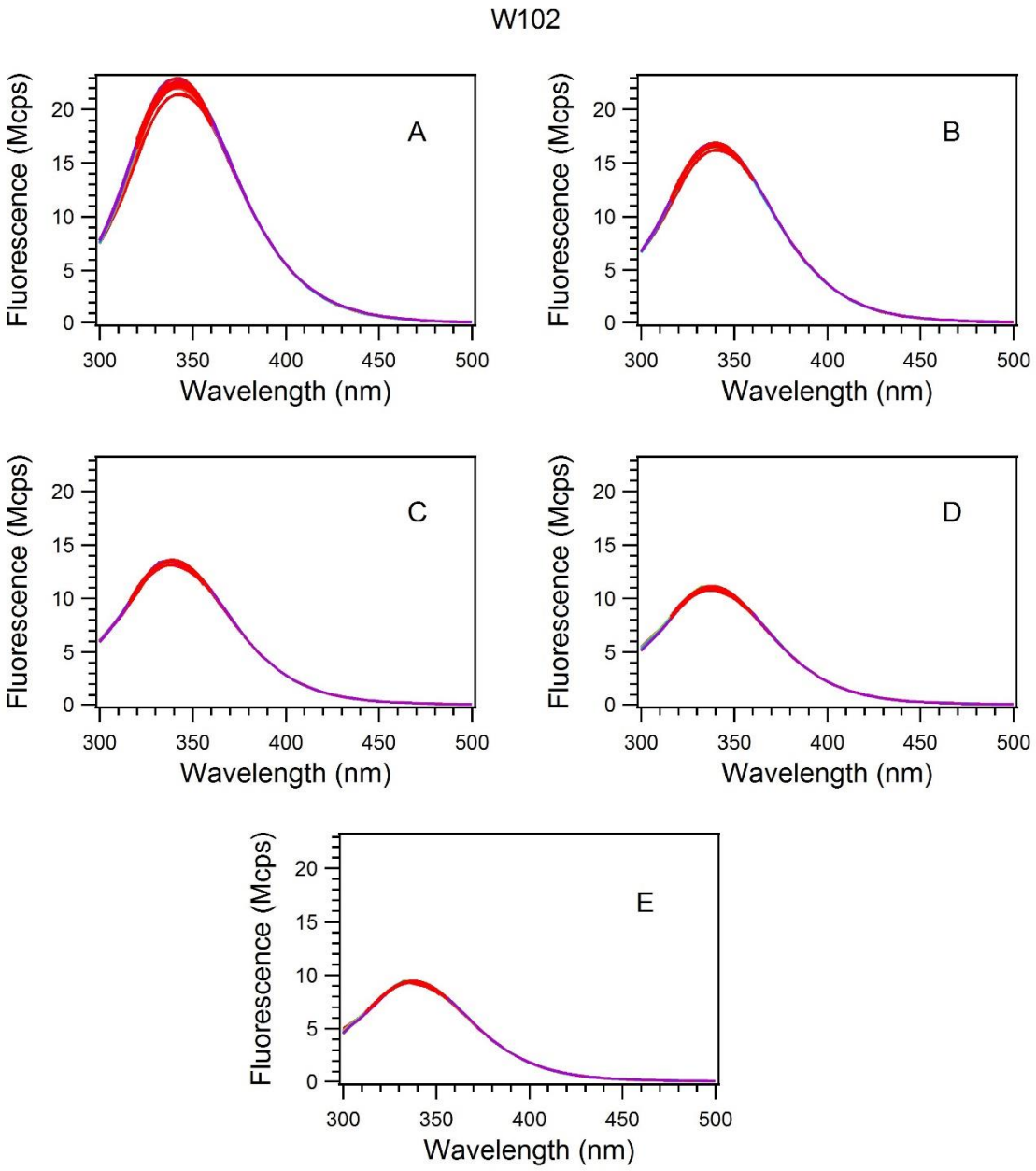

Figure S53: W102 DPPC Experiment Data. Depicted are the fluorescence spectra for the 0.0M (A), 0.1M (B), 0.2M (C), 0.3M (D) and 0.4M (E) acrylamide samples for all 60 min of the experiment. Gaussian fits are in red.

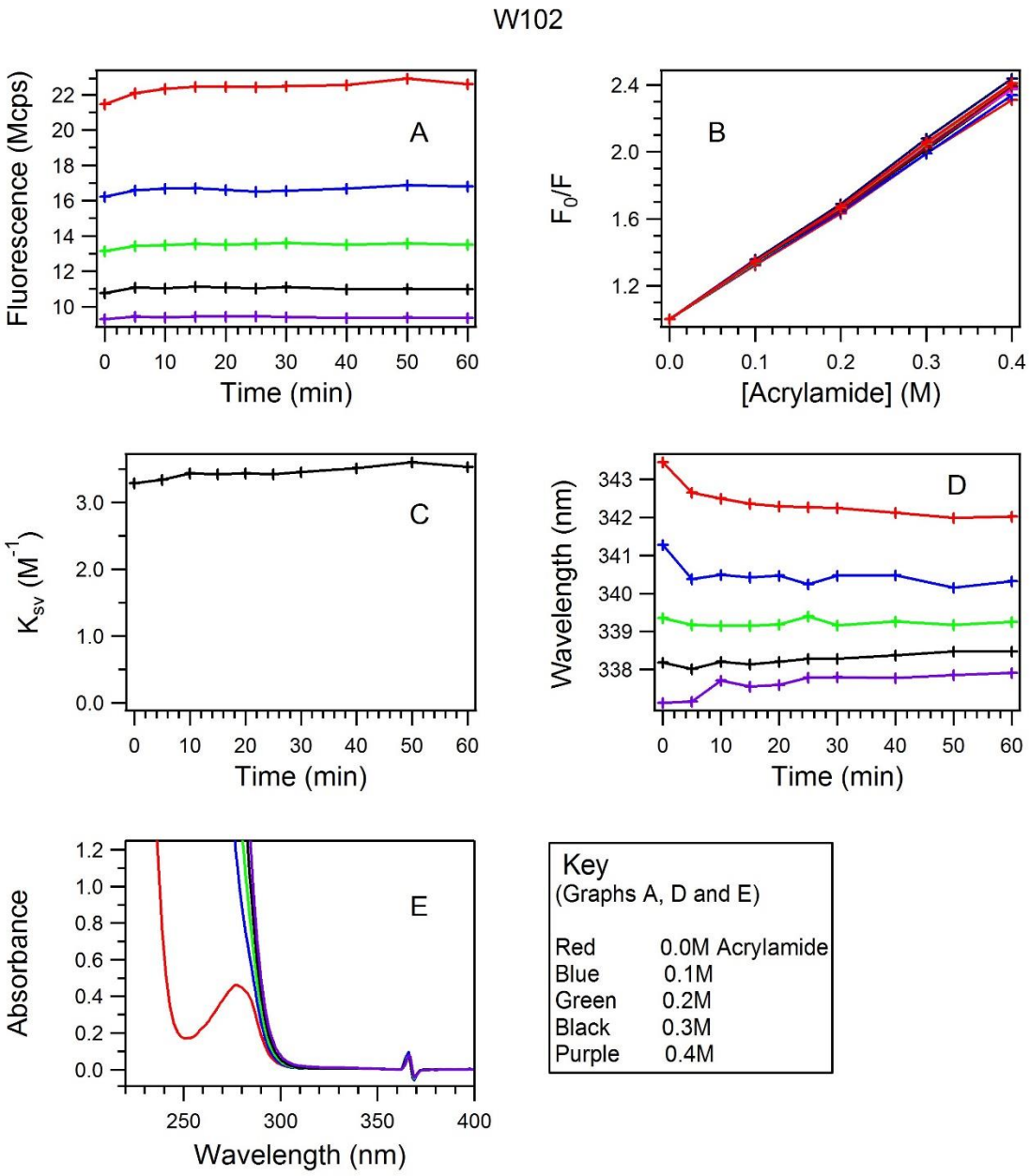

Figure S54: W102 DPPC Experiment Data Workup. Panel A depicts fluorescence maxima from the gaussian fits for each sample and time point. For panels A, D and E, red corresponds to the 0.0M acrylamide sample, blue to the 0.1M sample, green to the 0.2M sample, black to the 0.3M sample and purple to the 0.4M sample. Panel B depicts Stern-Volmer plots for each time point in the experiment. Panel C depicts the linear slope (K_{SV}) of the Stern-Vomer plots in panel B over the time of the experiment. Panel D depicts the shift of maximum wavelength of emission for all samples over the time of the experiment. Panel E depicts absorbance spectra for all samples.

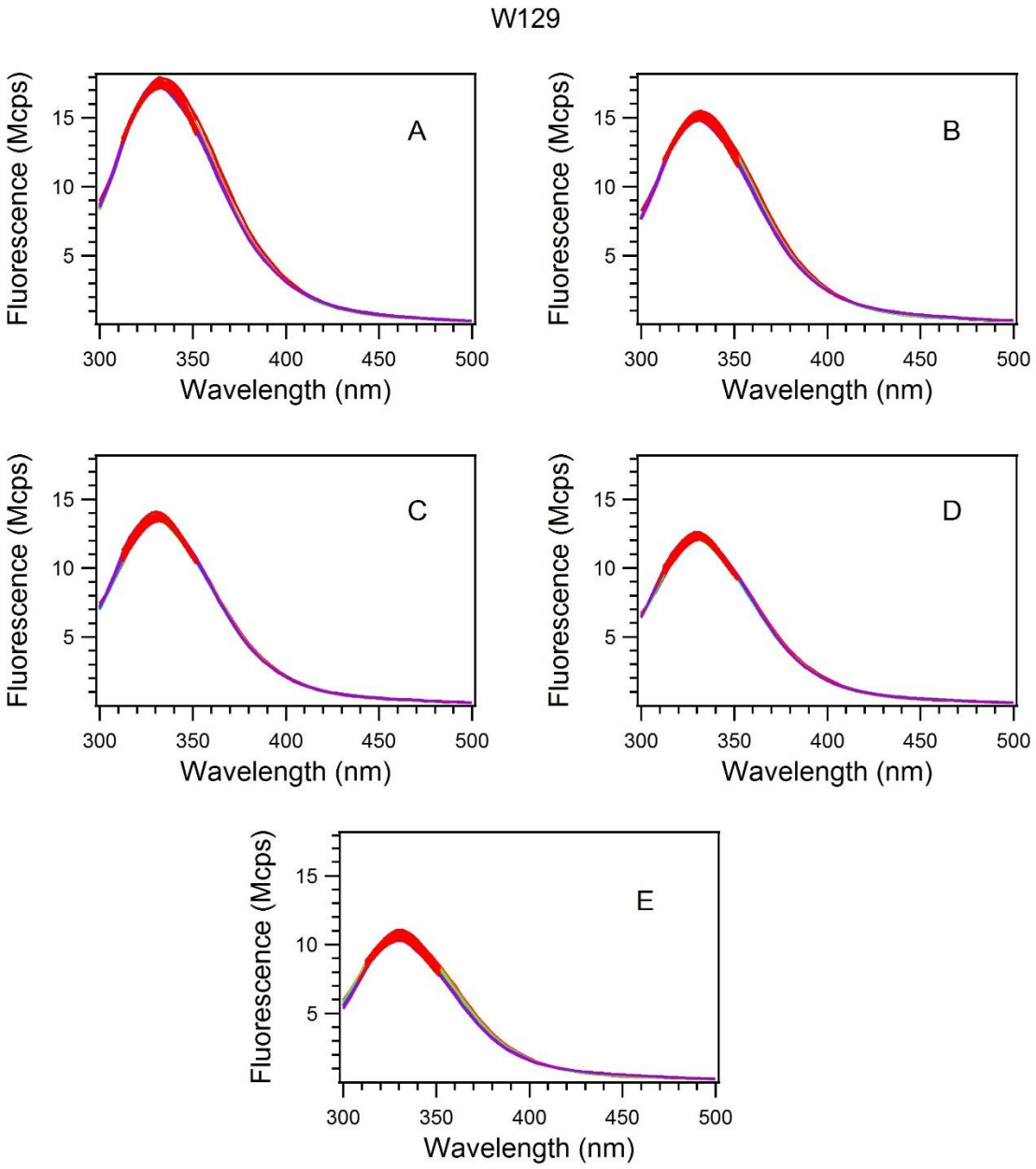

Figure S55: W129 DPPC Experiment Data. Depicted are the fluorescence spectra for the 0.0M (A), 0.1M (B), 0.2M (C), 0.3M (D) and 0.4M (E) acrylamide samples for all 60 min of the experiment. Gaussian fits are in red.

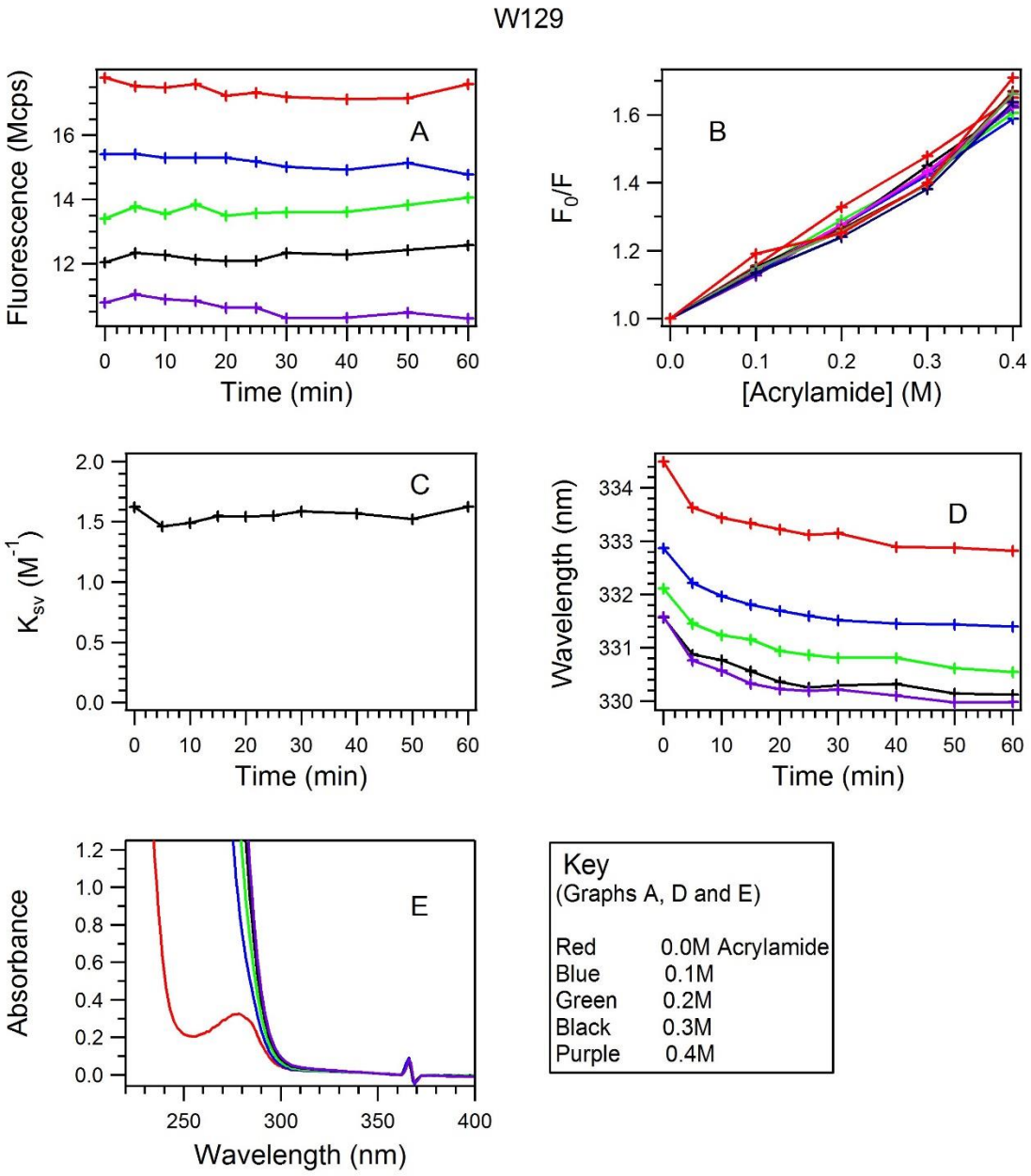

Figure S56: W129 DPPC Experiment Data Workup. Panel A depicts fluorescence maxima from the gaussian fits for each sample and time point. For panels A, D and E, red corresponds to the 0.0M acrylamide sample, blue to the 0.1M sample, green to the 0.2M sample, black to the 0.3M sample and purple to the 0.4M sample. Panel B depicts Stern-Volmer plots for each time point in the experiment. Panel C depicts the linear slope (K_{SV}) of the Stern-Vomer plots in panel B over the time of the experiment. Panel D depicts the shift of maximum wavelength of emission for all samples over the time of the experiment. Panel E depicts absorbance spectra for all samples.

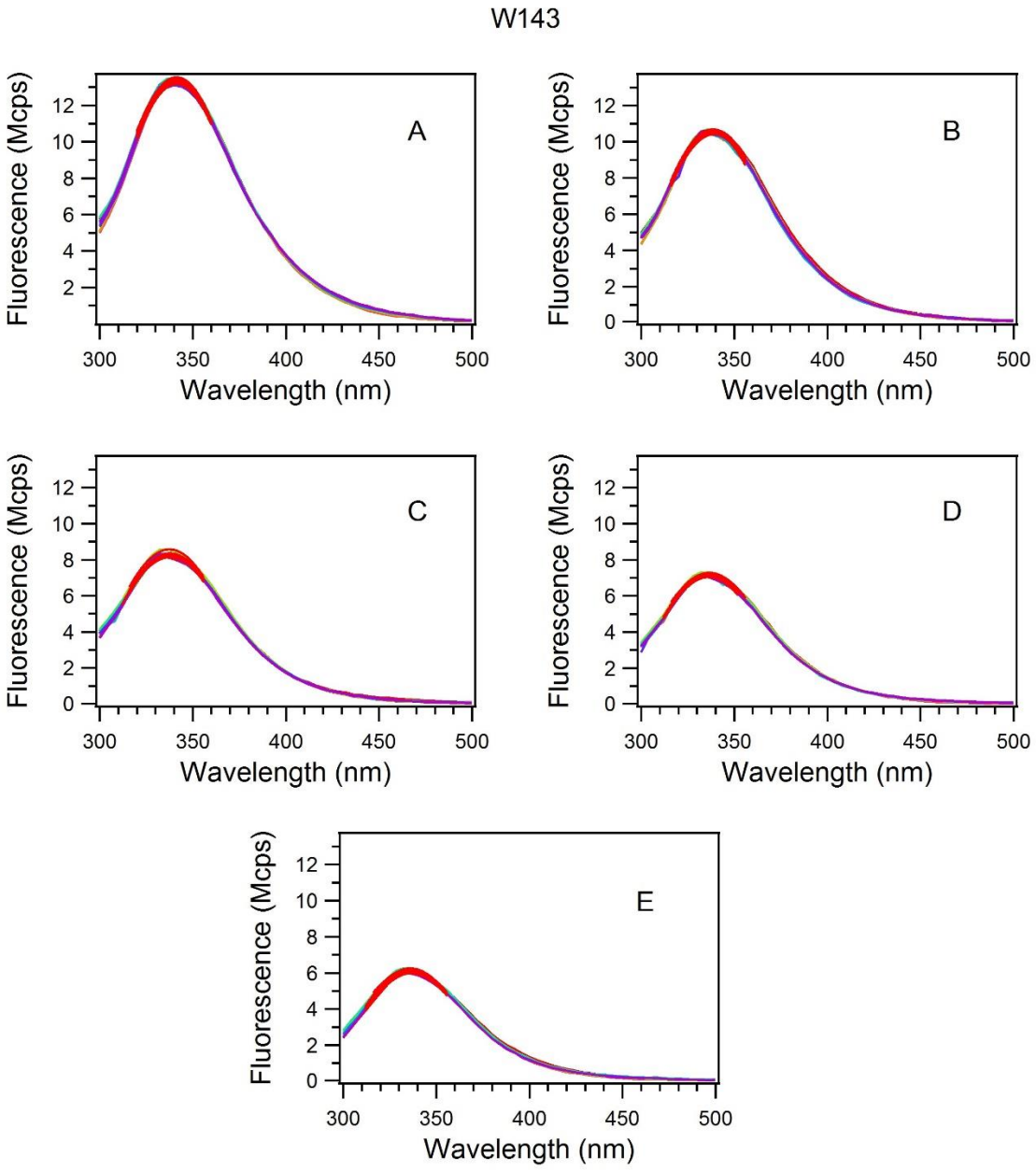

Figure S57: W143 DPPC Experiment Data. Depicted are the fluorescence spectra for the 0.0M (A), 0.1M (B), 0.2M (C), 0.3M (D) and 0.4M (E) acrylamide samples for all 60 min of the experiment. Gaussian fits are in red.

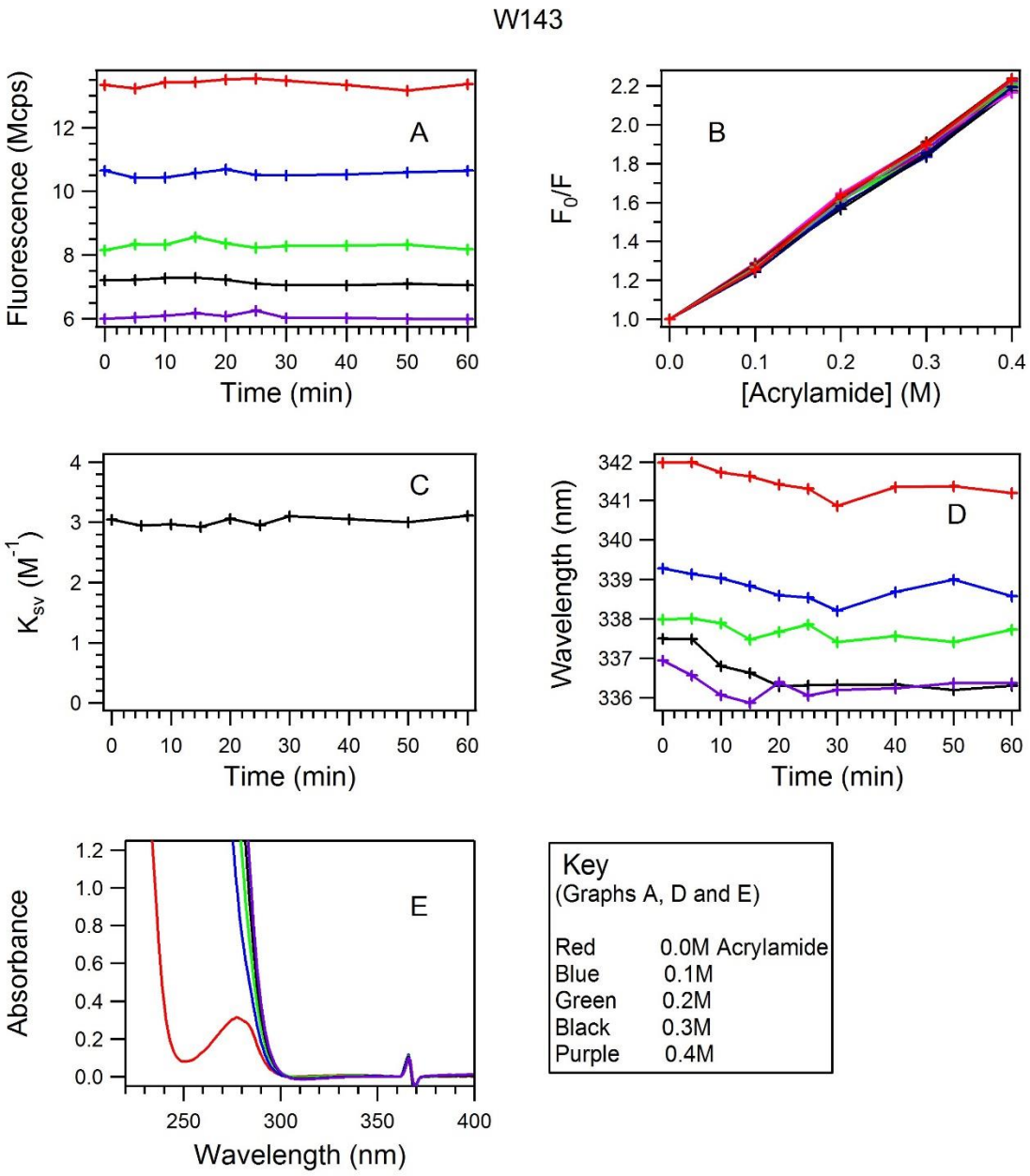

Figure S58: W143 DPPC Experiment Data Workup. Panel A depicts fluorescence maxima from the gaussian fits for each sample and time point. For panels A, D and E, red corresponds to the 0.0M acrylamide sample, blue to the 0.1M sample, green to the 0.2M sample, black to the 0.3M sample and purple to the 0.4M sample. Panel B depicts Stern-Volmer plots for each time point in the experiment. Panel C depicts the linear slope (K_{SV}) of the Stern-Vomer plots in panel B over the time of the experiment. Panel D depicts the shift of maximum wavelength of emission for all samples over the time of the experiment. Panel E depicts absorbance spectra for all samples.

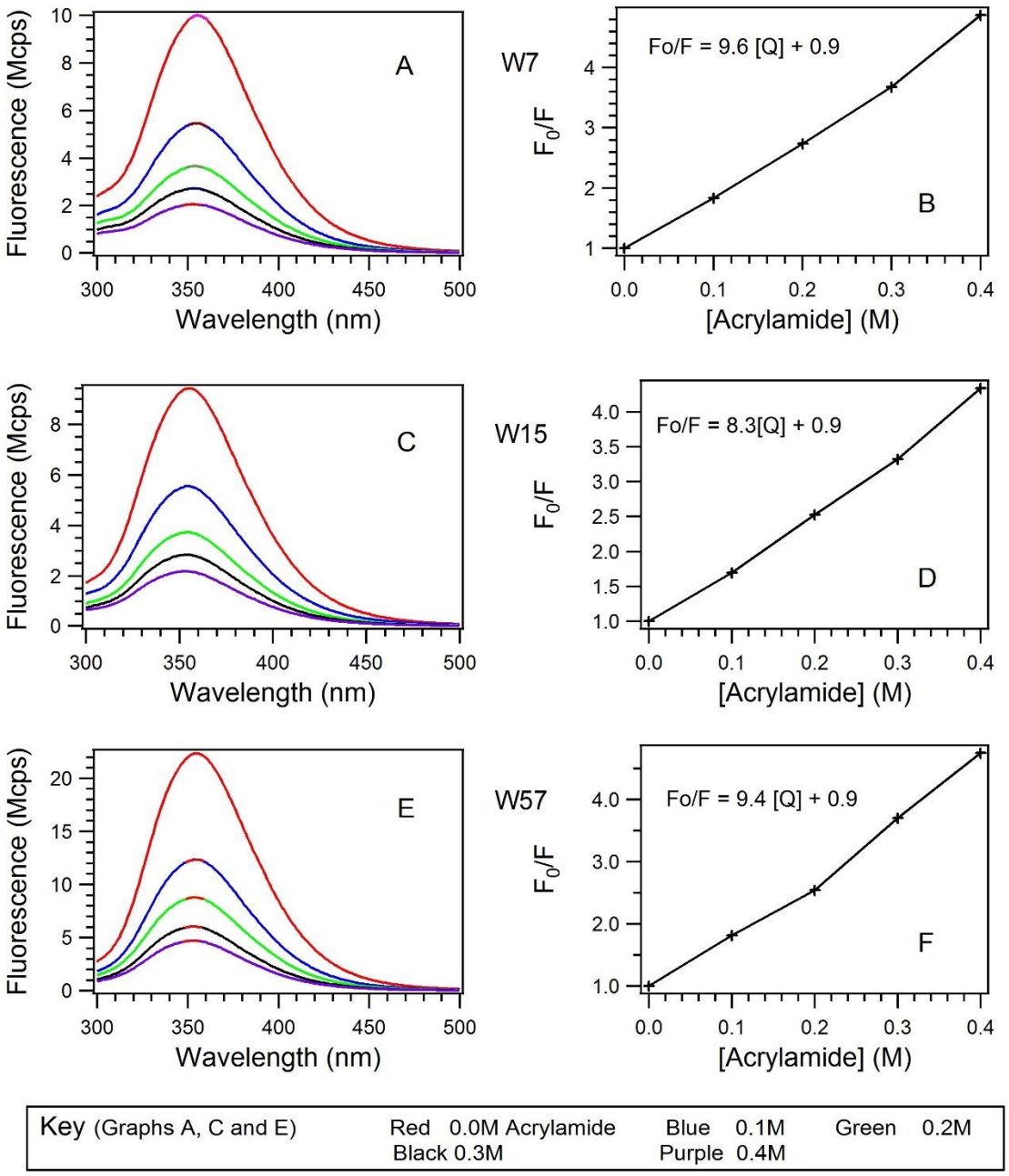

Figure S59: W7, W15 and W57 8M Urea Experiments. Panels A, C and E depict 'quenching trends' for OmpA mutants W7, W15 and W57 respectively in 8M urea with no SUVs. Panels B, D and F depict Stern-Volmer plots constructed from the fluorescence data in panels A, C and E respectively.

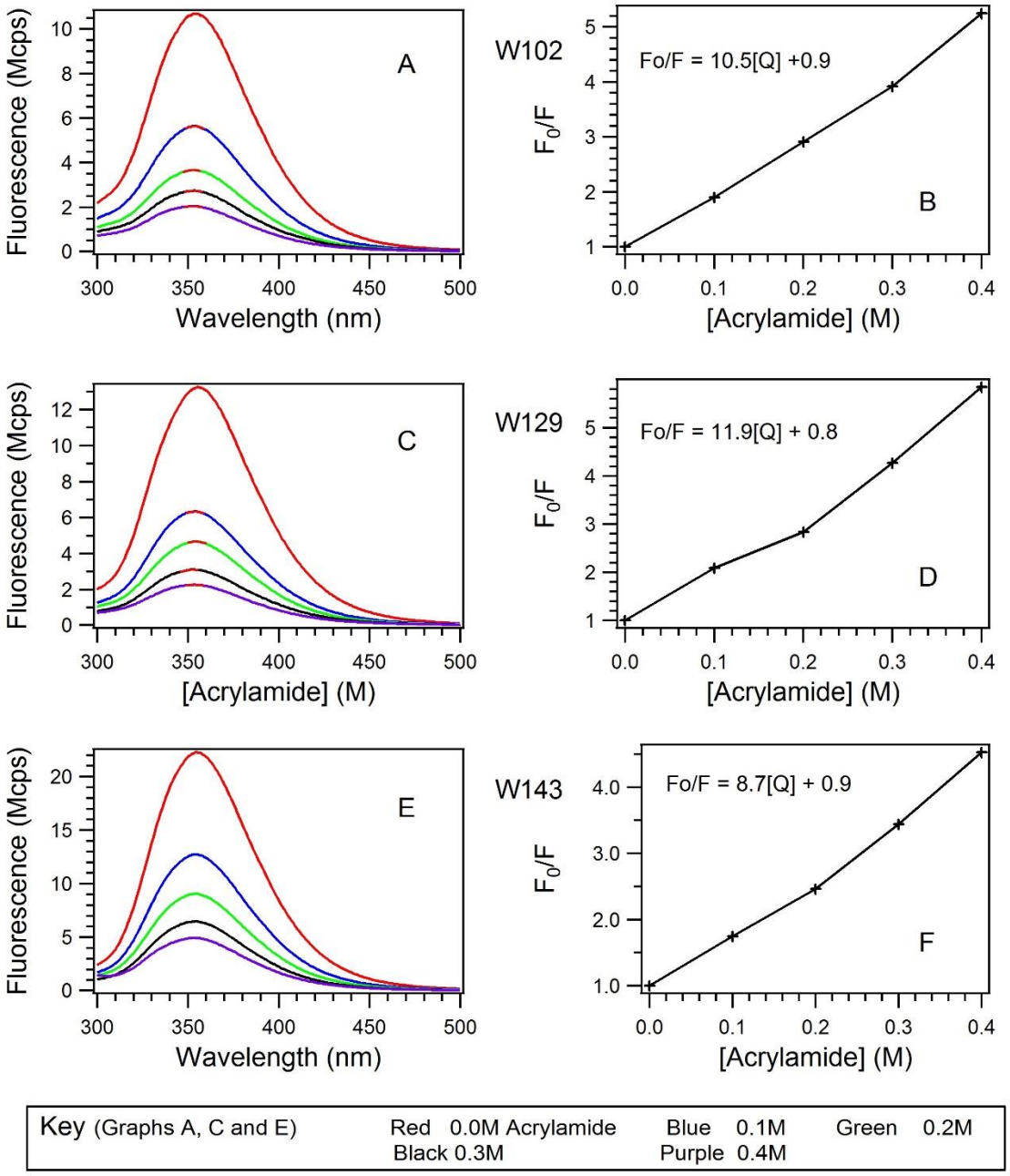

Figure S60: W102, W129 and W143 8M Urea Experiments. Panels A, C and E depict 'quenching trends' for OmpA mutants W102, W129 and W143 respectively in 8M urea with no SUVs. Panels B, D and F depict Stern-Volmer plots constructed from the fluorescence data in panels A, C and E respectively.

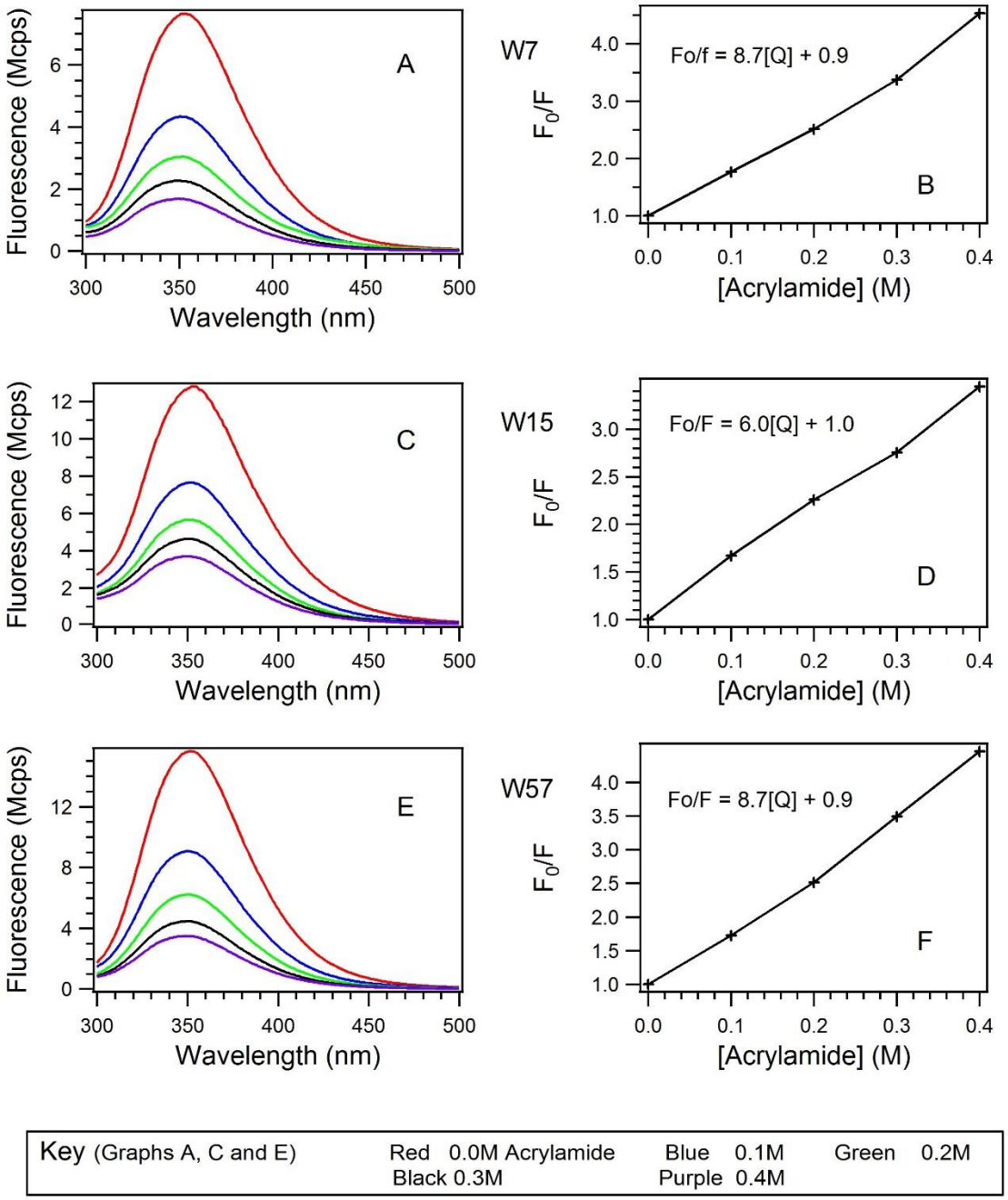

Figure S61: W7, W15 and W57 0.5 M Urea Experiments. Panels A, C and E depict 'quenching trends' for OmpA 1W mutants W7, W15 and W57 respectively in 0.5 M urea with no SUVs. Panels B, D and F depict Stern-Volmer plots constructed from the fluorescence data in panels A, C and E respectively.

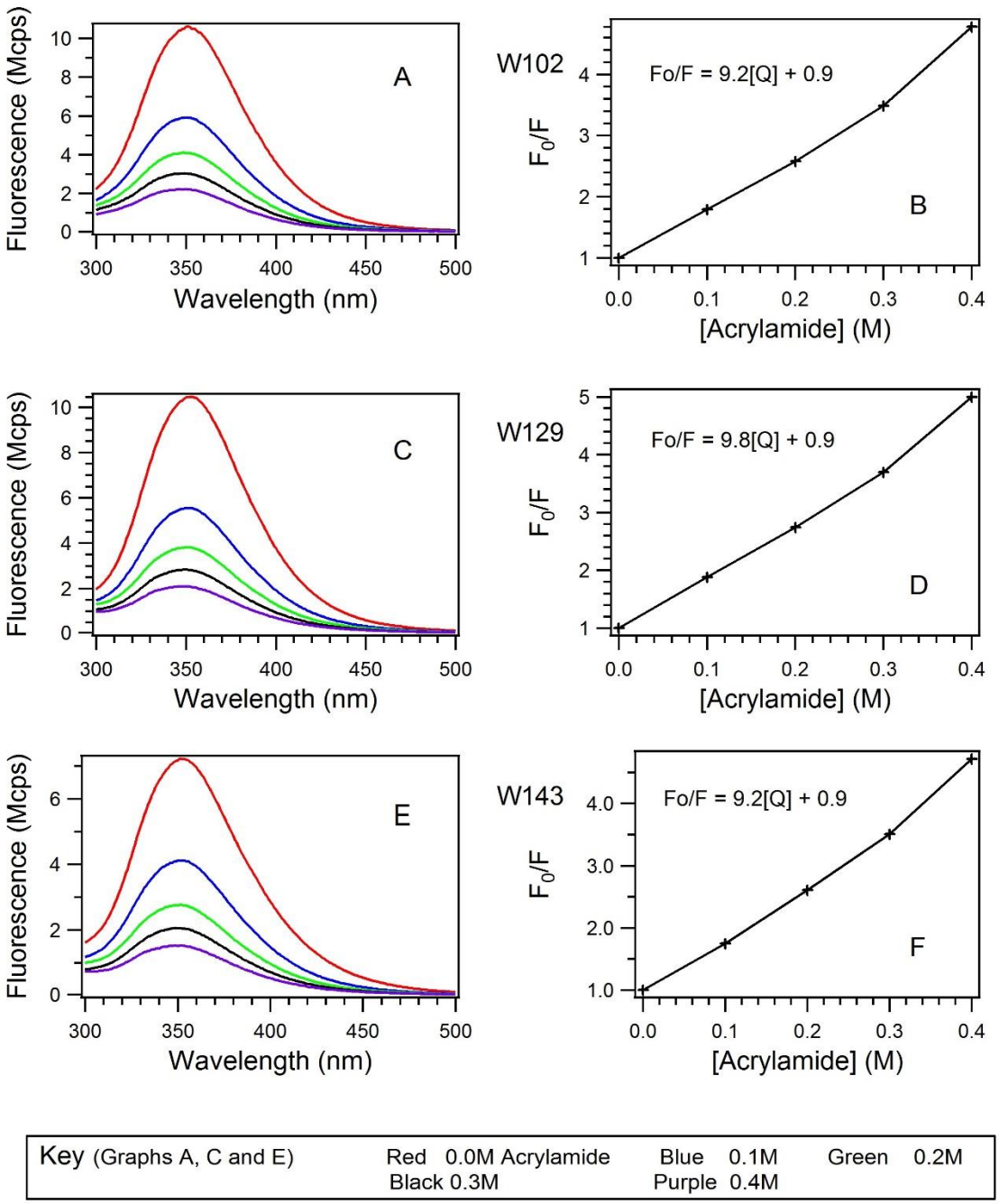

Figure S62: W102, W129 and W143 0.5 M Urea Experiments. Panels A, C and E depict 'quenching trends' for OmpA 1W mutants W102, W129 and W143 respectively in 0.5 M urea with no SUVs. Panels B, D and F depict Stern-Volmer plots constructed from the fluorescence data in panels A, C and E respectively.

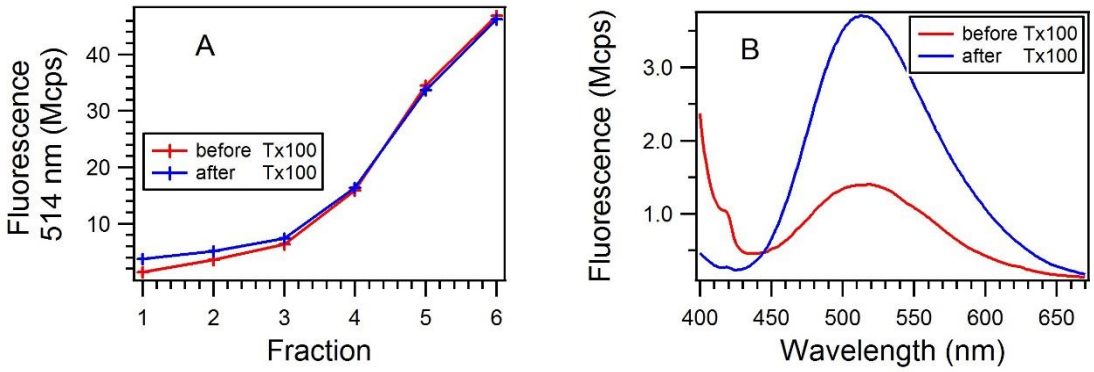

Figure S63: ANTS DPX Experiment 1 Fraction Selection. Panel A shows the fluorescence intensity at 514nm of fractions 1 thorugh 6 before (red) and after (blue) triton X-100. Panel B shows the fluorescence spectra for fraction 1 before (red) and after (blue) triton X-100.

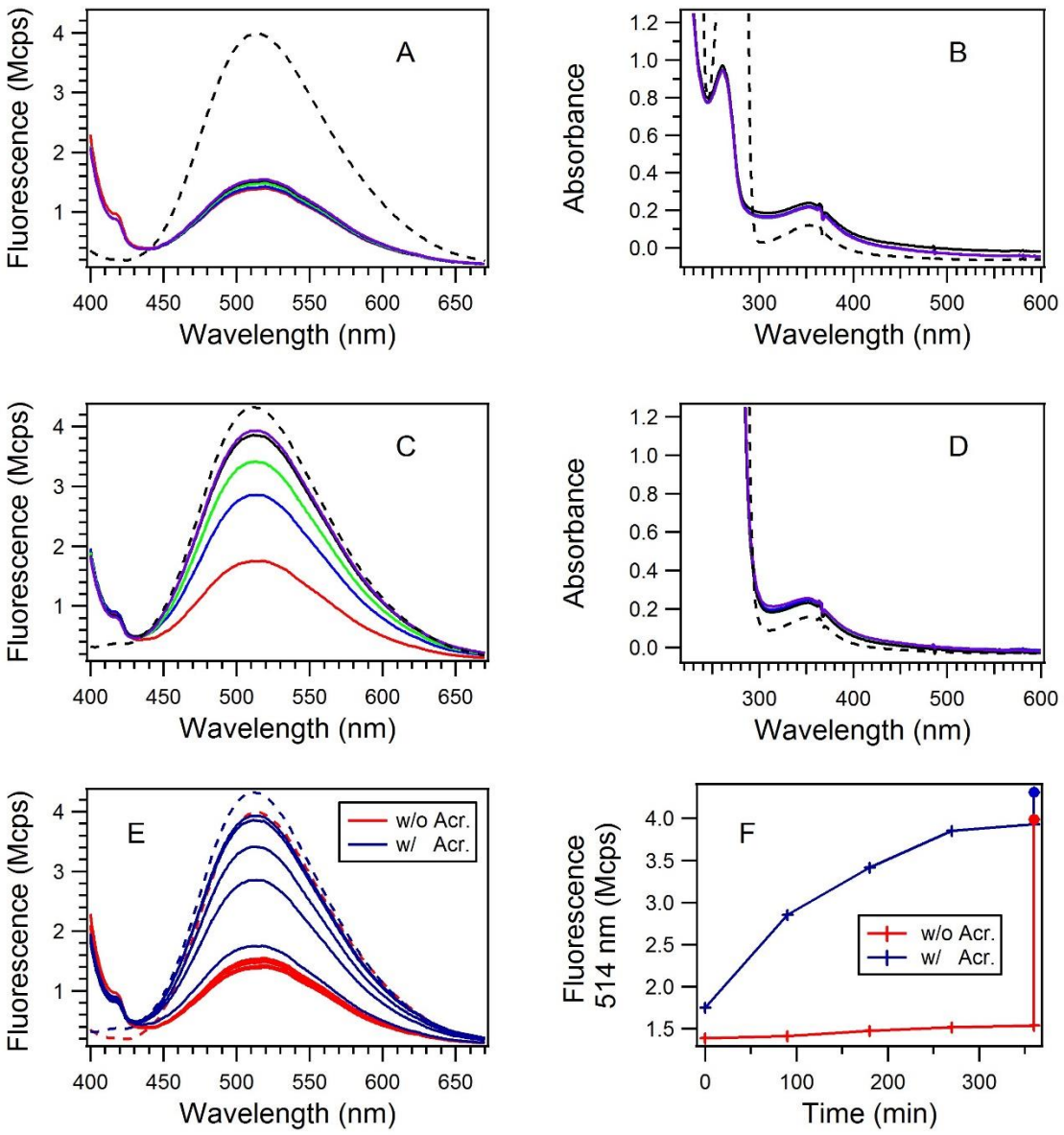

Figure S64: ANTS DPX Experiment 1 Fraction 1. Panel A depicts the fluorescence intensity of DMPC SUVs encapsulating ANTS and DPX from fraction 1 over a period of 6 hours and at 6 hours with triton X-100 (dashed). Panel B depicts the absorbance spectra of the sample in panel A at the same times. Panel C depicts the fluorescence intensity of 2mg/ml DMPC SUVs encapsulating ANTS and DPX from fraction 1, with 0.4M acrylamide, over a period of 6 hours and at 6 hours with triton X-100 (dashed). Panel D depicts the absorbance spectra of the sample in panel C at the same times. Panel E depicts The fluorescence intensity of ANTS and DPX in the absence (red) and in the presence of acrylamide (blue). Panel F depicts the fluorescence maxima of the samples in panel E; the circles indicate the fluorescence intensity after Triton X-100.

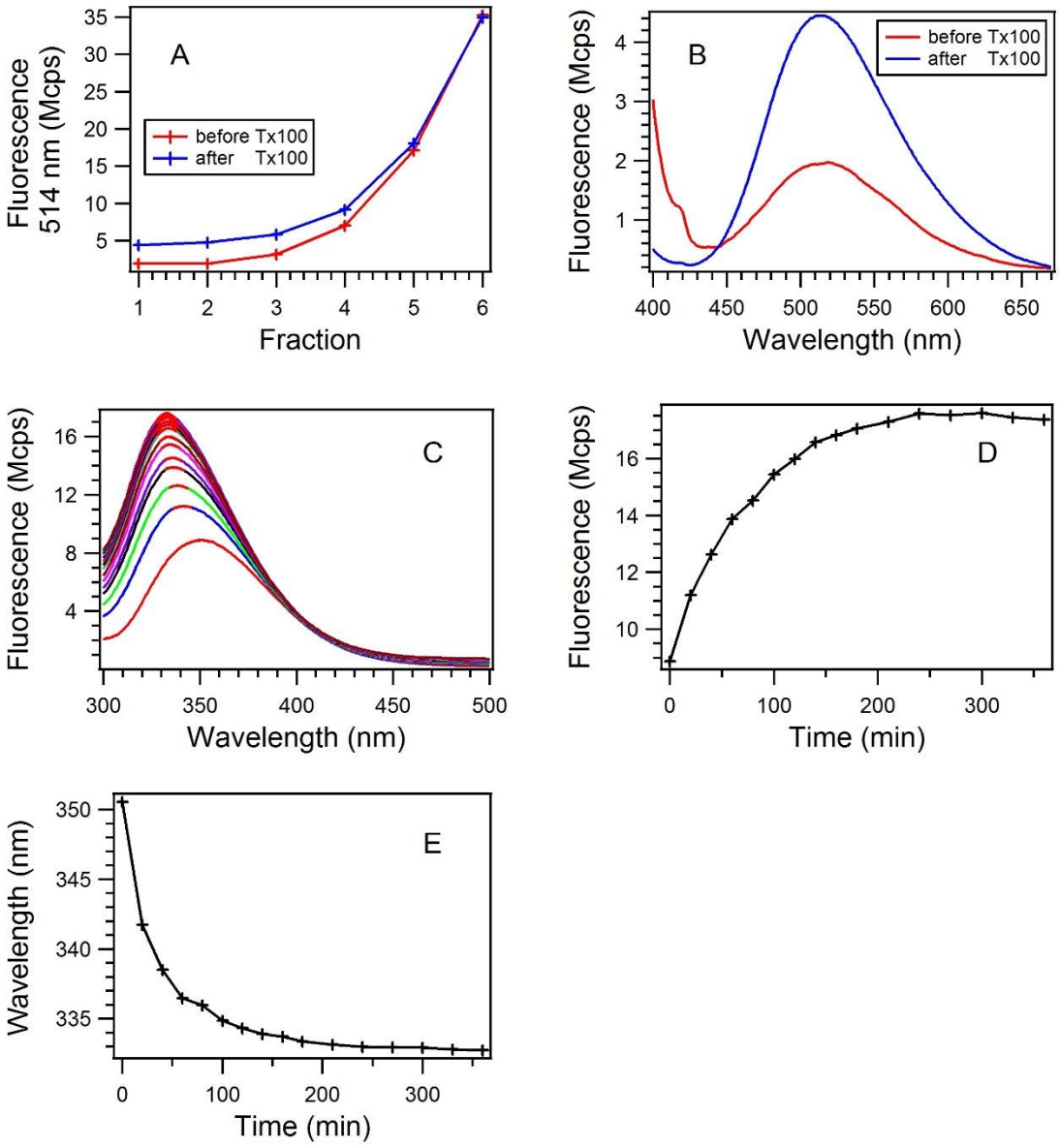

Figure S65: ANTS DPX and OmpA Experiment. Panel A shows the fluorescence intensity at 514nm of fractions 1 thorugh 6 before (red) and after (blue) triton X-100. Panel B shows the fluorescence spectra for fraction 1 before (red) and after (blue) triton X-100. Panel C shows the fluorescence intensity of the tryptophan residue of the W57 OmpA mutant. As it folds into DMPC SUVs encapsulating ANTS and DPX. Spectra were acquired at 20 minute intervals for the first 3 hours and then at 30 minute intervals for the last 3 hours. Panel D shows the increase in fluorescence quantum yeild as the trp residue inserts into the lipid bilayer. Panel E shows the 'blue shift' of λ_{max} as the trp residue inserts into the lipid bilayer. The data in panels D and E are from gaussian fits to the data in panel C.

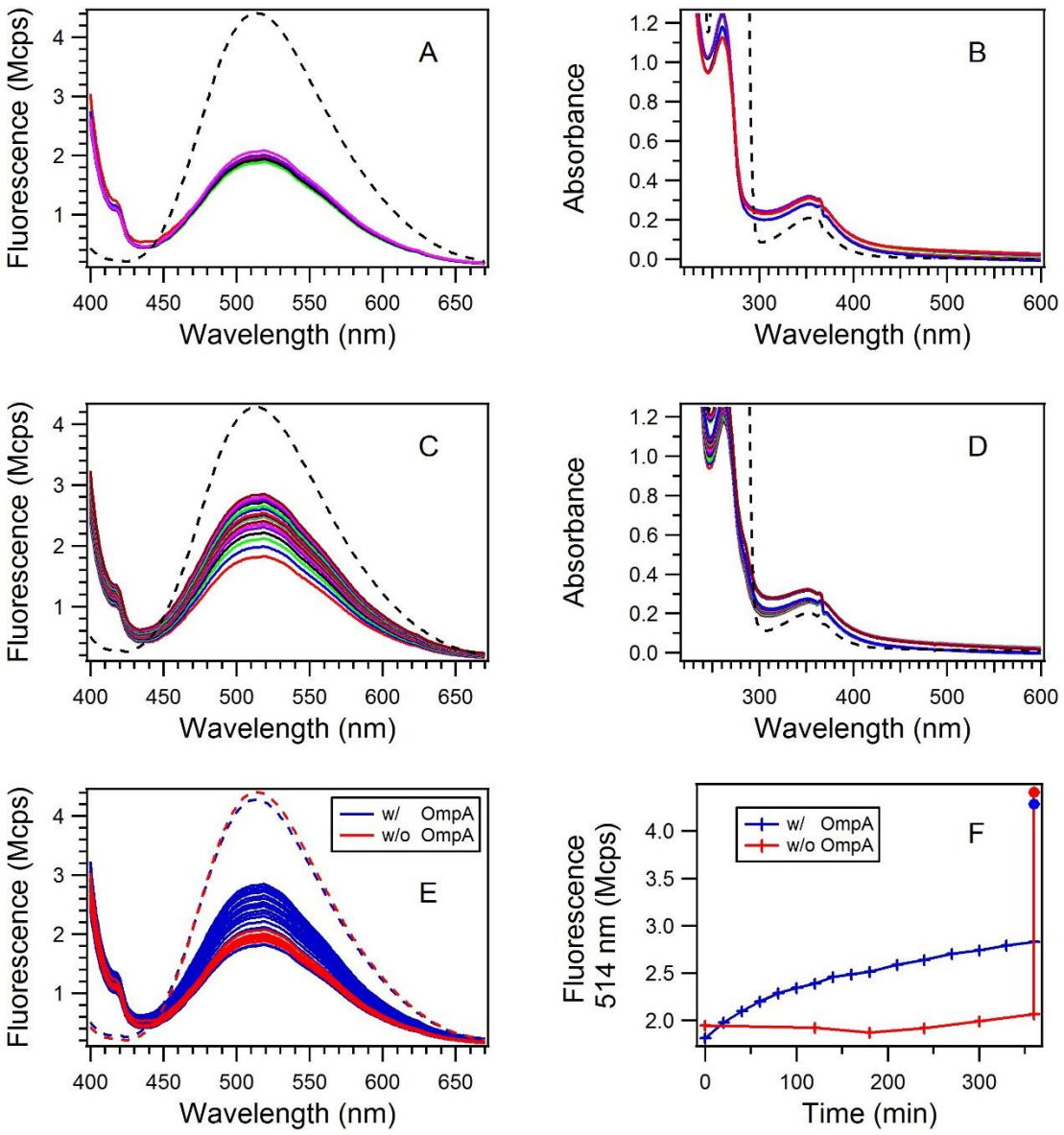

Figure S66: ANTS DPX and OmpA Experiment continued. Panel A depicts the fluorescence intensity of DMPC SUVs encapsulating ANTS and DPX from fraction 1 over a period of 6 hours and at 6 hours with triton X-100 (dashed). Panel B depicts the absorbance spectra of the sample in panel A at the same times. Panel C depicts the fluorescence intensity of DMPC SUVs encapsulating ANTS and DPX from fraction 1, with ~10 μM W57 OmpA, over a period of 6 hours and at 6 hours with triton X-100 (dashed). Panel D depicts the absorbance spectra of the sample in panel C at the same times. Panel E depicts The fluorescence intensity of ANTS and DPX in the absence (red) and in the presence of W57 OmpA (blue). Panel F depicts the fluorescence maxima of the samples in panel E plotted versus time; the circles indicate the fluorescence intensity after Triton X-100.

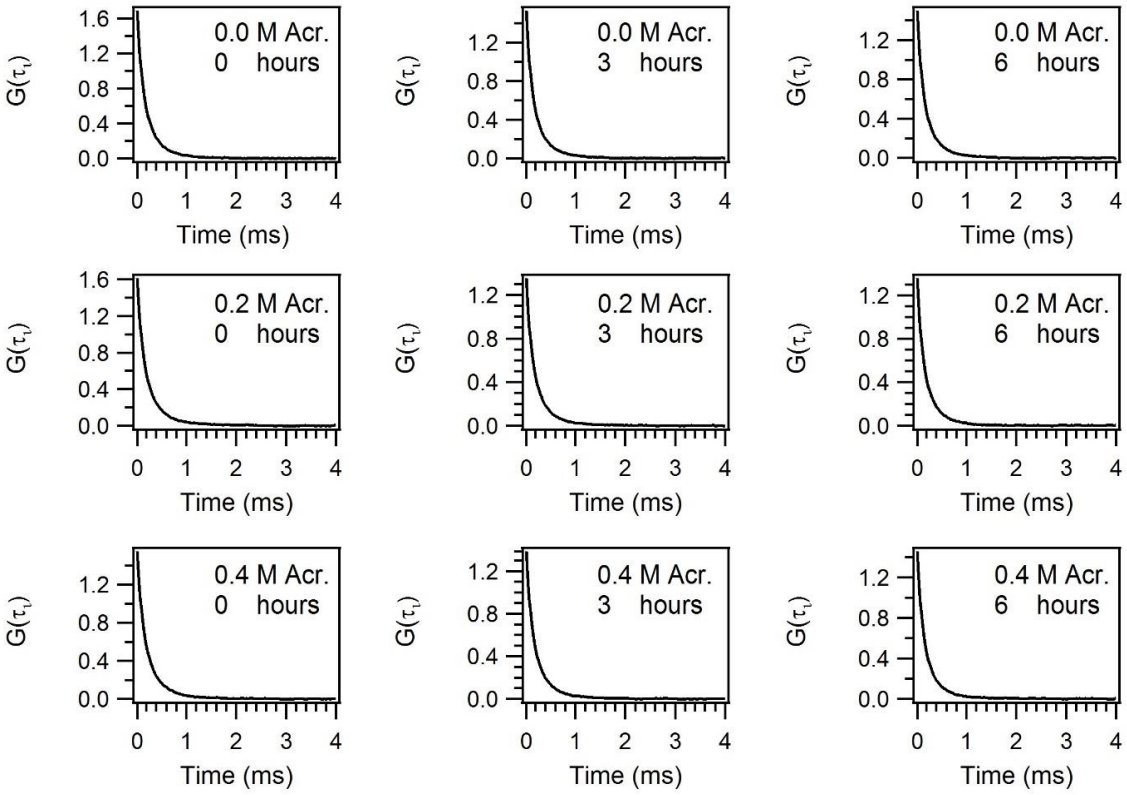

Figure S67: Autocorrelation curves. Samples of sonicated DMPC were prepared in 0.0 (top row), 0.2 (middle row) and 0.4 M (bottom row) acrylamide and were monitored by DLS at 0 (left column), 3 (middle column) and 6 hours (right column). The autocorrelation of the Rayleigh scatter is shown in these plots. The corresponding exponential and doulble exponential fit information as well as the calculated hydrodynamic radii are included in table 3.

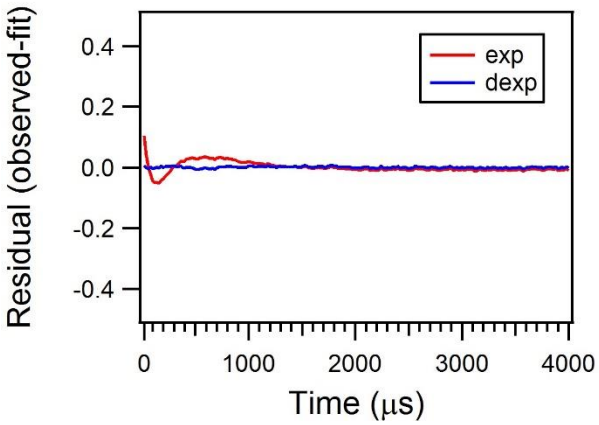

Figure S68: Autocorrelation data residual plot. Shown here are representative residual plots for the exponential fit (red) and double exponential fit (blue) to the autocorrelation data for the 0.0 M acrylamide sample at time zero hours. The residuals indicate that the double exponential fit is a more appropriate fit for these data. Only one is shown because the autocorrelation data are so similar across the variables of time and acrylamide concentration. Despite the superiority of the double exponential fit, the decay constants from both fits were used for calculation of hydrodynamic radii for comparison (Table 3).

Appendix 2. Custom IGOR Macros

```
Function GaussFitXY(GraphNameStr, xaxis)
// E.g., maxint("Graph0", q11_datx)
	String GraphNameStr // if "", use the top most graph
	Wave xaxis
	String list = TraceNameList(GraphNameStr,";",1) // create a list of traces on graph
	Variable numItems = ItemsInList( list )
	if ( numItems == 0 )
		//quit if number of waves is zero
		return 0
	endif
	Make/O/N=(numItems) maxYvalue, maxXpnt, maxXvalue, maxgYvalue, maxgXvalue
	String text = ""
	String buffer
	text += "\rFit Results: \r"
	sprintf buffer, "WaveName\tRange\tgxMax\tgYMax\t\r"; text += buffer
	String traceName
	Variable index, j
	for( index = 0; index < numItems ; index += 1 )
		traceName = StringFromList(index, list,";")
		wavestats/q $traceName
		maxYvalue[index]=V_max
		maxXpnt[index]=V_maxRowLoc
		j = maxXpnt[index]
		maxXvalue[index]=xaxis[j]
		Wave wname = $traceName
		CurveFit/M=2/Q/W=2 gauss, wname[maxXpnt[index]-
5,maxXpnt[index]+5]/X=xaxis[maxXpnt[index]-5,maxXpnt[index]+5]/D
```

Figure A1. GaussFitXY Macro. This macro was written to apply Gaussian fits to the fluorescence data for the quenching experiemnts. The macro is continued on the next page.

```
Wave W_coef

		maxgYvalue[index]=W_coef[0]+W_coef[1]

		maxgXvalue[index]=W_coef[2]

		sprintf buffer, "%s\t[ %g %g ]\t%.2f\t%g\r", traceName, xaxis[maxXpnt[index]-5], xaxis[maxXpnt[index]+5], maxgXvalue[index], maxgYvalue[index]

		text += buffer

		endfor

		Print "No. Waves Fitted: ", numItems

		text += "\r--------\r"

		String noteName =  "Note_" + StringFromList(0, list,";")

		print notename

		if (WinType(noteName)==0)

			NewNotebook/N=$noteName/F=1

			Notebook $noteName, fstyle=1, fSize=11

		endif

		Notebook $noteName, fstyle=0, fSize=11, tabs=34, text=text

		DoWindow/K $(StringFromList(0, list,";")+"_fitResults")

		Edit/N=$(StringFromList(0, list,";")+"_fitResults")  maxXpnt, maxXvalue, maxgXvalue, maxYvalue, maxgYvalue

End
```

Figure A1. GaussFitXY Macro, continued. This is the latter half of a macro was written to apply Gaussian fits to the fluorescence data for the quenching experiemnts.

```
Function sternvolmerplots(GraphNameStr, xaxis, acr)
// E.g., maxint("Graph0", q11_datx)
	String GraphNameStr // if "", use the top most graph
	Wave xaxis, acr
	String list = TraceNameList(GraphNameStr,";",1) // create a list of traces on graph
	Variable numItems = ItemsInList( list ) // should be 5 for my expt.
	if ( numItems == 0 )
		//quit if number of waves is zero
		return 0
	endif

	Variable numpts
	wavestats/q  xaxis
	numpts= V_npnts  // usually the number of time points that I have
	display  // make a blank graph
	Variable i   // this index # indicates the time point
	String outwName
	for( i = 0; i < numpts ; i += 1 )
		make/FREE/N=(numItems) f_temp  // make a wave for each time point with numitems entries.
		Variable j  // this index indicates the trace  for each different concentration of acrylamide
		String traceName
		for(j = 0; j< numItems; j += 1) // this loop is supposed to fill the wave made in the outer for loop with the entries indexed for each trace in list
			traceName = StringFromList(j, list,";")
			Wave wname = $traceName
			f_temp[j]=wname[i] //tempWave[j]=wname[i]
		endfor
		outwName = "fof_" + num2str(i)
```

Figure A2. SternVolmerPlots Macro. This macro was written to make Stern-Volmer plots for each time point in the experiment from the data in the rainbow graphs. The macro is continued on the next page.

```
Make/FREE/N=(numItems) fof_temp

                fof_temp = f_temp[0]/f_temp

                Duplicate/O fof_temp, $outwName

                appendtograph $outwName vs acr  // add each new stern volmer plot to the
blank graph during each iteration of the outer for loop

        endfor

End
```

Figure A2. SternVolmerPlots Macro, continued. This is the latter half of the macro that was written to make Stern-Volmer plots for each time point in the experiment from the data in the rainbow graphs.

References

1. Almén, M. S.; Nordström, K. J. V.; Fredriksson, R.; Schiöth, H. B., Mapping the human membrane proteome: a majority of the human membrane proteins can be classified according to function and evolutionary origin. *BMC Biology* **2009,** *7*, 50-50.

2. Wallin, E.; Heijne, G. V., Genome-wide analysis of integral membrane proteins from eubacterial, archaean, and eukaryotic organisms. *Protein Science* **1998,** *7* (4), 1029-1038.

3. Arinaminpathy, Y.; Khurana, E.; Engelman, D. M.; Gerstein, M. B., Computational analysis of membrane proteins: the largest class of drug targets. *Drug discovery today* **2009,** *14* (23-24), 1130-1135.

4. PDB Text Search for: protein. http://www.rcsb.org/pdb/results/results.do?qrid=FB547C65&tabtoshow=Current.

5. White, S. Membrane Proteins Of Known 3D Structure. http://blanco.biomol.uci.edu/mpstruc/ (accessed 7-29-2016).

6. ACS, S. References. https://scifinder.cas.org/scifinder/view/scifinder/scifinderExplore.jsf (accessed 6/15/2016).

7. Voet, D. V., J. ;Pratt, C. , *Fundamentals of Biochemistry: Life at the Molecular Level*. 4th ed.; Wiley: Hoboken, New Jersey, 2012.

8. Kampen, K. R., Membrane Proteins: The Key Players of a Cancer Cell. *The Journal of Membrane Biology* **2011,** *242* (2), 69-74.

9. Martens, J. R.; Gelband, C. H., Ion Channels in Vascular Smooth Muscle: Alterations in Essential Hypertension. *Experimental Biology and Medicine* **1998,** *218* (3), 192-203.

10. Jackson, W. F., Ion Channels and Vascular Tone. *Hypertension* **2000,** *35* (1), 173-178.

11. Yin, J.; Huang, F.; Yi, Y.; Yin, L.; Peng, D., EGCG attenuates atherosclerosis through the Jagged-1/Notch pathway. *International Journal of Molecular Medicine* **2015,** *37* (2), 398-406.

12. Gadsby, D. C.; Vergani, P.; Csanady, L., The ABC protein turned chloride channel whose failure causes cystic fibrosis. *Nature* **2006,** *440* (7083), 477-483.

13. Rask-Andersen, M.; Almén, M. S.; Schiöth, H. B., Trends in the exploitation of novel drug targets. *Nat Rev Drug Discov* **2011,** *10* (8), 579-590.

14. McPhail, G. L., Clancy, J.P. , Ivacaftor: The first therapy acting on the primary cause of cystic fibrosis. *Drugs of Today* **McPhail, G.L., Clancy, J.P. ,** *49* (4), 253-60.

15. Kleinschmidt, J. H.; Tamm, L. K., Folding Intermediates of a β-Barrel Membrane Protein. Kinetic Evidence for a Multi-Step Membrane Insertion Mechanism. *Biochemistry* **1996,** *35* (40), 12993-13000.

16. Tamm, L. K.; Hong, H.; Liang, lding and assembly of β-barrel membrane p B., Fo roteins. *Biochimica et Biophysica Acta (BBA) - Biomembranes* **2004,** *1666* (1–2), 250-263.

17. Bryngelson, J. D.; Onuchic, J. N.; Socci, N. D.; Wolynes, P. G., Funnels, pathways, and the energy landscape of protein folding: A synthesis. *Proteins: Structure, Function, and Bioinformatics* **1995,** *21* (3), 167-195.

18. Clantin, B.; Delattre, A.-S.; Rucktooa, P.; Saint, N.; Méli, A. C.; Locht, C.; Jacob-Dubuisson, F.; Villeret, V., Structure of the Membrane Protein FhaC: A Member of the Omp85-TpsB Transporter Superfamily. *Science* **2007,** *317* (5840), 957.

19. Gentle, I.; Gabriel, K.; Beech, P.; Waller, R.; Lithgow, T., The Omp85 family of proteins is essential for outer membrane biogenesis in mitochondria and bacteria. *The Journal of Cell Biology* **2003,** *164* (1), 19–24.

20. Xu, J.; Bjursell, M. K.; Himrod, J.; Deng, S.; Carmichael, L. K.; Chiang, H. C.; Hooper, L. V.; Gordon, J. I., A Genomic View of the Human-Bacteroides thetaiotaomicron Symbiosis. *Science* **2003,** *299* (5615), 2074.

21. Bergman, E. N., Energy contributions of volatile fatty acids from the gastrointestinal tract in various species. *Physiological Reviews* **1990,** *70* (2), 567.

22. HMP NIH Human Microbiome Project. http://hmpdacc.org/ (accessed 8/24/2016).

23. Lin, J.; Huang, S.; Zhang, Q., Outer membrane proteins: key players for bacterial adaptation in host niches. *Microbes and Infection* **2002,** *4* (3), 325-331.

24. Urfer, M.; Bogdanovic, J.; Lo Monte, F.; Moehle, K.; Zerbe, K.; Omasits, U.; Ahrens, C. H.; Pessi, G.; Eberl, L.; Robinson, J. A., A Peptidomimetic Antibiotic Targets Outer Membrane Proteins and Disrupts Selectively the Outer Membrane in Escherichia coli. *J Biol Chem* **2015**.

25. Foulds, J.; Chai, T.-J., Isolation and characterization of isogenic E. coli strains with alterations in the level of one or more major outer membrane proteins. *Canadian Journal of Microbiology* **1979,** *25* (3), 423-427.

26. Chen, R.; Schmidmayr, W.; Krämer, C.; Chen-Schmeisser, U.; Henning, U., Primary structure of major outer membrane protein II (ompA protein) of Escherichia coli K-12. *P Natl Acad Sci USA* **1980,** *77* (8), 4592-4596.

27. Le Coutre, J.; Whitelegge, J. P.; Gross, A.; Turk, E.; Wright, E. M.; Kaback, H. R.; Faull, K. F., Proteomics on Full-Length Membrane Proteins Using Mass Spectrometry. *Biochemistry* **2000,** *39* (15), 4237–4242.

28. Vogel, H.; Jähnig, F., Models for the structure of outer-membrane proteins of Escherichia coli derived from raman spectroscopy and prediction methods. *Journal of Molecular Biology* **1986,** *190* (2), 191-199.

29. Sonntag, I.; Schwarz, H.; Hirota, Y.; Henning, U., Cell envelope and shape of Escherichia coli: multiple mutants missing the outer membrane lipoprotein and other major outer membrane proteins. *Journal of Bacteriology* **1978,** *136* (1), 280-285.

30. Chai, T.; Foulds, J., Demonstration of a missing outer membrane protein in tolG mutants of Escherichia coli. *Journal of Molecular Biology* **1974,** *85* (3), 465-474.

31. Alphen, L. v.; Havekes, L.; Lugtenberg, B., Major outer membrane protein d of Escherichia coli K 12. *Febs Lett* **1977,** *75* (1), 285-290.

32. Datta, D. B.; Arden, B.; Henning, U., Major proteins of the Escherichia coli outer cell envelope membrane as bacteriophage receptors. *Journal of Bacteriology* **1977,** *131* (3), 821-829.

33. Schweizer, M.; Hindennach, I.; Garten, W.; Henning, U., Major Proteins of the Escherichia coli Outer Cell Envelope Membrane. Interaction of Protein II* with Lipopolysaccharide. *Eur J Biochem* **1978,** *82* (1), 211-217.

34. Surrey, T.; Jähnig, F., Kinetics of Folding and Membrane Insertion of a β-Barrel Membrane Protein. *J Biol Chem* **1995,** *270* (47), 28199-28203.

35. Surrey, T.; Jähnig, F., Refolding and oriented insertion of a membrane protein into a lipid bilayer. *P Natl Acad Sci USA* **1992,** *89* (16), 7457-7461.

36. Rodionova, N. A.; Tatulian, S. A.; Surrey, T.; Jaehnig, F.; Tamm, L. K., Characterization of two membrane-bound forms of OmpA. *Biochemistry* **1995,** *34* (6), 1921-1929.

37. Pautsch, A.; Schulz, G. E., High-resolution structure of the OmpA membrane domain1. *Journal of Molecular Biology* **2000,** *298* (2), 273-282.

38. Arora, A.; Abildgaard, F.; Bushweller, J. H.; Tamm, L. K., Structure of outer membrane protein A transmembrane domain by NMR spectroscopy. *Nat Struct Mol Biol* **2001,** *8* (4), 334-338.

39. Schiffer, M.; Chang, C. H.; Stevens, F. J., The function of tryptophan residues in membrane proteins. *Protein Engineering* **1992,** *5* (3), 213-214.

40. Cowan, S. W.; Rosenbusch, J. P., Folding pattern diversity of integral membrane proteins. *Science* **1994,** *264* (5161), 914-916.

41. Vivian, J. T.; Callis, P. R., Mechanisms of Tryptophan Fluorescence Shifts in Proteins. *Biophys J 80* (5), 2093-2109.

42. Dornmair, K.; Kiefer, H.; Jähnig, F., Refolding of an integral membrane protein. OmpA of Escherichia coli. *J Biol Chem* **1990,** *265* (31), 18907-18911.

43. Kleinschmidt, J. H.; den Blaauwen, T.; Driessen, A. J. M.; Tamm, L. K., Outer Membrane Protein A of Escherichia coli Inserts and Folds into Lipid Bilayers by a Concerted Mechanism. *Biochemistry* **1999,** *38* (16), 5006-5016.

44. Bulieris, P. V.; Behrens, S.; Holst, O.; Kleinschmidt, J. H., Folding and Insertion of the Outer Membrane Protein OmpA Is Assisted by the Chaperone Skp and by Lipopolysaccharide. *J Biol Chem* **2003,** *278* (11), 9092-9099.

45. Kang, G.; López-Peña, I.; Oklejas, V.; Gary, C. S.; Cao, W.; Kim, J. E., Förster resonance energy transfer as a probe of membrane protein folding. *Biochimica et Biophysica Acta (BBA) - Biomembranes* **2012,** *1818* (2), 154-161.

46. Lakowicz, J. R., *Principles of Fluorescence Spectroscopy*. Springer: New York, 2006.

47. Evans, R. F.; Kuntz, R. R.; Volkert, W. A.; Ghiron, C. A., Flash Photolysis of N-Acetyl-L-Tryptophanamide: The Relationship Between Radical Yields and Fluorescence Quenching. *Photochem Photobiol* **1978,** *27* (5), 511-515.

48. Tallmadge, D. H.; HuEbnert, J. S.; Borkman, R. F., ACRYLAMIDE QUENCHING OF TRYPTOPHAN PHOTOCHEMISTRY AND PHOTOPHYSICS. *Photochem Photobiol* **1989,** *49* (4), 381-386.

49. Lakowicz, J. R.; Zelent, B.; Gryczynski, I.; Kuba, J.; Johnson, M. L., Distance-Dependent Fluorescence Quenching of Tryptophan BY Acrylamide. *Photochem Photobiol* **1994,** *60* (3), 205-214.

50. Eftink, M. R.; Ghiron, C. A., Dynamics of a protein matrix revealed by fluorescence quenching. *P Natl Acad Sci USA* **1975,** *72* (9), 3290-3294.

51. Eftink, M. R.; Ghiron, C. A., Fluorescence quenching studies with proteins. *Analytical Biochemistry* **1981,** *114* (2), 199-227.

52. Krylov, N. A.; Pentkovsky, V. M.; Efremov, R. G., Nontrivial Behavior of Water in the Vicinity and Inside Lipid Bilayers As Probed by Molecular Dynamics Simulations. *ACS Nano* **2013,** *7* (10), 9428-9442.

53. Kleinschmidt, J. H.; Tamm, L. K., Time-Resolved Distance Determination by Tryptophan Fluorescence Quenching: Probing Intermediates in Membrane Protein Folding. *Biochemistry* **1999,** *38* (16), 4996-5005.

54. Qu, J.; Mayer, C.; Behrens, S.; Holst, O.; Kleinschmidt, J. H., The Trimeric Periplasmic Chaperone Skp of Escherichia coli Forms 1:1 Complexes with Outer Membrane Proteins via Hydrophobic and Electrostatic Interactions. *Journal of Molecular Biology* **2007,** *374* (1), 91-105.

55. Cheung, M. S.; García, A. E.; Onuchic, J. N., Protein folding mediated by solvation: Water expulsion and formation of the hydrophobic core occur after the structural collapse. *Proceedings of the National Academy of Sciences* **2002,** *99* (2), 685-690.

56. Sheinerman, F. B.; Brooks Iii, C. L., Calculations on folding of segment B1 of streptococcal protein G1. *Journal of Molecular Biology* **1998,** *278* (2), 439-456.

57. Bartlett, G. J.; Porter, C. T.; Borkakoti, N.; Thornton, J. M., Analysis of Catalytic Residues in Enzyme Active Sites. *Journal of Molecular Biology* **2002,** *324* (1), 105-121.

58. Levy, Y.; Onuchic, J. N., Water and proteins: A love–hate relationship. *P Natl Acad Sci USA* **2004,** *101* (10), 3325-3326.

59. Kauzmann, W., Some Factors in the Interpretation of Protein Denaturation1. In *Advances in Protein Chemistry*, C.B. Anfinsen, M. L. A. K. B.; John, T. E., Eds. Academic Press: 1959; Vol. Volume 14, pp 1-63.

60. Dill, K. A., Dominant forces in protein folding. *Biochemistry* **1990,** *29* (31), 7133-7155.

61. Sanchez, K. M.; Gable, J. E.; Schlamadinger, D. E.; Kim, J. E., Effects of Tryptophan Microenvironment, Soluble Domain, and Vesicle Size on the Thermodynamics of Membrane Protein Folding: Lessons from the Transmembrane Protein OmpA. *Biochemistry* **2008,** *47* (48), 12844-12852.

62. Sanchez, Katheryn M.; Kang, G.; Wu, B.; Kim, Judy E., Tryptophan-Lipid Interactions in Membrane Protein Folding Probed by Ultraviolet Resonance Raman and Fluorescence Spectroscopy. *Biophys J* **2011,** *100* (9), 2121-2130.

63. Biomedicals, M. TRITON® X-100, 02300221. http://www.mpbio.com/product.php?pid=02300221&country=223 (accessed 8/20/2016).]
64. Ladokhin, A. S.; Wimley, W. C.; White, S. H., Leakage of membrane vesicle contents: determination of mechanism using fluorescence requenching. *Biophys J* **1995,** *69* (5), 1964-1971.

65. Berne, B. J. P., R. , *Dynamic light scattering: with applications to chemistry, biology, and physics*. Dover: Mineola, New York, 2006.

66. NYU New York University Scientific Visualization Center; Lipids Section. https://www.nyu.edu/pages/mathmol/library/lipids/ (accessed 8/11/2016).

67. Danoff, E. J.; Fleming, K. G., The soluble, periplasmic domain of OmpA folds as an independent unit and displays chaperone activity by reducing the self-association propensity of the unfolded OmpA transmembrane β-barrel. *Biophys Chem* **2011,** *159* (1), 194-204.

68. Leonenko, Z. V.; Finot, E.; Ma, H.; Dahms, T. E. S.; Cramb, D. T., Investigation of Temperature-Induced Phase Transitions in DOPC and DPPC Phospholipid Bilayers Using Temperature-Controlled Scanning Force Microscopy. *Biophys J* **2004,** *86* (6), 3783-3793.

69. Sanchez, K. M.; Neary, T. J.; Kim, J. E., Ultraviolet Resonance Raman Spectroscopy of Folded and Unfolded States of an Integral Membrane Protein. *The Journal of Physical Chemistry B* **2008,** *112* (31), 9507-9511.

70. Caputo, G. A.; London, E., Using a Novel Dual Fluorescence Quenching Assay for Measurement of Tryptophan Depth within Lipid Bilayers To Determine Hydrophobic α-Helix Locations within Membranes. *Biochemistry* **2003,** *42* (11), 3265-3274.

71. Kang, G. Fluorescence and energy transfer studies of membrane protein folding. UCSD, 2015.

72. Kang, G.; López-Peña, I.; Bhakta, S.; Kim, J. E., Probing Membrane Protein Structure and Dynamics by Fluorescence Spectroscopy. In *Encyclopedia of Analytical Chemistry*, John Wiley & Sons, Ltd: 2013.

73. Malmberg, C. G.; Maryott, A. A., Dielectric Constant of Water from 0 0 to 1000 C. *Journal of Research of the National Bureau of Standards* **1956,** *56* (1).

74. Raudino, A.; Mauzerall, D., Dielectric properties of the polar head group region of zwitterionic lipid bilayers. *Biophys J* **1986,** *50* (3), 441-449.

75. Bellemare, F.; DeMendoncaFragata, M., Polarity studies on the head group of single-layered phosphatidylcholine- -tocopherol vesicles. *Journal of Colloid and Interface Science 77* (1), 243-251.

76. Fettiplace, R.; Andrews, D. M.; Haydon, D. A., The thickness, composition and structure of some lipid bilayers and natural membranes. *The Journal of Membrane Biology* **1971,** *5* (3), 277-296.

77. CRC, *Handbook of Chemistry and Physics*. 43 ed.; The Chemical Rubber Publishing Company: Cleveland Ohio, 1961.

78. Badawi, H. M.; Al-Khaldi, M. A. A.; Al-Abbad, S. S. A.; Al-Sunaidi, Z. H. A., Rotational barriers in monomeric CH2CX–COOH and CH2CX–CONH2 (X is H or CH3) and vibrational analysis of methacrylic acid and methacrylamide. *Spectrochimica Acta Part A: Molecular and Biomolecular Spectroscopy* **2007,** *68* (3), 432-442.

79. Lewis, B. A.; Engelman, D. M., Lipid bilayer thickness varies linearly with acyl chain length in fluid phosphatidylcholine vesicles. *Journal of Molecular Biology* **1983,** *166* (2), 211-217.